DIVISION OF BIOMEDICAL ENGINEERING

DEPARTMENT OF HUMAN BIOLOGY

UNIVERSITY OF CAPE TOWN

Project title:

MECHANICAL PROPERTIES OF OESOPHAGEAL SQUAMOUS CELL CARCINOMA CELLS DURING CHEMOTHERAPY

Dissertation:

In fulfilment of the requirements for the degree:

MSc in Biomedical Engineering (MM054HUB05)

By:

MARTIN KIWANUKA (KWNMAR005)

Supervisor:

Prof. Thomas Franz

Co-supervisors:

Assoc. Prof. Neil Davies

Date:

June 2021

Declaration

I, **Martin Kiwanuka**, hereby declare that the work on which this dissertation/thesis is based is my original work (except where acknowledgements indicate otherwise). Neither the entire work nor any part of it has been, is being, or will be submitted for another degree in this or any other university.

I authorize the University of Cape Town to reproduce for research either the whole or any portion of its contents in any manner whatsoever.

Signature: ……

Date: ……

Abstract

Oesophageal cancer (OC) is the seventh most common and sixth deadliest cancer worldwide, with oesophageal squamous cell carcinoma (OSCC) the most prevalent subtype, responsible for over 90 % of all OC cases in Southern and Eastern Africa and South-East and Central Asia. Most OSCC patients present for diagnosis at later stages of cancer development since it is asymptomatic at its early stages. Chemotherapy combined with radiotherapy or surgery is the most effective method used to treat OSCC. However, it is mainly affected by treatment failure due to chemoresistance. Recent studies have highlighted the role of cell mechanics in the development of cancer and chemoresistance. Therefore, this study investigates the association between exposure to chemotherapeutic drugs and changes in the mechanical properties of human OSCC of South African origin.

Cell lines (WHCO1) derived from biopsies of primary OSCC from South African patients were cultured in 2D and 3D environments and treated with 2 µM Paclitaxel. Ethanol was used as the vehicle control in the 2D study, whereas untreated cells were used as controls in both 2D and 3D studies. Mitochondrial Particle Tracking Microrheology (MPTM) and VAMPIRE algorithm were used to characterize the intracellular stiffness (N = 142 cells) and morphology (N = 251 cells) of OSCC cells, respectively, after 24 and 48 hours of treatment.

Results show that treatment of OSCC cells with Paclitaxel led to an increase in their intracellular stiffness as early as 24 hours after treatment, and this continued increasing until 48 hours for cells in 2D. No significant differences were observed between the controls at both 24 and 48 hours indicating that the increase in intracellular stiffness of OSCC cells was due to Paclitaxel treatment. In contrast to 2D, the intracellular stiffness of cells in 3D decreased after 24 hours of treatment with Paclitaxel, with cells at 48 hours softer than those at 24 hours. In addition, the untreated cells in 3D at 48 hours were stiffer than those at 24 hours at short delay times (τ = 0.15 and 0.9 s, $p < .05$), indicating that the increase in intracellular stiffness of Paclitaxel-treated cells in 3D might not have only been due to drug treatment.

Furthermore, treatment of OSCC with Paclitaxel led to a significant increase in cell area and perimeter for the cells in 2D at both 24 and 48 hours of treatment compared to the controls ($p < .005$) but not in 3D. No significant differences were observed between the controls at both 24 and 48 hours indicating that the increase in cell area and perimeter in cells in 2D was due to Paclitaxel treatment. Additionally, treating OSCC cells with Paclitaxel did not affect the morphological heterogeneity of cells in 2D. However, it led to a decrease in the heterogeneity of cells in 3D after 48 hours of treatment. Based on the study findings, there are changes in intracellular stiffness, morphology, and heterogeneity associated with the treatment of OSCC cells with Paclitaxel.

Dedication

I dedicate this dissertation and master's degree to my late father, Mr. Kiwanuka Waliggo Lawrence (September 1963 – July 2007); mother, Ms. Namyalo Scovia; grandfather and guardian, Mr. Mpagi John Mary; brothers, Mr. Waliggo Junior Lawrence and Mr. Nsowe Deogratious; and my sister Ms. Nalutoogo Sharon, for all the love, support, and encouragement throughout my life and academic journey.

Acknowledgements

I would like to thank my supervisor, Prof. Thomas Franz, for the continuous scientific guidance, mentorship, and encouragement throughout my master's studies. Thank you for being interested in advancing my academic career and all the local and international opportunities you introduced me to.

I would also like to thank my co-supervisor, Assoc. Prof. Neil Davies for introducing me to the field of cell biology and for accepting me into your molecular biology laboratory for my tissue culture experiments. Thank you for taking the time to review my thesis and for all the guidance and advice you gave me during my master's studies.

Special thanks to Prof. Iqbal Parker of the Division of Medical Biochemistry & Structural Biology, University of Cape Town (UCT), for providing us with the oesophageal squamous cell carcinoma cell line (WHCO1) that we used in our study. Thanks to Ms. Humaira Lambarey (Parker's lab) for training me in cell culture.

My sincere thanks to Mrs. Helen Ilsley and Ms. Silindile Ngcobo from the Cardiovascular Research Unit (CVRU) at UCT for training me in cell and tissue culturing and always being available whenever I needed advice or assistance with my experiments.

Thanks to Professor Dirk Lang and the entire team at the Confocal and Light Imaging Facility at the UCT for training me in confocal imaging and assisting with my imaging work even during the most challenging times of the COVID-19 pandemic. I highly appreciate your commitment to helping me finish all my imaging work in time and guidance and advice with image analysis.

Thanks to all the members of the Mechanobiology group and CVRU (2019 - 2021) at the UCT for your encouragement and constructive feedback on the different aspects of my research.

Sincere thanks to Ms. Ghodeejah Higgins for all the guidance in planning my experiments and training in mitochondrial Particle Tracking Microrheology, and statistical analysis. I highly appreciate your willingness always to assist me in every way possible whenever I got stuck with my work.

Special thanks to Ms. Juliet Nagawa for making my transition into the Mechanobiology group, UCT, and Cape Town, in general, smooth, and always being available to review my documents, including the thesis. Thank you for the introductory training in statistics and the assistance and guidance with my statistical analysis work whenever there was a need.

My sincere thanks also go to Ms. Catherine Namayega for booking me a house that became a home for me in Cape Town for two good years and welcoming me with a special meal. Thank you for all the assistance with my academic and non-academic work throughout the years of my master's degree.

I would also like to thank the staff members of UCT, especially those in the Division of Biomedical Engineering, Department of Human Biology, and Faculty of Health Sciences, for the continual administrative support.

And finally, I am grateful for the African Biomedical Engineering Mobility scholarship (ABEM) funded by the Intra-African Academic Mobility Scheme of the European Commission's Education, Audiovisual and Culture Executive Agency; South African Medical Research Council (SAMRC) and UCT for funding my master's studies.

All the glory to the almighty God!

Table of Contents

Declaration i

Abstract ii

Dedication iii

Acknowledgements iv

List of Figures vii

List of Tables xi

List of Abbreviations xiii

Chapter 1 Introduction and Background 1

1.1 Overview of dissertation 1

1.2 Introduction to cancer 1

1.3 Cancer prevalence and distribution 2

1.4 Epidemiology and the pathogenesis of oesophageal cancer 3

1.5 Clinical presentation of oesophageal cancer 5

1.6 Diagnosis and staging of oesophageal cancer. 5

1.7 Treatment of oesophageal cancer 8

1.7.1 Surgery 8

1.7.2 Chemotherapy and radiotherapy 8

1.8 Cell mechanics and mechanobiology 9

1.8.1 Structure and function of a cell 9

1.8.2 The cytoskeleton and its role in cell mechanics 11

1.8.3 The extracellular environment and cell mechanics 12

1.8.4 Cell mechanics and mechanobiology case studies 14

1.8.5 Experimental tools and methods to study cell mechanics. 15

1.9 Research aims and objectives. 18

Chapter 2 Materials and Methods 20

2.1 Overview 20

2.2 Cell culture 20

2.3 Seeding densities and viability determination 20

2.4 Chemotherapeutic drug treatment 22

2.4.1 2D experiments 22

2.4.2 3D experiments 23

2.5 Mitochondrial Particle-Tracking Microrheology 23

2.5.1 Mitochondrial staining 23

2.5.2 Time-lapse Imaging 24

2.5.3 Image processing and data analysis 24

2.6 Cell morphological analysis 25
2.7 Statistical analysis 27
Chapter 3 Results 28
3.1 Intracellular stiffness of WHCO1 cells 28
3.1.1 Effect of Paclitaxel treatment on the intracellular stiffness of WHCO1 cells in 2D environments 28
3.1.2 Effect of Paclitaxel treatment on the intracellular stiffness of WHCO1 cells in 3D environments 32
3.1.3 Effect of dimensionality on the intracellular stiffness of WHCO1 cells. 36
3.2 Morphology for WHCO1 cells 37
3.2.1 Effect of Paclitaxel treatment on the morphology of WHCO1 cells in 2D environments 38
3.2.2 Effect of Paclitaxel treatment on the morphology of WHCO1 cells in 3D environments 40
3.2.3 Effect of dimensionality on the morphology of WHCO1 cells 40
3.2.4 Shape analysis and heterogeneity of the treated and untreated WHCO1 cells 41
3.2.5 Heterogeneity in the treated and untreated WHCO1 cells in 2D environments 41
3.2.6 Heterogeneity in the treated and untreated WHCO1 cells in 3D environments 43
Chapter 4 Discussion 45
4.1 Intracellular stiffness 45
4.2 Morphology 47
4.3 Dimensionality 48
Chapter 5 Conclusion and recommendations 49
References 51
Appendix 63
Supplementary Information for Chapter 2 63
Supplementary Information for Chapter 3 66

List of Figures

Figure 1.1: Allocation of cancer incidences and mortality in the world continents in 2018. Reused with permission from Bray et al. (2018). 3
Figure 1.2: An illustration of oesophageal cancer (http://umr.adam.com). 4
Figure 1.3: cancer incidences and mortalities by the ten most prevalent cancers in 2018 as reported by the World Health Organization (2020)..... 4
Figure 1.4: Oesophageal cancer wound as viewed on an endoscope. A: OSCC. B: Large fatal and bleeding OAC. Reused from Lagergren and Lagergren (2010) with permission from BMJ Publishing Group Ltd. 6
Figure 1.5: Stages of oesophageal cancer using the tumor, node and metastases (TNM) staging classification. Tis (HGD) symbolizes high-grade dysplasia; T1a, a tumor that has invaded the lamina propria; T1b, a tumor that has penetrated muscularis mucosae or submucosa; T2, a tumour that has penetrated muscularis propria; T3, a tumour that has invaded the adventitia; T4a, a tumour that has extended to the pleura and T4b, shows a tumor that has spread into the aorta and neighbouring tissues. M1 symbolizes the presence of distant metastases whereas N0 stands for no metastases in the lymph nodes; N1, a tumour that has metastasized to one or two lymph nodes; N2, metastases in three to six lymph nodes and N3 signifies a tumor that has spread to seven or more lymph nodes. Reused with permission from Rice et al. (2017). 7
Figure 1.6: An illustration of the structure of a eukaryotic showing its major components. Reused with permission from Bao and Suresh (2003)..... 10
Figure 1.7: Particle-Tracking Microrheology. Video microscopy is performed to monitor and capture videos of the movement of tracer particles within the medium. Particle-tracking is performed to construct particle trajectories from the displacement of tracer particles within the medium, and finally, time lag-dependent mean-squared displacements are computed from the particle trajectories using appropriate software (Schultz and Furst 2012)..... 18
Figure 2.1: Neubauer chamber counting grid as seen under the light microscope. Cells in squares labelled one are counted to calculate the number of viable and non-viable cells (https://www.emsdiasum.com). 21
Figure 2.2: Procedure for MPTM. From left to right on the top row are an illustration of treated and untreated WHCO1 cells in 2D and 3D environments. It is followed by a representative of cells fluorescently labelled with MitoTracker green solution (green color represents the mitochondria of the cells fluorescently labelled with Mitotrackers), a confocal microscope used for time-lapse imaging of cells, and lastly, examples of images captured with a confocal microscope. The second row illustrates the procedure for post-image processing and data analysis. On the left is a representation

of particle trajectories (see inset) constructed using TrackMate in Image J to trace the displacement of mitochondria within the cell cytoplasm. In the centre is a graph representing time-dependent MSDs that were computed from particle trajectories using custom algorithms in MATLAB, and at the right is the plot of fluidity calculated from the slope of time-dependent logarithmic MSDs. 25
Figure 2.3: Illustration of the VAMPIRE analysis. A: a thousand equidistant points along the contour of cells were used to describe the contour of the cells. B: The unaligned identified cell shapes (left) were then combined and aligned as shown on the right. C: principal component analysis of the coordinates on the contours of the aligned cells was performed to acquire principal components (PC 1, PC 2…, PC N). D: the cell shapes were then reconstructed from a reduced number of principal components comprising 95 % shape variations among all analyzed cells. E: K-means clustering was then applied to the group of cell data described by the principal components to obtain representative shape modes. Reused with permission from Phillip et al. (2021). 26
Figure 3.1: Confocal images of Paclitaxel-treated, ethanol-treated, and untreated WHCO1 cells in 2D environments after 24 and 48 hours of treatment. The images are taken from a pool of 1000 frames captured in 140 seconds using a confocal microscope. The images were captured for N = 12 and 14 Paclitaxel treated cells at 24 and 48 hours of treatment, 11 for each of the ethanol-treated cells at 24 and 48 hours, and 17 and 14 for untreated cells at 24 and 48 hours, respectively. Scale bars (white) represent 5 µm. 28
Figure 3.2: Microrheological characterization of WHCO1 cells in 2D environments. (a) MSD versus delay time curves for Paclitaxel-treated cells at 24 (PTX 24) and 48 (PTX 48) hours of incubation. (b) Fluidity versus delay time curves for Paclitaxel-treated cells at 24 and 48 hours of treatment. (c) MSD versus delay time plots for cells treated with ethanol for 24 (ETH 24) and 48 (ETH 48) hours. (d) Fluidity versus delay time curves for ethanol-treated cells at 24 and 48 hours of treatment. (e) MSD curves for the untreated at 24 (UNT 24) and 48 (UNT 48) hours of incubation. (f) Fluidity curves for untreated cells at 24 and 48 hours. Error bars are SEM for one independent repeat experiment (n = 2), N = 12 and 14 for Paclitaxel-treated cells at 24 and 48 hours of treatment, respectively, N = 11 for each of the ethanol-treated cells at 24 and 48 hours of treatment, and N =17 and 14 for untreated cells incubated for 24 hours 48 hours, respectively. Statistical analysis was carried out using a two-way ANOVA. 30
Figure 3.3: Microrheology of WHCO1 cells at 24 hours of treatment in 2D environments. (a) MSD versus delay time curves for untreated (UNT), ethanol-treated (ETH), and Paclitaxel-treated cells (PTX). (b) Fluidity versus delay time curves for untreated, ethanol-treated, and Paclitaxel-treated cells. Error bars are SEM for one independent repeat experiments (n = 2), N=17 (UNT), 11 (ETH), and 12 (PTX). N refers to the number of cells in each condition. A total of 40 cells were analyzed. Statistical analysis was carried out using a two-way ANOVA. 31

Figure 3.4: Microrheology of WHCO1 cells at 48 hours of treatment in 2D environments. (a) MSD versus delay time curves for Untreated, ethanol-treated, and Paclitaxel-treated cells. (b) Fluidity versus delay time curves for untreated, ethanol-treated, and Paclitaxel-treated cells. Error bars show SEM for one independent repeat experiment (n = 2), N=14, 11, and 14 for untreated, ethanol-treated, and Paclitaxel-treated cells, respectively. Statistical analysis was carried out using a two-way ANOVA. 32
Figure 3.5: Confocal images of Paclitaxel-treated and untreated WHCO1 cells embedded in 3D environments after 24 and 48 hours. The images are taken from a pool of 1000 frames captured in 150 seconds using a confocal microscope. The images were captured for N = 21 and 10 Paclitaxel treated cells at 24 and 48 hours of treatment, respectively, and 19 and 13 for the untreated cells at 24 and 48 hours. Scale bars (white) represent 5 µm. 33
Figure 3.6: Microrheological characterization of WHCO1 cells in 3D environments. (a) MSD versus delay time curves for Paclitaxel-treated cells at 24 and 48 incubation hours. (b) Fluidity versus delay time curves for Paclitaxel-treated cells at 24 and 48 hours. (c) MSD versus delay time plots for untreated cells 24 and 48 hours of incubation. (d) Fluidity versus delay time curves for untreated cells at 24 and 48 hours of incubation. Error bars indicate SEM for one independent repeat experiment (n = 2), N = 21 and 10 for Paclitaxel-treated cells at 24 and 48 hours of treatment, respectively, and N = 19 and 13 for untreated cells incubated for 24 hours 48 hours, respectively. Statistical analysis was carried out using a two-way ANOVA. 34
Figure 3.7: Microrheology of WHCO1 cells at 24 hours of treatment in 3D environments. (a) MSD versus delay time curves for Untreated and Paclitaxel-treated cells. (b) Fluidity versus delay time curves for untreated and Paclitaxel-treated cells. Error bars show SEM for one independent repeat experiment (n = 2), N = 19 and 21 for untreated and Paclitaxel-treated cells, respectively. Statistical analysis was carried out using a two-way ANOVA. 35
Figure 3.8: Microrheology of WHCO1 cells at 48 hours of treatment in 3D environments. (a) MSD versus delay time curves for Untreated and Paclitaxel-treated cells. (b) Fluidity versus delay time curves for untreated and Paclitaxel-treated cells. Error bars show SEM for one independent repeat experiment (n = 2), N = 13 and 10 for untreated and Paclitaxel-treated cells, respectively. Statistical analysis was carried out using a two-way ANOVA. 35
Figure 3.9: Comparison of MSDs and fluidity for WHCO1 cells in 2D and 3D environments at a delay time of 2.1 seconds. (a) MSDs for Paclitaxel-treated and untreated WHCO1 cells at 24 and 48 hours of treatment. (b) Fluidity for Paclitaxel-treated and untreated WHCO1 cells at 24 and 48 hours of treatment. PTX_24, PTX_48, UNT_24, and UNT_48 stand for Paclitaxel-treated and Untreated cells at

24 and 48 hours of treatment. Error bars indicate SEM. ** and *** indicate p < 0.005 and 0.0005, respectively. Statistical analysis was carried out using a three-way ANOVA. 37
Figure 3.10: Morphology analysis of treated and untreated cells. (a) Cell area, (b) perimeter, (c) circularity, and (d) aspect ratio of Paclitaxel-treated and Untreated WHCO1 cells at 24 and 48 hours of treatment in 2D and 3D environments. Error bars are SEM for one independent repeat experiment (n = 2). For 2D experiments, N = 27 and 22 for Paclitaxel-treated cells at 24 and 48 hours, respectively. N = 43 and 23 for the ethanol-treated cells at 24 and 48 hours and 42 and 37 for the untreated cells at 24 and 48 hours, respectively. For the 3D experiments, N = 15, 11 for Paclitaxel-treated cells at 24 (PTX_24) and 48 (PTX_48) hours of treatment, respectively, and 16 and 15 for untreated cells at 24 (UNT_24) and 48 (UNT_48) hours of treatment, respectively. *, **, *** indicate p < 0.025, 0.005, and 0.0005, respectively. Statistical analysis was carried out using a three-way ANOVA. 39
Figure 3.11: Shape modes obtained for WHCO1 cells in 2D and 3D environments. (a) Registered objects are showing actual boundaries of cells selected randomly from individual shape modes. (b) Shape mode dendrogram demonstrating the morphology of the different shape modes (1 through 10) detected and their similarity..... 41
Figure 3.12: Cellular heterogeneity for treated and untreated WHCO1 cells in 2D environments, (a) cells treated with Paclitaxel for 24 hours (N = 27), (b) cells treated with Paclitaxel for 48 hours (N = 22), (c) cells treated with ethanol for 24 hours (N = 43), (d) ethanol-treated cells at 48 hours of treatment (N = 23), (e) and (f) untreated cells at 24 (N = 42) and 48 (N = 37) hours of incubation, respectively obtained using VAMPIRE analysis. The numbers above the bars are representative of the abundance of cells in each shape mode. The shape modes are shown in Figure 3.11 (b)..... 43
Figure 3.13: Cellular heterogeneity for treated and untreated cells in 3D environments, (a) cells treated with Paclitaxel for 24 hours (N = 15), (b) cells treated with Paclitaxel for 48 hours (N = 11), (c) untreated cells incubated for 24 hours (N = 16), and (d) untreated cells incubated for 48 hours (N = 15) obtained using VAMPIRE analysis. The numbers above the bars are representative of the abundance of cells in each shape mode. The shape modes are shown in Figure 3.11(b). 44

List of Tables

Table S. 1: Summaries of mean MSDs (μm^2) and standard deviations of mitochondrial fluctuations from 79 individual WHCO1 cells in 2D environments at 24 and 48 hours of treatment. PTX and UNT stand for Paclitaxel-treated and untreated cells, respectively. MSDs at τ = 0.7 s were transformed using a logarithmic function, whereas τ = 6.3, 7.7 and 9.1 s were transformed using a square root function, respectively, after failing the normality test. 66

Table S. 2: Summaries of mean fluidity and standard deviations of mitochondrial fluctuations from 79 individual WHCO1 cells in 2D environments at 24 and 48 hours of treatment. PTX and UNT stand for Paclitaxel-treated and untreated cells, respectively. Fluidity values at τ = 6.3 and 9.1 s were transformed using a logarithmic and square root function, respectively, after failing the normality test. 66

Table S. 3: Two-way ANOVA results summarising the significance of the interaction between drug treatment intervention (untreated and Paclitaxel-treated cells) and duration of treatment (24 and 48 hours) in MSDs and fluidity at the different delay times for the cells in 2D. 67

Table S. 4: Pairwise comparisons of MSDs of Paclitaxel-treated (PTX or P) and untreated (UNT or U) in 2D environments at 24 and 48 hours of treatment. For example, PTX (24 Vs 48) compares MSDs for Paclitaxel-treated cells at 24 and 48 hours. 67

Table S. 5: Pairwise comparisons of fluidity for Paclitaxel-treated (PTX or P), ethanol-treated (ETH or E) and untreated (UNT, or U) in 2D environments at 24 and 48 hours of treatment. 68

Table S. 6: Summarises of mean MSDs (μm^2) and standard deviations of mitochondrial fluctuations from 63 individual WHCO1 cells embedded in 3D environments at 24 and 48 hours of treatment. PTX and UNT stand for Paclitaxel-treated and untreated cells, respectively. 69

Table S. 7: Summaries of mean fluidity and standard deviations of mitochondrial fluctuations from 63 individual WHCO1 cells embedded in 3D environments at 24 and 48 hours of treatment. PTX and UNT stand for Paclitaxel-treated and untreated cells, respectively. Fluidity at τ = 1.5 s was transformed using a square root function after failing the normality test. 70

Table S. 8: Two-way ANOVA results summarising the significance of the interaction between drug treatment intervention (untreated and Paclitaxel-treated cells) and duration of treatment (24 and 48 hours) in MSDs and fluidity at the different delay times for the cells in 3D. 71

Table S. 9: Pairwise comparisons of MSDs of Paclitaxel-treated (PTX) and untreated (UNT) in 3D environments at 24 and 48 hours of treatment. For example, PTX (24 Vs 48) compares MSDs for Paclitaxel-treated cells at 24 and 48 hours. 72

Table S. 10: Pairwise comparisons of fluidity for Paclitaxel-treated (PTX) and untreated (UNT) in 3D environments at 24 and 48 hours of treatment. 73

Table S. 11: Summaries of mean MSDs and fluidity and standard deviations of mitochondrial fluctuations from single WHCO1 cells in 2D and 3D environments at 24 and 48 hours of treatment. PTX and UNT stand for Paclitaxel-treated and untreated cells, respectively. The MSDs and fluidity are compared at τ = 2.1 s. MSDs were transformed using the square root function after failing the normality test. 74
Table S. 12: Pairwise comparisons of MSDs and fluidity for Paclitaxel-treated (PTX) and untreated (UNT) in 2D and 3D environments at 24 and 48 hours of treatment. 74
Table S. 13: Summaries of mean and standard deviations for the area, perimeter, circularity, and aspect ratio from WHCO1 cells in 2D and 3D environments at 24 and 48 hours of treatment. PTX and UNT stand for Paclitaxel-treated and untreated cells, respectively. 75
Table S. 14: Pairwise comparisons for mean area, perimeter, circularity, and aspect ratio for Paclitaxel-treated (PTX) and untreated (UNT) in 2D and 3D environments at 24 and 48 hours of treatment..... 76
Table S. 15: VAMPIRE analysis results showing the abundance of cells in each of the conditions in each shape mode. P_24, P_48, E_24, E_48, U_24, and U_48 represent the number of Paclitaxel-treated cells at 24 and 48 hours, ethanol-treated cells at 24 and 48 hours, and untreated cells at 24 and 48 hours, respectively. 78

List of Abbreviations

2D	Two-dimensional
3D	Three-dimensional
AC	Adenocarcinoma
AFM	Atomic force microscopy
AJCC	American Joint Committee on Cancer
ALL	Acute lymphoblastic leukaemia
AML	Acute myeloid leukaemia
ANOVA	Analysis of variance
CCD	Charge-coupled device
CO_2	Carbon dioxide
CT	Computed tomography
cTNM	Clinical tumour, node, and metastases
DMEM	Dulbecco's Modified Eagle Medium
DNA	Deoxyribonucleic acid
ECM	Extracellular matrix
EDTA	Ethylenediaminetetraacetic Acid
FBS	Foetal bovine serum
G-actin	Globular actin
HEPES	Hydroxyethyl piperazineethanesulfonic acid
IC50	Half maximal inhibitory concentration
MATLAB	Matrix Laboratory
MPTM	Mitochondrial Particle-Tracking Microrheology
MSD	Mean-square displacement
MTC	Magnetic twisting cytometry
MTOC	Microtubule-organizing centre
NA	Numerical aperture
OAC	Oesophageal adenocarcinoma
OSCC	Oesophageal squamous cell carcinoma
PBS	Phosphate-buffered saline
PET	Positron emission tomography
PH	Potential of Hydrogen
PTM	Particle Tracking Microrheology
pTNM	Pathologic tumour, node, and metastases

SCC	Squamous cell carcinoma
SPSS	Statistical Package for Social Sciences
TNM	Tumour, node, and metastases
USA	United States of America
VAMPIRE	Visually Aided Morpho-Phenotyping Image Recognition
WHCO	Wits Human Carcinoma of the Oesophagus
ypTNM	Post-neoadjuvant pathologic tumour, node, and metastases

Chapter 1 Introduction and Background

1.1 Overview of dissertation

This master's degree dissertation focuses on investigating the effect of chemotherapeutic drug exposure on the mechanical properties of human oesophageal cancer cells in two- (2D) and three-dimensional (3D) environments. The study is based on the hypothesis that cell stiffness and morphology changes are associated with chemotherapeutic drug exposure and the development of chemoresistance in cancer patients. If determined, cell stiffness and morphology changes could serve as biomechanical markers for the early detection, rapid diagnosis, and evaluation of the efficacy of chemotherapy in cancer patients in South Africa and the world in general. Oesophageal squamous cell carcinoma (OSCC) cell line, WHCO1, established from biopsies of South African oesophageal cancer patients, were used in this study. To achieve the aim of the study, we evaluated the effect of chemotherapeutic drug treatment on the mechanical properties of non-resistant human OSCC in 2D and 3D environments using mitochondrial-particle-tracking microrheology (MPTM).

Chapter one entails the background information related to cancer and cell mechanobiology. It includes a brief introduction to cancer, its global prevalence and distribution, the epidemiology and pathogenesis of oesophageal cancer, the cancer type studied in this project. The chapter further discusses the stages of oesophageal cancer development and its diagnostic and treatment methods. It also briefly introduces cell mechanics and mechanobiology and reviews the experimental tools and techniques used to study the mechanical properties of cells.

The second chapter describes the research methods and materials used in our study, including 2D and 3D cell culturing techniques, mitochondrial particle-tracking microrheology, morphology analysis using Visually Aided Morpho-Phenotyping Image Recognition (VAMPIRE) software and statistical analysis using SPSS (Statistical Package for Social Sciences) for windows. Chapter three describes the results obtained from our experimental and computational studies demonstrating the effect of chemotherapeutic treatment on the cell stiffness and morphology of human OSCC cells embedded in 2D and 3D environments. Chapter four discusses the results of our study, whereas conclusions and recommendations are stated in chapter five.

1.2 Introduction to cancer

Cancer is defined as a persistent, dysregulated cellular growth that results from alterations in various gene expressions. The alterations in gene expressions result from prolonged exposure of cells to cancer-promoting environmental and lifestyle factors, including smoking, diet, radiation, infections, and pollution. However, they can also develop due to internal factors, for instance, genetic anomalies,

hormonal imbalances, and immune responses. Alterations in gene expression can lead to an imbalance in cell replication and death, aiding abnormal or dysregulated cell growth. The abnormal cells can locally invade tissues, spread to lymph nodes, and metastasize to distant body organs, leading to death if not detected and treated earlier. According to Anand *et al.* (2008), genetic anomalies are responsible for approximately 5-10% of all cancer incidents, whereas about 90-95% of the rest of the cancers are attributed to environmental and lifestyle factors.

The most common cancers, called carcinomas, develop from epithelial tissue. The epithelium comprises cells that line the walls of cavities, channels and tubes in the body and the skin, which serves as the external covering of the entire body. The carcinomas are responsible for more than 80% of cancer-related mortalities (Weinberg 2007). These include cancers originating from the gastrointestinal tract, that is, the mouth, oesophagus, stomach, and small and large intestines, in addition to those arising from the skin, mammary glands, pancreas, lung, liver, ovary, uterus, prostate, gall bladder, and urinary bladder. Furthermore, carcinomas are categorized into squamous cell carcinomas (SCC) and adenocarcinomas (AC). SCC originates from epithelial cells that line cavities or channels in the body to protect the underlying cell population. In contrast, AC arises from epithelial cells that specialize in secreting substances such as mucous layer into the ducts or cavities they line.

The non-epithelial cancers include sarcomas, lymphomas, and neuroectodermal malignancies. Sarcomas are derived from the connective tissues in the body; lymphomas constitute cancers from blood-forming tissue and cells of the immune system. In contrast, neuroectodermal malignancies originate from cells that form various central and peripheral nervous system components. Other cancers that do not fit into the four major classifications include melanomas, small-cell lung carcinomas, and teratomas. Malignancies often manifest as solid masses detectable via physical inspection or diverse imaging techniques due to their distinct physical properties.

1.3 Cancer prevalence and distribution

Despite efforts to alleviate the cancer burden, its incidence and mortality are increasing rapidly worldwide. World Health Organization (2020) report revealed that approximately eighteen million cancer incidents and ten million deaths occurred worldwide in 2018. Furthermore, it also predicted that the global burden of cancer would increase to about twenty-nine to thirty-seven million new cases by 2040, with the most significant increase in developing countries.

Figure 1.1 below illustrates the global allocation of cancer incidences and mortality in 2018. Of the 18 million new cancer incidences and 9.6 million deaths reported in 2018 worldwide by Bray *et al.* (2018), 5.8% (1,055,000) new cases and 7.3% (700,000) deaths occurred in Africa. According to the World Health Organization (2020), lower-income countries and people with the lowest financial status within

these countries reported the worst cancer outcomes. Scaling-up cancer control is, therefore, crucial in improving cancer outcomes and lives globally.

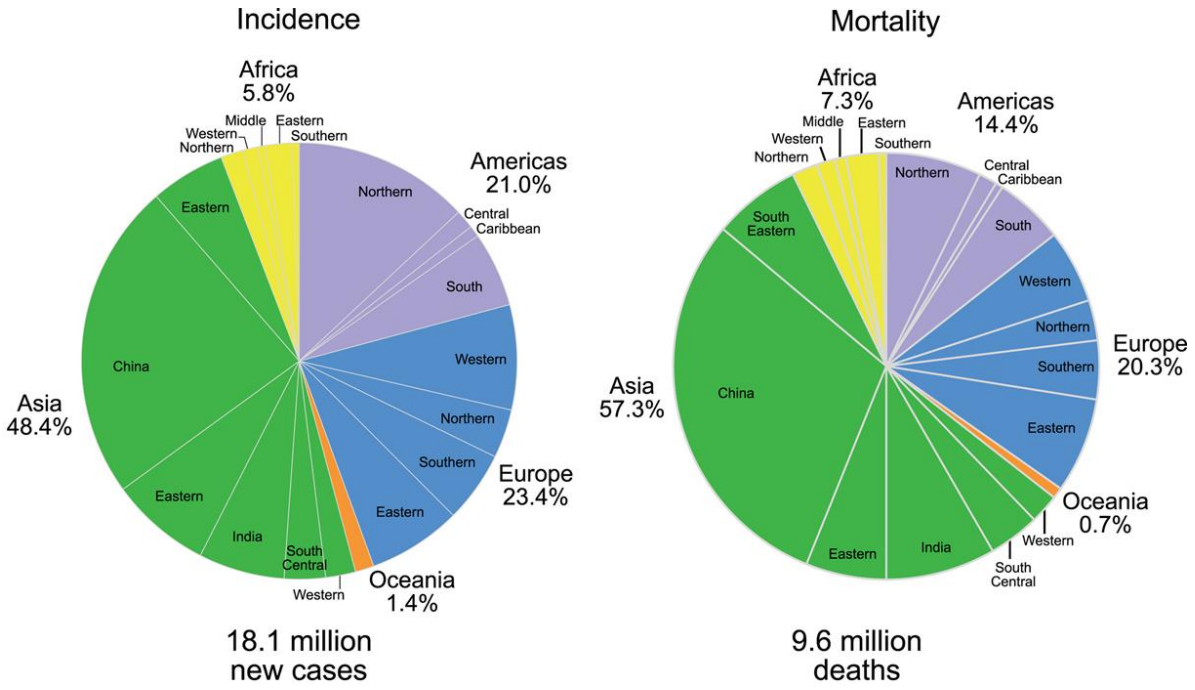

Figure 1.1: Allocation of cancer incidences and mortality in the world continents in 2018. Reused with permission from Bray et al. (2018).

1.4 Epidemiology and the pathogenesis of oesophageal cancer

Oesophageal cancer affects the oesophagus, which is the tube connecting the mouth to the stomach (Figure 1.2) and is listed among the ten most prevalent cancers worldwide (Figure 1.3). In 2018, it ranked as the seventh most pervasive and the sixth deadliest cancer with about 579,000 (3.2% of 18.1 million) cancer incidences and 508,800 (5.3% of 9.6 million) deaths reported globally (Bray *et al.* 2018) (Figure 1.3).

Approximately 70% of the oesophageal cancer cases occur in men, and it is most prevalent in Eastern and Southern African countries (Bray *et al.* 2018). Oesophageal cancer is typically asymptomatic initially, and most patients present at a late stage when their chances of survival are dismal. As a result, it has poor treatment outcomes, with a five-year survival rate reported at about 15% to 25% (Pennathur *et al.* 2013). Best outcomes occur when the disease is diagnosed in its early stages.

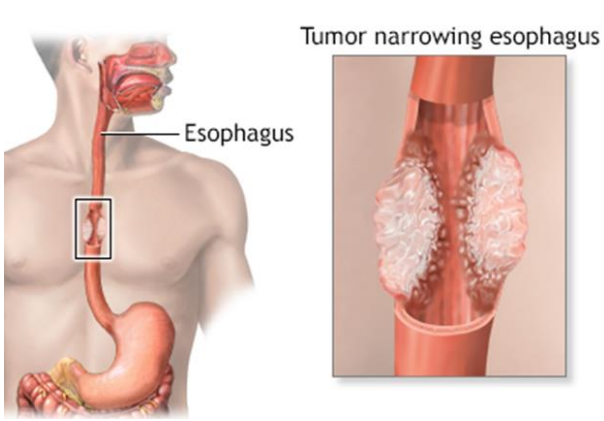

Figure 1.2: An illustration of oesophageal cancer (http://umr.adam.com).

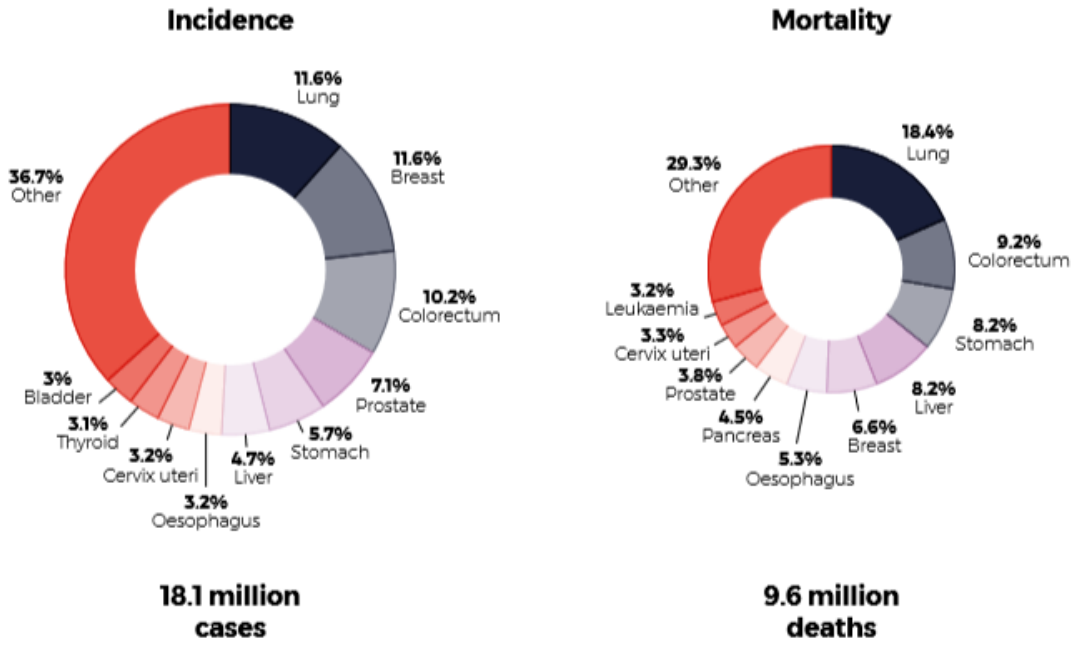

Figure 1.3: cancer incidences and mortalities by the ten most prevalent cancers in 2018 as reported by the World Health Organization (2020).

Furthermore, oesophageal cancer is categorized into oesophageal squamous cell carcinoma (OSCC) and oesophageal adenocarcinoma (OAC), the most prevalent histological subgroups. Oesophageal squamous cell carcinoma originates from squamous epithelial cells lining the upper two-thirds of the oesophagus, whereas OAC occurs in the lower third of the oesophagus and generally develops from Barrett mucosa (Barrett mucosa occurs as a result of acid reflux from the stomach leading to thickening of the flat cells lining the oesophagus) (Arnold *et al.* 2017). The known risk factors of oesophageal cancer include heavy consumption of alcohol, tobacco smoking, injuries to the oesophagus, thoracic radiation, poor diet, excess body weight and chronic gastro-oesophageal reflux disease (Jemal *et al.* 2011, Pennathur *et al.* 2013, Tan *et al.* 2016, Thun *et al.* 2017). Notably, OSCC is

the most prevalent subtype in South-East and Central Asia and Southern and Eastern Africa and is responsible for approximately 90% of all the oesophageal cancer cases. In contrast, OAC is most prevalent in high-income countries (Arnold *et al.* 2017, Arnold *et al.* 2015, Tan *et al.* 2016).

Oesophageal cancer and cancer in general are, therefore, a growing burden in low-and middle-income countries and the world, and there is a need for interventions to improve its treatment and diagnostic methods.

1.5 Clinical presentation of oesophageal cancer

Most oesophageal cancer patients are diagnosed at a later stage of disease development. This late diagnosis is because of the elasticity of the oesophagus, making it difficult to detect any abnormal growths unless continued screening and surveillance are performed. At diagnosis, most of the patients present with progressive dysphagia, which is caused by substantial penetration of the cancerous cells into the lumen of the oesophagus, pain triggered by the invasion of cancer cells into the neighbouring structures and involuntary weight loss (Bird-Lieberman and Fitzgerald 2009, Lagergren *et al.* 2017, Schlansky *et al.* 2006). Other symptoms include an abnormal change in the voice due to the tumour growing on the left laryngeal nerve, relentless coughing associated with a fistula between the oesophagus and the respiratory tract, and noticeable metastases in the lymph nodes. All these symptoms occur late into the development of oesophageal cancer (Lagergren and Lagergren 2010).

1.6 Diagnosis and staging of oesophageal cancer

Endoscopy followed by the histopathological assessment of biopsies is the standard method used to diagnose oesophageal cancer (Figure 1.4) (Alexandersson 2018, Bloomfeld *et al.* 2005, Lagergren *et al.* 2017). Endoscopy helps locate and determine the presence of the tumour, its size and the existence, and the severity of Barrett's oesophagus. After confirmation of the presence of oesophageal cancer, computed tomography, endoscopic ultrasound, and positron emission tomography using fluorodeoxyglucose and combined with computed tomography (PET/CT) can be performed to detect regional and distant metastases for staging purposes (Chadwick *et al.* 2016, Findlay *et al.* 2015).

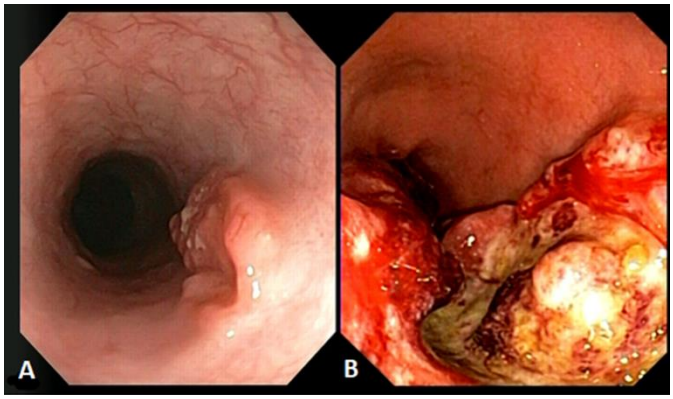

Figure 1.4: Oesophageal cancer wound as viewed on an endoscope. A: OSCC. B: Large fatal and bleeding OAC. Reused from Lagergren and Lagergren (2010) with permission from BMJ Publishing Group Ltd.

Oesophageal cancer is staged using the tumour, node, and metastases (TNM) staging method developed by the American Joint Committee on Cancer (AJCC) and the different stages are categorized into clinical, pathological, and post-neoadjuvant groups (D'journo 2018, Rice and Blackstone 2020, Rice *et al.* 2017). T in the TNM acronym is divided into Tis, T1, T2, T3 and T4. Tis symbolizes high-grade dysplasia; T1, a tumour that has invaded the lamina propria, muscularis mucosae, or submucosa; T2, a tumour that has penetrated the muscularis propria; T3, a tumour that has extended to the adventitia; and T4 representing a tumour that has spread into neighbouring tissues. Additionally, N is subdivided into N0, signifying no metastases in the lymph nodes; N1, a tumour that has metastasized to one or two lymph nodes; N2, a tumour that has metastasized to a range of three to six lymph nodes; and N3 representing a tumour that has spread to seven or more lymph nodes. Furthermore, M is also subdivided into M0, indicating no metastases to the distant tissues and organs and M1 signifying the presence of distant metastases (Figure 1.5).

The stages classified under the pathologic stage group (pTNM) for OAC are Stage 0, which represents high-grade glandular dysplasia, Tis; Stage IA (T1aN0M0G1), Stage IB (T1aN0M0G2 and T1bN0M0G1-2), and Stage IC (T1N0M0G3 and T2N0M0G1-2). Others are Stage IIA (T2N0M0G3), Stage IIB (T3N0M0 and T1N1M0), Stage IIIA (T2N1M0 and T1N2M0), Stage IIIB (T2N2M0, T3N1-2M0, and T4aN0-1M0), Stage IVA (T4aN2M0, T4bN0-2M0, and PTanyN3M0), and Stage IVB for cancers having metastases to distant organs (M1). The pathological stage groups for OSCC include Stage 0, indicating high-grade glandular dysplasia, Tis, Stage IA (T1aN0M0G1), Stage IB (T1aN0M0G2-3, T1bN0M0, and T2N0M0G1), Stage IIA (T2N0M0G2-3, T3N0M0, and T3N0M0G1), Stage IIB (T3N0M0G2-3 and T1N1M0). The rest of the OSCC stages (Stage III and Stage IV) are identical to those of OAC. G1, G2, and G3 in the tumour groupings indicate a well-differentiated, moderately differentiated, and poorly differentiated tumour, respectively. The pTNM categories are determined microscopically after surgical or endoscopic resection before any treatment is performed.

Stages categorized under the clinical-stage group (cTNM) for OAC are Stage 0, which consists of Tis, Stage I (T1N0M0), Stage IIA (T1N1M0), Stage IIB (T2N0M0), Stage III (T2N1M0 and T3-4aN0M0), Stage IVA (T4bN0-1M0 and N2-N3M0), and Stage IVB, which consists of all M1 cancers. Furthermore, the cTNM stage groups for OSCC consist of Stage 0 (Tis); Stage I (T1N0-1M0); Stage II (T2N0-1M0 and T3N0M0); Stage III (T3N1M0 and T1-3N2M0), Stage IVA (T4N0-2M0 and N3M0), and Stage IVB consisting of M1 cancers. For cTNM, the TNM groups are generally determined by imaging rather than microscopic analysis of the oesophageal resection before any treatment.

The stages under post-neoadjuvant pathological stage groups (ypTNM) of oesophageal cancer include Stage I (T0-2N0M0), Stage II (T3N0M0), Stage IIIA (T0-2N1M1), Stage IIIB (T1-3N2M0, T3N1M0, and T4aN0M0), Stage IVA (T4aN1-2M0, T4bN0-2M0, and TanyN3M0), and Stage IVB, which consists of M1 cancers. All the stages are identical for both OSCC and OAC. The ypTNM stages are determined after treatment.

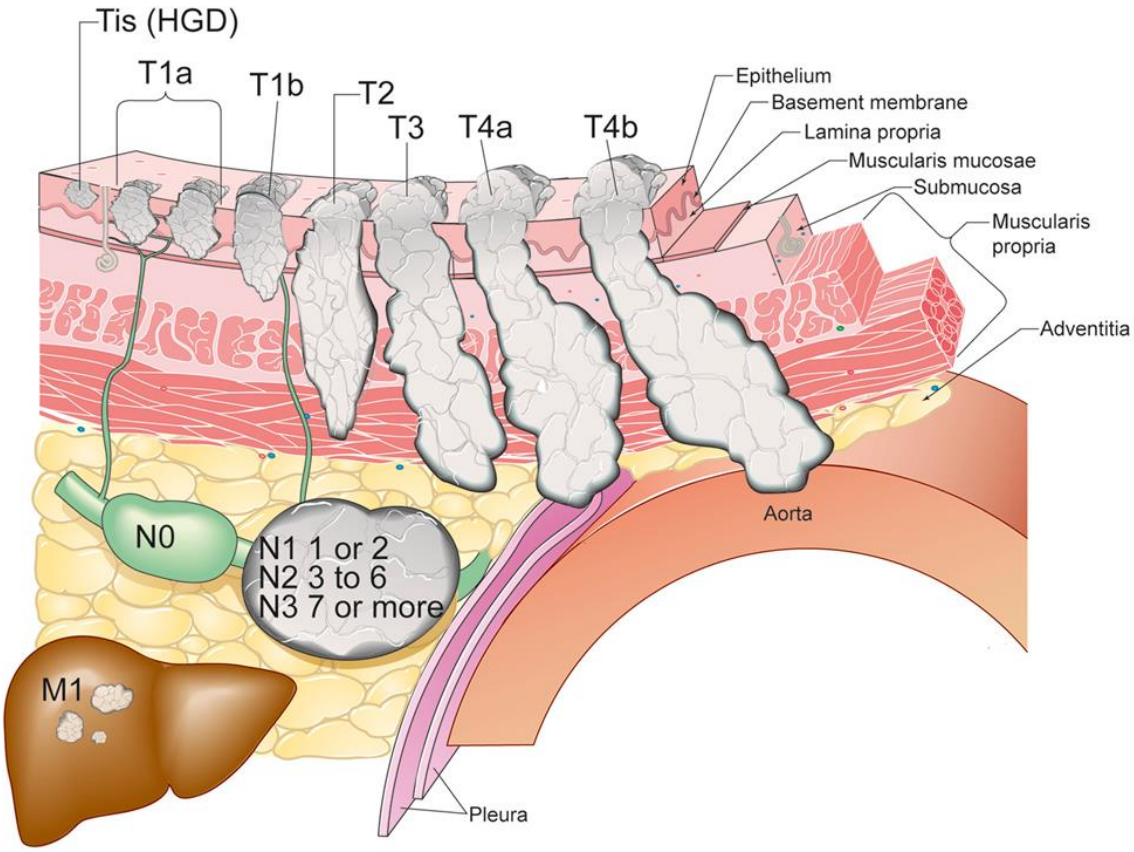

Figure 1.5: Stages of oesophageal cancer using the tumor, node and metastases (TNM) staging classification. Tis (HGD) symbolizes high-grade dysplasia; T1a, a tumor that has invaded the lamina propria; T1b, a tumor that has penetrated muscularis mucosae or submucosa; T2, a tumour that has penetrated muscularis propria; T3, a tumour that has invaded the adventitia; T4a, a tumour that has extended to the pleura and T4b, shows a tumor that has spread into the aorta and neighbouring tissues. M1 symbolizes the presence of distant metastases whereas N0 stands for no metastases in the lymph nodes; N1, a tumour that has metastasized to one or two lymph nodes; N2, metastases in three

to six lymph nodes and N3 signifies a tumor that has spread to seven or more lymph nodes. Reused with permission from Rice et al. (2017).

1.7 Treatment of oesophageal cancer

The choice of method for oesophageal cancer treatment is dependent on the cancer stage of cancer, tumour location, comorbidities, and the age of the patient. For patients without metastases, endoscopic or surgical therapy is the best choice for in situ and stage IA oesophageal cancer in patients fit for surgery. Surgical treatment with or without perioperative chemoradiotherapy is also recommended for other oesophageal cancer stages without metastases for patients appropriate for surgery. For patients with locally advanced oesophageal cancer or metastases in the lymph nodes, chemotherapy or chemoradiotherapy followed by surgery is recommended for those fit for surgery.

1.7.1 Surgery

Oesophagectomy or oesophageal resection is the surgical procedure used in the treatment of oesophageal cancer. It involves removing part of the upper and lower oesophageal tract or the entire oesophagus and reconstructing it using a colon or bowel portion. It is divided into transthoracic and trans-hiatal oesophagectomy. In transthoracic oesophagectomy, an incision through the abdomen, followed by a thoracic incision or even a neck incision, is performed to complete the oesophageal resection (Mckeown 1976). In contrast, in trans-hiatal oesophagectomy, an abdominal and cervical incision are the only ones necessary to complete the resection (Gurusamy *et al.* 2016, Orringer and Sloan 1978, Yamamoto *et al.* 2013). Other minimally invasive surgical options include laparoscopy and thoracoscopy (Dapri *et al.* 2008, Luketich *et al.* 2000, Senkowski *et al.* 2006, Yamamoto *et al.* 2013). Furthermore, for in situ or stage IA oesophageal carcinoma, endoscopic mucosal or submucosal resection can also be carried out to excise the whole cancer tissue and avoid complete removal of the oesophagus (Isomoto *et al.* 2013, Kim HH *et al.* 2012, Ning *et al.* 2017).

1.7.2 Chemotherapy and radiotherapy

The purpose of chemotherapy in treating oesophageal cancer is to induce the death of cancer cells that have metastasized to other body parts and shrink the primary tumour so that surgery can easily be performed. Radiotherapy kills cancer cells and can also slow down their growth by damaging their deoxyribonucleic acid (DNA). The chemotherapeutic drugs that have been used in oesophageal cancer treatment include carboplatin, Paclitaxel, cisplatin, fluorouracil, and oxaliplatin. Several clinical trials have tested the effectiveness of a combination of some of the chemotherapeutic drugs with or without radiotherapy followed by surgery to treat oesophageal cancer. These trials have revealed that chemoradiotherapy followed by surgery is associated with higher rates of oesophageal cancer tumour

response (Klevebro *et al.* 2016, Shapiro *et al.* 2015, Von Dobeln *et al.* 2019, Working 2002, Ychou *et al.* 2011).

However, the clinical effectiveness of chemoradiation therapy and patient outcomes are associated with treatment failures, mainly due to radiation and chemoresistance (Kim JJ and Tannock 2005, Nyhan *et al.* 2016, O'sullivan G *et al.* 1999). This resistance can be attributed to the repopulation of tumour cells that have survived radiation and chemotherapy during the treatment cycle. Radiation and chemoresistance are the leading causes of oesophageal cancer recurrence in patients. The reported one-, three-, and five-year survival rates of oesophageal cancer patients after tumour recurrence are 45.9%, 10.6%, and 6.4%, respectively (Su *et al.* 2014, Zhen *et al.* 2018). Therefore, there is a need to monitor the effectiveness of chemoradiotherapy for early detection of chemoresistance and oesophageal cancer recurrence in cancer patients.

1.8 Cell mechanics and mechanobiology

Cell mechanics and mechanobiology is a multi-disciplinary field that integrates cell biology, biomechanics, and biophysical principles to understand the physiology and pathophysiology of proteins, cells, tissues, and organs. The problems of interest in this field range from intracellular interactions of proteins and organelles that control gene transcription or drive cell migration to the biophysical interactions between cells and the extracellular environment. Cells in their environments within the human body undergo various external and internal events crucial for maintaining their function, such as cell-cell and cell-extracellular environment communication, cell division and growth, proliferation, migration, and apoptosis (Bao and Suresh 2003, Chen CS *et al.* 2004).

Cells typically respond to these intracellular and extracellular events by altering their physical properties such as cell shape and cytoskeletal concentration and organization or activation of the intracellular or extracellular signalling processes (Bausch and Kroy 2006, Geiger and Bershadsky 2002, Kasza *et al.* 2007, Orr *et al.* 2006, Rodriguez *et al.* 2013). These cellular responses can lead to cells becoming stiff or soft, an influx of calcium into cells, changes in cellular morphologies, an increase in focal adhesions, and disease states like cancer (Rodriguez *et al.* 2013, Unal *et al.* 2014). In summary, cell mechanics and mechanobiology focus on studying and understanding the biomechanical processes within the cell and cell interactions with its extracellular environment and their associated biological and functional outcomes.

1.8.1 Structure and function of a cell

A cell is the smallest structural, functional, and biological unit of all living organisms. It is composed of the cell membrane, cytoskeleton, cytoplasm, nucleus, and organelles, as seen in Figure 1.6. The cell membrane is a thin layer that physically separates the cell's interior from the extracellular

environment. It contains protein receptors, which carry out functions such as transporting specific molecules through to the cell's interior or exterior, communicating with neighbouring cells and the extracellular environment (ECM) and binding the cell to its environment. Additionally, the cell membrane's strength contributes to the cell's mechanical support, whereas its flexibility enables cells to divide, grow, and locomote. The cytoskeleton constitutes a network of proteins, including actin filaments, microtubules, and intermediate filaments. It is responsible for determining and maintaining cell shape and stiffness, taking part in cell division and motility, and the movement of organelles and other substances within the cells and between cell populations and the ECM. The cytoskeleton is further discussed in detail in section 1.8.2.

The cytoplasm consists of a jelly-like fluid (cytosol) within which several organelles and particles making up the cell are suspended, as seen in Figure 1.6. It provides mechanical support to the cells by exerting pressure against the cell's membrane, thus maintaining its shape. Additionally, the cytoplasm is a site for cell processes such as cell division, protein synthesis and metabolism and transports organelles around the cell interior. Furthermore, organelles' crowdedness within the cytoplasm can increase the cell's intracellular stiffness and reduce the diffusion rate of molecules and other substances within the cell (Zimmerman and Minton 1993). The nucleus, the most prominent organelle within the cell, contains DNA that carries all genetic information. It regulates and promotes the expression of genes and DNA replication during the cell division cycle. The nucleus also governs the cell's structure by transcribing DNA that encodes structural proteins such as actin and keratin.

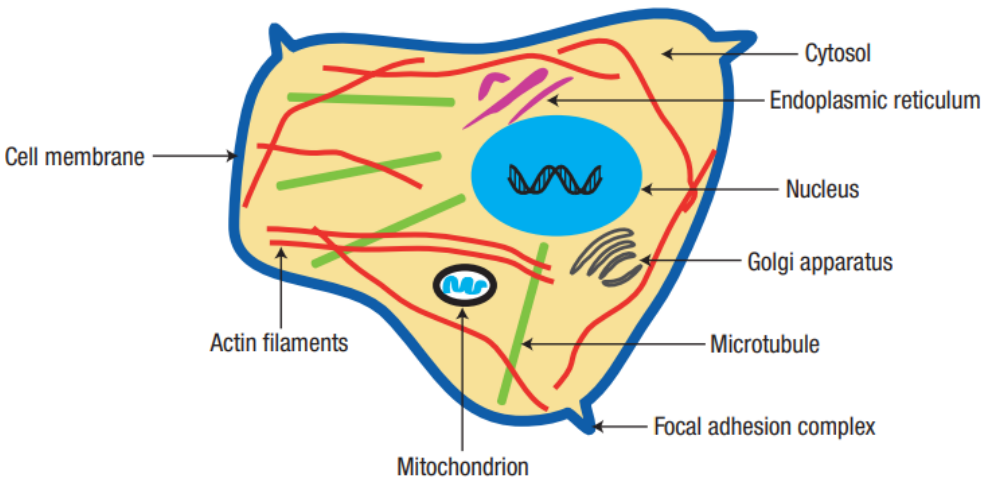

Figure 1.6: An illustration of the structure of a eukaryotic showing its major components. Reused with permission from Bao and Suresh (2003).

1.8.2 The cytoskeleton and its role in cell mechanics

The physical and mechanical properties of cells, such as stiffness and morphology, are governed by the cytoskeletal components (actin filaments, microtubules, and intermediate filaments) and associated proteins (Fletcher and Mullins 2010, Moeendarbary and Harris 2014, Suresh 2007). Additionally, the cytoskeletal components and associated protein are crucial in cellular functions such as cell division, cell cycle regulation, mechanotransduction, cell motility, and apoptosis. Furthermore, the concentration and molecular composition of cytoskeletal filaments are essential in determining the global deformability of cells; response to biomechanical signals from the interior of the cell or the extracellular microenvironment and determining cell-cell or cell-extracellular matrix interactions (Pritchard *et al.* 2014, Suresh 2007).

Any alterations to the cytoskeletal dynamics and organization during the above-mentioned cellular processes can lead to changes in the physical properties of cells, such as stiffness and morphology; and the development of diseases such as cancer (Kumar and Weaver 2009, Malandrino *et al.* 2018, Pachenari *et al.* 2014, Park 2016, Unal *et al.* 2014). Therefore, quantifying the alterations in the cytoskeletal dynamics and cell mechanics (such as morphology and stiffness) can serve as markers for detecting the onset of diseases, diagnosing disease states, monitoring disease progression, and testing drugs.

1.8.2.1 Microtubules

Microtubules are hollow, long cylindrical structures with an outer diameter of approximately 25 nm. Microtubules generally emanate from a single microtubule-organizing centre (MTOC) adjacent to the nucleus (Baker E. L. 2010, De Forges *et al.* 2012). Microtubules comprise monomers of α-tubulin and β-tubulin in a helical arrangement organized into small hollow cylinders. Microtubules are stiffer than all other cytoskeletal components and have a persistence length of approximately 5 mm (Fletcher and Mullins 2010, Mofrad 2009). They are more dynamic than the rest of the cytoskeleton components and continuously undergo polymerization and depolymerization (Mitchison and Kirschner 1984, Mofrad 2009). Furthermore, microtubules organize themselves into mitotic spindles that separate chromosomes into two identical sets during cell division (Fletcher and Mullins 2010, Jordan and Wilson 2004, Sharp *et al.* 2000).

1.8.2.2 Actin filaments

Actin filaments are double-helical polymers made up of globular actin monomers (G-actin) with an elasticity ranging from 1 to 2 GPa and a diameter of approximately 7 nm (Baker E. L. 2010, Mofrad 2009, Rodriguez *et al.* 2013). They are considered the most abundant structural components of all cells and constitute about 10 % of all proteins in non-muscle cells (Cooper and Hausman 2004, Mofrad

2009, Suresh 2007) and approximately 20% of all proteins in muscle cells (Suresh 2007). Actin filaments undergo polymerization and depolymerization regulated by factors such as ion concentrations. They, therefore, can rapidly assemble and disassemble, forming filopodia protrusions and lamellipodia extensions that are essential in cell migration (Cooper and Hausman 2004, Fletcher and Mullins 2010, Goley and Welch 2006, Suresh 2007). Furthermore, actin filaments can organize themselves into bundles (stress fibers) or a mesh with the help of actin-binding proteins. Actin fibers mostly form when the cell needs additional strength in response to increased mechanical forces; thus, the actin fibers adhere to the focal adhesion spots at a higher density (Suresh 2007).

1.8.2.3 Intermediate filaments

Intermediate filaments are made up of tetramer sub-units called protofilaments, assembled into large rope-like structures with a diameter of about 8-10 nm and a persistence length of about 1 µm (Mofrad 2009, Mucke *et al.* 2004, Rodriguez *et al.* 2013). Intermediate filaments are the softest cytoskeletal components and are resistant to tensional forces much more than compressional forces (Fletcher and Mullins 2010). Intermediate filaments are more stable in terms of polymerization and depolymerization than actin filaments and microtubules, and they are crucial in maintaining the mechanical strength of cells and tissues (Herrmann *et al.* 2007). Intermediate filaments are divided into two types: one forms a meshwork surface beneath the nucleus's inner membrane, and the other spreads throughout the cell cytoplasm (Herrmann *et al.* 2007).

1.8.3 The extracellular environment and cell mechanics

The microenvironment of cells includes neighbouring cells, signalling molecules, and blood vessels, all held together by the ECM, its main constituent. The ECM consists of glycosaminoglycans, proteoglycans, glycoproteins, polysaccharides, and various proteins such as collagen, elastin, and laminin. The ECM has a distinctive chemical, physical and mechanical properties and provides structural support to the cells within tissues (Kim SH *et al.* 2011, Lu *et al.* 2012). Additionally, cell-ECM interactions are crucial in maintaining healthy tissue and controlling cellular activities, including proliferation, migration, adhesion, and survival (Hynes 2009, Malta *et al.* 2016, Stern *et al.* 2009, Ulrich *et al.* 2009).

Cancer onset and progression lead to stiffening of the tumour microenvironment due to an increase in ECM deposition and cross-linking. The tumour microenvironment, as a result, becomes stiffer than the microenvironment of healthy cells. This difference in stiffness is used in the early detection of cancer in soft tissues such as the breast by palpation, detecting increased hardness of the cancer tissues compared to healthy tissue (Huang and Ingber 2005, Mahoney and Csima 1982).

Typically, cells interact with the ECM in a feedback loop to maintain healthy tissues. For example, cells constantly secrete, break down or rearrange the ECM components to change the ECM properties, such as stiffness. In turn, any alterations in the ECM can bring about variations in cellular activities and behaviour. This feedback mechanism enables cells and tissues to maintain normal homeostasis and function (Butcher *et al.* 2009, Lu *et al.* 2012, Samuel *et al.* 2011). Any interruptions to this regulatory feedback mechanism can lead to the development and progression of diseases like cancer. For example, during the early stages of cancer development, cancer cells secrete lysyl oxidase, a protein that enhances ECM cross-linking, leading to alterations in the ECM mechanical properties (such as stiffness) (Decitre *et al.* 1998). Therefore, both cancer and healthy cells contribute to the remodelling and stiffening of the extracellular matrix.

Cells can sense changes in the ECM's stiffness and respond by undergoing various molecular and cellular scale changes, such as regulating cell morphology, focal adhesions, proliferation, the tension in the cytoskeleton, and stiffness through mechanotransduction (Mcbeath *et al.* 2004, Rajagopalan *et al.* 2004). Specifically, previous studies have reported that an increase in substrate stiffness increases the basal area, the number of focal adhesions, and the proliferation of healthy cells (Folkman and Moscona 1978, Quinlan *et al.* 2011, Sun *et al.* 2018). Additionally, these studies have reported that the stiffness of healthy cells increases with an increase in the environmental stiffness to the point of matching their mechanical properties. However, some other studies have also reported that cancer cells tend to be insensitive to variations in the ECM stiffness, thus enhancing their ability to survive *in vivo* (Lin HH *et al.* 2015, Rianna and Radmacher 2017, Tilghman *et al.* 2010).

Two- (2D) and three-dimensional (3D) *in vitro* culture systems have been established to mimic the *in vivo* extracellular matrix and its interaction with cells. Most of the in-vitro studies in cancer research have been conducted in 2D culture systems such as plastic Petri dishes due to their simplicity and affordability. However, these do not accurately mimic the mechanical properties and the topographical structures of the *in vivo* ECM due to their higher stiffness and flatness. 3D culture systems are more physiologically relevant as they mimic the ECM more accurately than the 2D culture systems. These include natural hydrogels such as collagen and synthetic hydrogels such as polyacrylamide and polyethylene glycol. These mechanical properties of matrices can easily be tuned and modulated to mimic those of the *in vivo* ECM, and they can facilitate protein absorptions and support focal adhesions. 2D and 3D matrices have been applied in several studies to investigate the effect of the mechanical properties of the ECM on the intracellular stiffness of cancer cells (Baker E. L. *et al.* 2009, Kim JE *et al.* 2018, Mak *et al.* 2014), cancer cell migration and invasion (Baker E. L. *et al.* 2011, Zaman *et al.* 2006), and anticancer drug testing (Charoen *et al.* 2014, Reynolds *et al.* 2017).

1.8.4 Cell mechanics and mechanobiology case studies

1.8.4.1 Cancer cells are softer than their healthy counterparts

Previous studies have demonstrated that cancerous cells are softer than their healthy counterparts and that the stiffness further diminishes with cancer progression. For example, studies comparing the stiffness of malignant and non-malignant breast cells found that malignant breast cells are significantly softer than their non-malignant counterparts (Li *et al.* 2008, Mandal *et al.* 2016, Nematbakhsh *et al.* 2017, Network *et al.* 2013). Similar results were obtained for thyroid (Prabhune *et al.* 2012, Rianna and Radmacher 2017), oral (Remmerbach *et al.* 2009), oesophageal (Fuhrmann *et al.* 2011), prostate (Faria *et al.* 2008, Lekka *et al.* 2012, Pogoda *et al.* 2021), and ovarian cancer (Babahosseini *et al.* 2014, Xu WW *et al.* 2012). Furthermore, atomic force microscopy (AFM) studies showed that malignant cells are more deformable than healthy cells originating from different organs (Cross *et al.* 2007, Grady *et al.* 2016). In contrast to most studies, a few studies have shown that malignant cells are stiffer than healthy cells. Such results have been found in cervical squamous carcinoma (Ding *et al.* 2015) and human lymphoid and myeloid cells (Rosenbluth *et al.* 2006).

1.8.4.2 Role of actin and microtubules in cell mechanics

Grady *et al.* (2016) subjected various cells to cytochalasin D (actin polymerization inhibitor) and nocodazole (microtubules polymerization inhibitor) to determine the role of actin filaments and microtubules in cell elasticity. Using AFM, this study revealed that actin filaments contribute more than the microtubules to the stiffness of healthy cells. Significant decreases in the elastic moduli of non-cancerous cells were found when treated with cytochalasin D than the control cells from the same origin. In contrast, no significant differences were detected in the nocodazole treated cells. The study also revealed that the disruption of microtubules affects cancer cell stiffness since the cancer cells treated with nocodazole exhibited increased stiffness compared to cytochalasin D treated cells and the healthy cells.

Other AFM studies also demonstrated that cytochalasin D treated cells exhibited a reduction in the stiffness of treated cells compared to the untreated cells (Pogoda *et al.* 2012, Ramos *et al.* 2014, Wakatsuki *et al.* 2001). Similar results were obtained with other drugs such as latrunculin A (Adamo *et al.* 2012, Kubitschke *et al.* 2017, Mihai *et al.* 2012) and latrunculin B (Louise *et al.* 2014, Wakatsuki *et al.* 2001) that disrupt the actin cytoskeleton. These studies show that the arrangement and density of actin filaments contribute to the stiffness of cells. Furthermore, previous studies also showed that treating cells with microtubule-stabilizing drugs such as Paclitaxel (Bober and Shah 2015, Kubitschke *et al.* 2017) and colchicine (Weber *et al.* 2019) significantly increases their stiffness.

1.8.4.3 *Chemotherapy alters cancer cell mechanics*

Previous research has shown that treatment of cancerous cells with chemotherapeutic drugs increases their stiffness. For example, using AFM, Lam *et al.* (2007) studied the effect of dexamethasone and daunorubicin chemotherapeutic drugs on the stiffness of acute lymphoblastic leukaemia (ALL) and acute myeloid leukaemia (AML), respectively. The stiffness of ALL and AML cells increased as they underwent cell death compared to the untreated leukaemia cells from the same patient. This increase in stiffness was attributed to the reorganization of the actin cytoskeleton due to polymerization and depolymerization during apoptosis. It was confirmed by treating cancer cells with cytochalasin D (inhibiting the actin cytoskeleton dynamics) together with the daunorubicin, which significantly suppressed cell stiffening as cells underwent death. Furthermore, Lam et al. also showed that the increase in leukaemia cancer cell stiffness following chemotherapy and cell death could substantially lead to vascular complications due to microcirculation obstruction.

Raudenska *et al.* (2019) treated prostate cancer cells with docetaxel and cisplatin, assessed the stiffness of cells that survived treatment using AFM, and determined the motility and invasion capacity of the treated cells using colony-forming assay, wound healing assay, coherence-controlled holographic microscopy, and real-time cell analysis. It was found that the cells that survived docetaxel and cisplatin treatment exhibited a higher stiffness and decreased motility and invasion capacity than the untreated cells. Furthermore, Sharma *et al.* (2014) characterized the stiffness of cisplatin-resistant and cisplatin-sensitive ovarian cancer cells using AFM and found that cisplatin-resistant cells exhibited a higher stiffness than the cisplatin-sensitive cells.

1.8.5 Experimental tools and methods to study cell mechanics

Several tools and methods have been established to study the mechanical properties of cells *in vitro* and determine their association with disease states such as cancer. These tools and techniques are commonly grouped into active or passive methods. Active methods apply controlled external forces such as magnetic or optical forces to manipulate the probes within a medium whose mechanical properties are being analyzed. These active methods include atomic force microscopy (AFM) (Deng *et al.* 2010, Radmacher *et al.* 1992), magnetic twisting cytometry (MTC) (Puig-De-Morales *et al.* 2001), optical tweezers or laser traps (Moffitt *et al.* 2008, Zhang and Liu 2008), magnetic tweezers (Gosse and Croquette 2002), micropipette aspiration (Hochmuth 2000, Thoumine and Ott 1997, Trickey *et al.* 2000).

In contrast to the active methods, in the passive techniques, the fluctuations of particles embedded within the cell due to thermal energy exerted by the cellular environments are detected and analyzed (Liu W and Wu 2018, Selvaggi *et al.* 2010). The passive methods include particle tracking

microrheology (PTM) (Mak *et al.* 2014, Selvaggi *et al.* 2010, Weihs *et al.* 2006, Wirtz 2009) and diffusion wave spectroscopy (Pine *et al.* 1990).

Some of the most common limitations of active methods include the possibility of damaging cells due to exerting excessive external forces on the cell surface and the inability to accurately distinguish the origin of responses from subcellular structures such as cell membrane, nucleus, and cytoplasm without making assumptions (Selvaggi *et al.* 2010, Wirtz 2009). Passive methods, such as PTM, can be used to overcome the above limitations. Particle Tracking Microrheology measures cells' intracellular mechanical properties without subjecting them to external forces. Furthermore, PTM makes it possible to characterize the mechanical properties of cells in more physiological environments such as a 3D ECM or *in vivo* much better than the active methods (Wirtz 2009). Particle tracking microrheology was selected for this current study due to its suitability in characterizing cells' intracellular mechanical properties, and it is discussed further in section 1.8.5.1.

1.8.5.1 Particle-Tracking Microrheology

Particle tracking microrheology is the most used passive method to investigate the intracellular mechanical properties of cells by tracking and analyzing the Brownian movements of tracer/probe particles embedded within the cell's cytoplasm (Mak *et al.* 2014, Selvaggi *et al.* 2010, Tseng *et al.* 2002, Wirtz 2009), see Figure 1.7 for the illustration of PTM. Nanometre or micrometre-sized tracer particles used in PTM are either synthetic or endogenous such as lipid granules and organelles or fluorescently labelled molecules (Weihs *et al.* 2006). Synthetic tracer particles are introduced into the cell cytoplasm through particle delivery systems such as ballistic particle injection, and the cells may get damaged in the process (Selvaggi *et al.* 2010). Consequently, endogenous organelles such as the mitochondria have recently been the most used tracer particles in PTM since they can easily be fluorescently labelled using dyes such as MitoTracker red/green (Mak *et al.* 2014). They also do not require specialized particle delivery systems to be embedded in the cell cytoplasm, thus being non-invasive and much safer. The use of mitochondria as tracer particles has been previously validated against endogenous particles by (Mak *et al.* 2014).

During PTM, a random force due to thermal energy is exerted on each tracer particle embedded in the cells' cytoplasm (Selvaggi *et al.* 2010, Tseng *et al.* 2002). This force dynamically deforms the medium surrounding the tracer particle to facilitate its displacement within the cytoplasm. Time-lapse images or videos of the Brownian movement of tracers are taken using a fluorescent microscope such as a confocal microscope equipped with a charge-coupled device (CCD) camera. These videos are analyzed using particle-tracking algorithms to construct particle trajectories that describe tracer particles' movement within the cytoplasm.

Time-dependent mean-squared displacements (MSD) are then computed from the particle trajectories using Eq. (1.1) and used to describe the particle motion dynamics and the intracellular viscoelastic properties (Baker E. L. *et al.* 2009, Selvaggi *et al.* 2010, Tseng *et al.* 2002).

$$\langle \Delta r^2(\tau)_{xy} \rangle = \langle [x(t+\tau) - x(t)]^2 + [y(t+\tau) - y(t)]^2 \rangle \quad (1.1)$$

where $\langle \Delta r^2(\tau)_{xy} \rangle$ is the 2D ensemble and time average MSD of particle trajectories, t is the elapsed time, τ is the delay time between the particle positions within the time-lapse images, and $[x(t), y(t)]$ are the time-dependent coordinates for each tracer particle within the cytoplasm. When particles diffuse through a viscoelastic medium like that of living cells, $\langle \Delta r^2(\tau)_{xy} \rangle$ becomes non-linear with time and can be defined using a time-dependent power-law relationship shown in Eq. (*1.2*) (Selvaggi *et al.* 2010, Tseng *et al.* 2002, Weihs *et al.* 2006):

$$\langle \Delta r^2(\tau) \rangle \sim t^{\alpha} \quad (1.2)$$

The slope of the log-log plot of $\langle \Delta r^2(\tau)_{xy} \rangle$, α, represents the diffusivity (fluidity) and is used to characterize the tracer particles' motion within the cytoplasm. A diffusivity or fluidity of α = 0 corresponds to the solid-like motion of the particles (stiffer medium). In contrast, fluidity of α = 1 corresponds to the purely diffusive fluid-like motion of particles (softer medium) (Selvaggi *et al.* 2010).

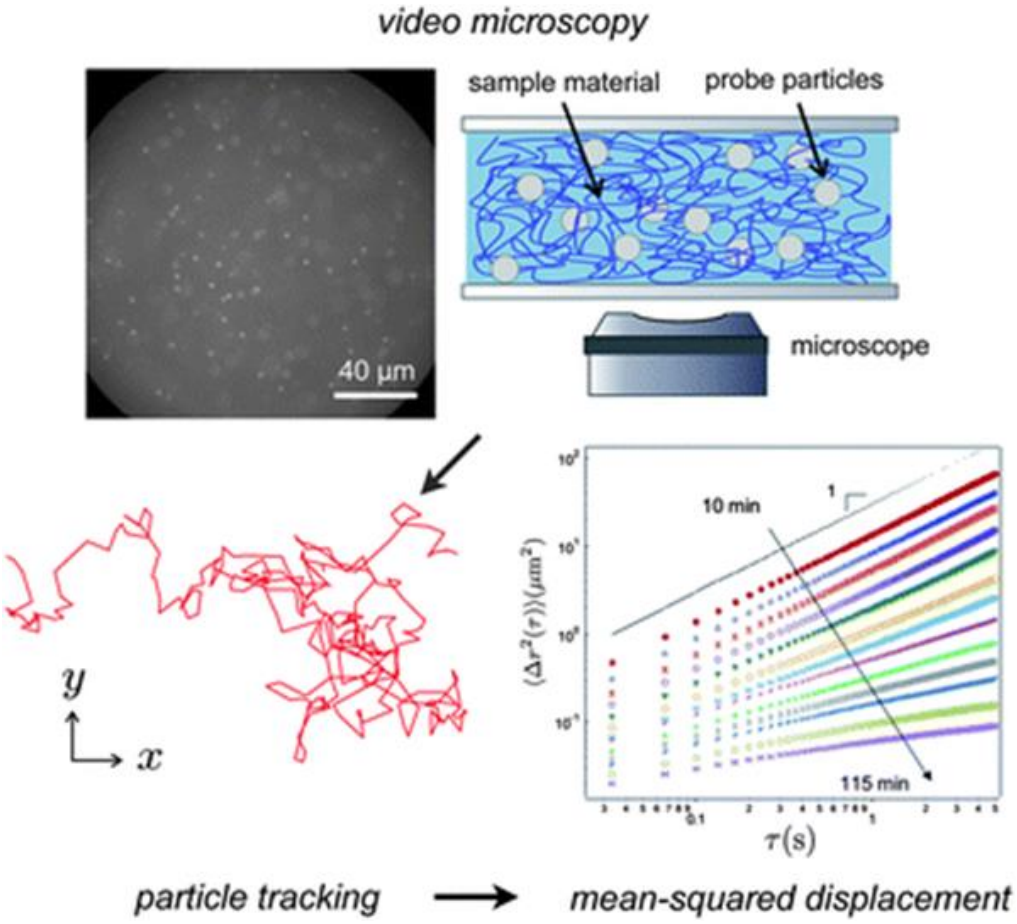

Figure 1.7: Particle-Tracking Microrheology. Video microscopy is performed to monitor and capture videos of the movement of tracer particles within the medium. Particle-tracking is performed to construct particle trajectories from the displacement of tracer particles within the medium, and finally, time lag-dependent mean-squared displacements are computed from the particle trajectories using appropriate software (Schultz and Furst 2012).

1.9 Research aims and objectives

To the author's knowledge, there are no studies on the mechanical properties of cancer cells and the effect of chemotherapeutic treatment using cancer cells from South African or African patients. There is, therefore, a need for information on how chemotherapeutic drugs affect the cells of patients who have grown up in socio-economic and dietary backgrounds in South Africa and Africa at large. Information on the mechanical signatures of cancer cells during disease progression and treatment with chemotherapeutic drugs in these patients will be crucial in complementing the genetic and molecular mechanisms in cancer diagnosis and evaluating the effectiveness of chemotherapy in African cancer patients.

Therefore, this research project aims to investigate the association between exposure to chemotherapeutic drugs and changes in the mechanical properties of human oesophageal squamous cell carcinoma of South African origin. Such cell stiffness changes may serve as biomechanical markers

for the early detection of chemoresistance and evaluation of chemotherapeutic drug efficacy in South African cancer patients.

The following objectives facilitate achieving the aim.

1. To evaluate the effect of drug treatment on the intracellular stiffness of non-resistant human oesophageal squamous cell carcinoma in two-dimensional environments. This objective was achieved by treating oesophageal squamous cell carcinoma cells (WHCO1) cultured in 2D environments with 2 µM paclitaxel for 24 and 48 hours then performing MPTM to determine the changes in the intracellular stiffness.
2. To evaluate the effect of drug treatment on the intracellular stiffness of non-resistant human oesophageal squamous cell carcinoma embedded in three-dimensional environments. WHCO1 cells were cultured in 3D environments (Type 1 Rat Tail Collagen) and then treated with 2 µM paclitaxel for 24 and 48 hours. MPTM was then used to determine the changes in the intracellular stiffness of the cells in comparison with the untreated cells.
3. To assess the effect of drug treatment on the morphology of non-resistant human oesophageal squamous cell carcinoma cells in both two and three-dimensional environments. WHCO1 cells seeded both in 2D and 3D environments were treated with 2 µM paclitaxel for 24 and 48 hours and changes in their morphology assessed using VAMPIRE algorithm.

Chapter 2 Materials and Methods

2.1 Overview

This study utilizes experimental and computational methods to characterize the mechanical properties of human oesophagal cancer cells during chemotherapy. Briefly, oesophagal squamous cell carcinoma cells, WHCO1, of South African origin, were cultured in two-dimensional (2D) and three-dimensional (3D) environments and treated with 2 µM of Paclitaxel for up to 48 hours. Ethanol was used to treat cells as vehicle control only in the 2D cultures to rule out the effect of ethanol on the cells, whereas the untreated cells were used as the controls. The intracellular stiffness of the treated and untreated cells was then assessed after 24 and 48 hours of treatment using Mitochondrial Particle-Tracking Microrheology (MPTM) previously validated (Mak *et al.* 2014). Morphology analysis of both the treated and untreated cells in 2D and 3D environments was performed using Visually Aided Morpho-Phenotyping Image Recognition (VAMPIRE) software.

2.2 Cell culture

A human oesophageal squamous cell carcinoma (OSCC) cell line, WHCO1, extracted from biopsies of primary oesophagal squamous cell carcinoma from a South African patient by Veale and Thomley in 1984 was used for the study (Paccez *et al.* 2015, Siyo *et al.* 2017, Smith *et al.* 2016). This cell line was donated by Prof. Iqbal Parker (Division of Medical Biochemistry & Structural Biology, Faculty of Health Sciences, University of Cape Town, South Africa). This cell line represents oesophageal squamous cell carcinoma prevalent in the least developed countries such as South Africa.

WHCO1 cells were cultured and maintained in DMEM, pH 7.3 (Dulbecco's Modified Eagle Medium, SIGMA, Life Science, USA), complemented with 10 % FBS (foetal bovine serum, Gibco, Life Technologies) and 1 % (v/v) streptomycin-penicillin stock (Gibco, Life Technologies). The cells were cultivated in T-25 tissue culture flasks and kept at 37°C and 5 % CO_2 in a humidified incubator. The growth media was changed every 2-3 days, and the cells were routinely sub-cultured once they reached 80-90 % confluence as assessed by viewing cells under an inverted microscope. See appendix for preparation of DMEM and growth media.

2.3 Seeding densities and viability determination

Seeding densities and cell viability for each experiment were determined by cell counting using trypan blue exclusion dye staining in a haemocytometer and a light microscope. Briefly, WHCO1 cells at 80-90 % confluence were washed with PBS (phosphate-buffered saline, Sigma-Aldrich, Life Science, USA) (see appendix for preparation of PBS) and then brought into suspension with 0.05 % Trypsin-EDTA (Ethylenediaminetetraacetic acid) (Biochrom GmbH, Germany). Subsequently, the cells were

centrifuged at 1,500 rpm and 20°C for 3 minutes to separate cells from the media containing Trypsin-EDTA. The cells were re-suspended in 1 ml of fresh media from which 20 µl of the cell solution was pipetted and diluted with 20 µl of 0.4 % trypan blue (Sigma-Aldrich, Life Science, USA). Trypan blue stains non-viable cells blue, whereas viable cells remain unstained and appear white under a microscope. 10 µl of the diluted cell solution was pipetted and introduced between the Neubauer chamber of the hemocytometer shown in Figure 2.1 and the glass coverslip. Subsequently, cells were viewed under a light microscope to count the number of viable and non-viable cells.

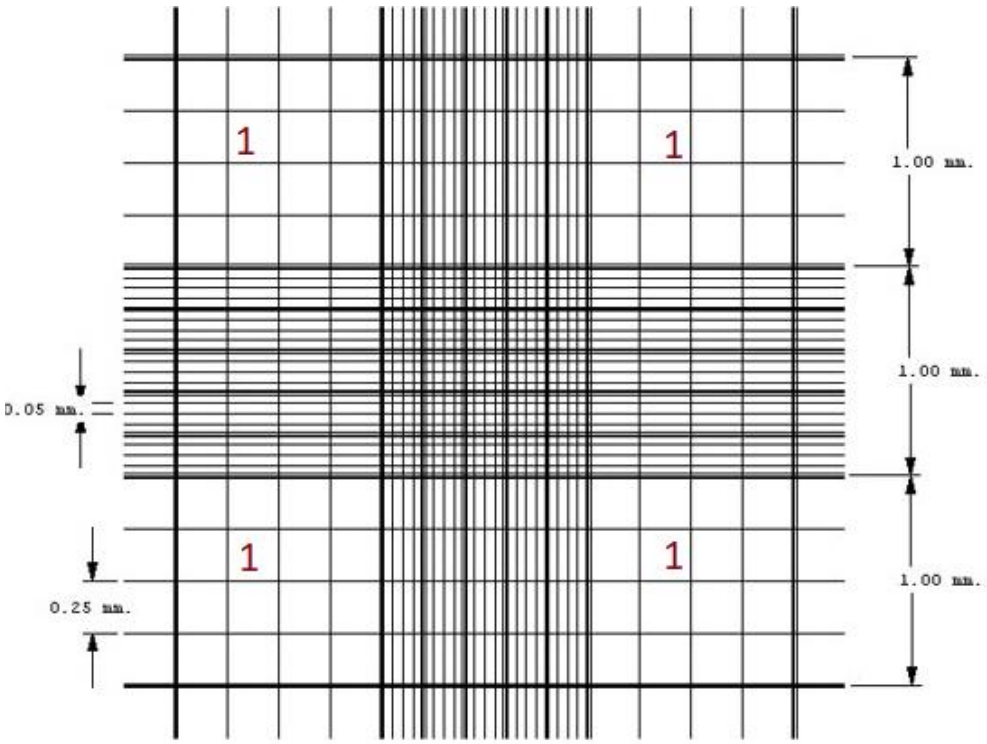

Figure 2.1: Neubauer chamber counting grid as seen under the light microscope. Cells in squares labelled one are counted to calculate the number of viable and non-viable cells (https://www.emsdiasum.com).

The concentrations of the live and dead cells and the percentage of live cells were then calculated using Eq. (2.1), (2.2), and (2.5), respectively.

$$Concentration\ of\ live\ cells\ [cells/ml]\ =\ A\ x\ C\ x\ D\ldots \quad (2.1)$$

$$Concentration\ of\ dead\ cells\ [cells/ml]\ =\ B\ x\ C\ x\ D \quad (2.2)$$

$$Total\ number\ of\ live\ cells\ =\ concentration\ of\ live\ cells\ x\ volume \quad (2.3)$$

$$Total\ number\ of\ cells\ =\ number\ of\ live\ cells\ +\ number\ of\ dead\ cells \quad (2.4)$$

$$Percentage\ viability\ =\left[\frac{number\ of\ live\ cells}{total\ number\ of\ cells}\right]\ x\ 100 \quad (2.5)$$

where:

- A is the average number of live cells counted; that is, the total number of live cells counted divided by the number of squares labelled one in Figure 2.1.
- B is the average number of dead cells counted; that is, the total number of dead cells counted divided by the number of squares labelled one in Figure 2.1.
- C is the dilution factor and,
- D the correction factor [10^4]

After determining the total number of viable cells, seeding densities for further experiments were determined using Eq. (2.6) below (the cells that were not used for experiments were frozen and stored in liquid nitrogen):

$$C_1V_1 = C_2V_2 \qquad (2.6)$$

Where:

- C_1 represents the concentration of viable cells in 1 ml,
- C_2 the number of cells required as the seeding density,
- V_1 the unknown volume of cells to be pipetted from the 1 ml of cell solution, and
- V_2 represents the 1 ml volume containing the counted viable cells.

2.4 Chemotherapeutic drug treatment

2.4.1 2D experiments

For 2D experiments, WHCO1 cells were cultured, as described in section 2.2 above. At 80-90 % confluence, the cells were sub-cultured, and 20,000 cells were seeded in each of the wells of two 35 mm 4-chambered glass-bottom dishes (Greiner Bio-One, Germany). The cells were then allowed to adhere to the surface of the dishes for 24 hours while being maintained at 37°C and 5 % CO_2. Subsequently, the growth media in one of the wells for each dish was replaced with media containing Paclitaxel (16.7 ml of Paclitaxel drug containing 49.7 % ethanol, Teva Pharmaceuticals (Pty) Ltd); ethanol in the second well and fresh growth media in the third well. One of the dishes was incubated for 24 hours and the other for 48 hours at 37°C and 5 % CO_2. A half-maximal inhibitory concentration (IC50) of 2 µM of Paclitaxel (see appendix for preparation of Paclitaxel), previously used by Dzobo *et al.* (2018) against WHCO1 cells, was used to treat the cells. Ethanol (0.014 % [v/v]; ethanol concentration in 2 µM of Paclitaxel) was used as a vehicle control to rule out the effect of ethanol on the cells, and untreated cells were used as the controls. The treated and untreated cells were then used in experiments described in sections 2.5 and 2.6.

2.4.2 3D experiments

For 3D experiments, WHCO1 cells cultured as described in section 2.2 were brought into suspension using Trypsin-EDTA centrifuged as described in section 2.3 and then embedded as single cells in Type I Rat Tail collagen solution (BD Bioscience, San Jose, CA) at a final concentration of 2 mg/ml. The collagen solution consisted of 49 µl of Type I Rat Tail collagen (stock solution of 8.21 mg/ml), 49 µl of neutralizing solution (100 mM HEPES, pH 7.4, SIGMA Life Science), and 20 µl ($1.4 \times 10^5\ cells$) of cell suspension and diluted with 82 µl of PBS (pH 7.4) to make a final concentration of 2 mg/ml (See appendix for preparation of collagen solution). Eight gels (200 µl of collagen solution) were made in total, and from these, 50 µl of collagen solution was pipetted into the wells of two 35 mm 4-chambered glass-bottom dishes (Greiner Bio-One, Germany), which were allowed to polymerize at 37°C and 5 % CO_2 in a humidified incubator for an hour. Two wells were used in each of the dishes.

The one hour of incubation and polymerization included an initial three minutes of incubation, after which the dishes were flipped over four times, with each flip lasting for 2 minutes to prevent cells from settling to the top or bottom surfaces of the gels and ensuring even distribution of the cells throughout the gel before polymerization. The collagen was then allowed to gel in the incubator for another 50 minutes. After complete gelation of collagen, 500 µl of fresh growth media was pipetted onto the gel in one of the wells of each dish (control/untreated cells), whereas the cells in the second well of each dish were treated with Paclitaxel (2 µM) in fresh growth media (final volume of 500 µl). One of the dishes was incubated for 24 hours and the other for 48 hours. The treated and untreated cells embedded in collagen gels were then used in experiments described in sections 2.5 and 2.6.

2.5 Mitochondrial Particle-Tracking Microrheology

Mitochondrial Particle-Tacking Microrheology (MPTM) works by measuring the rheological properties of cells, such as viscoelasticity, by computing the trajectories of the mitochondrial fluctuations within the cytoplasm of the cells. Mitochondria are used as the trackers since they are endogenous and abundant within the cell cytoplasm. They also have comparable mean-square displacements (MSDs) to those of exogenously injected micro-particles (Guo *et al.* 2014, Mak *et al.* 2017). This MPTM method was used to evaluate the impact of chemotherapeutic treatment on the cell stiffness of OSCC cells (WHCO1), and it is as previously described by Mak *et al.* (2014). See Figure 2.2 for an illustration of the MPTM procedure.

2.5.1 Mitochondrial staining

After the 24 and 48 hours of incubation, cells cultured in 2D and 3D environments and treated as discussed in sections 2.2 and 2.4 were incubated with MitoTracker green solution (Life Technologies, Carlsbad, CA) for 30 and 45 minutes, respectively, for cells in 2D and 3D environments to label the

mitochondria within the cell cytoplasm fluorescently. 100 nM and 400 nM of MitoTracker green solution in fresh growth media were used for 2D and 3D experiments. See appendix for preparation of the MitoTracker solution. The concentrations of MitoTracker green used for both cells in 2D and 3D were first optimized as higher concentrations were toxic for cells in a 2D environment, especially the ones treated with Paclitaxel. In contrast, lower concentrations of MitoTracker green could not properly label the mitochondria within cells embedded in 3D environments, making them difficult to trace. In both cases, the cells were incubated at 37^0C and 5 % CO_2 in a humid incubator. The cells that survived Paclitaxel treatment in both 2D and 3D environments were imaged as described in section 2.5.2.

2.5.2 Time-lapse Imaging

After labelling, time-lapse images of cells in each condition were captured using a confocal microscope (Zeiss LSM 880 Airy-scan, Germany) equipped with a charge-coupled device (CCD) camera. A 63 X 1.4 NA oil immersion objective was used. The confocal microscope was also equipped with a temperature and gas-controlled incubator. All cells were incubated at 37^oC and 5 % CO_2 in the incubation chamber of the confocal microscope throughout the imaging sessions and were allowed a minimum of five minutes to settle before any imaging was performed. These five minutes permitted the temperature and circulation of carbon dioxide within the medium of cells and incubation chamber to reach the equilibrium conditions and helped reduce drift in the cells, which might have happened due to the handling of cells. Time-lapse images were acquired for at least ten individual cells in each condition in both 2D and 3D environments. In the 3D experiments, only cells near the centre of the gel were located and imaged to prevent the border effects of gels on the cells. For each cell, 1000 frames were captured within a duration of 140 s and 150 s (approximately seven frames per second) for cells in 2D and 3D, respectively. All cells that seemed to be undergoing cellular division were excluded in the experimental analysis to concentrate on single cells. All the imaging for this study was carried out at the Confocal and Light Microscope Imaging Facility, University of Cape Town.

2.5.3 Image processing and data analysis

TrackMate, a plugin in Fiji Image J (Tinevez J-Y and Herbert 2020, Tinevez JY *et al.* 2017), was used to process the acquired time-lapse images for each cell in all conditions to construct particle trajectories, which describe the displacement of the mitochondria within the cell cytoplasm. Only the mitochondria with an estimated diameter of 1 µm were included in the trajectories. The maximum allowed linking distance between successive mitochondria was set at 0.5 µm, and the maximum frame interval accepted in the construction of trajectories was five frames. The trajectories were filtered, and only those that contained at least 75 mitochondria tracked for longer than 95 seconds were considered for further analysis. The particle trajectories were then analyzed using the MSD-Analyzer algorithm

(Tarantino *et al.* 2014, Tinevez J-Y and Herbert 2020) in MATLAB (Math Works, Inc., 2020) to compute the time-dependent mean-square displacements (MSDs) of the mitochondria within each cell. Furthermore, fluidity (diffusivity coefficient, α), which is the slope of the log-log plot of MSDs ($\Delta r^2(t)$) versus times (t) curves were calculated using Eq. (2.7) below.

$$\frac{\partial In[\Delta r^2(t)]}{\partial Int} \qquad (2.7)$$

Fluidity is used to quantitatively characterize the displacement of tracer particles in the cytoplasm of cells. See section 1.8.5.1 on how fluidity values are used to define the intracellular stiffness of cells.

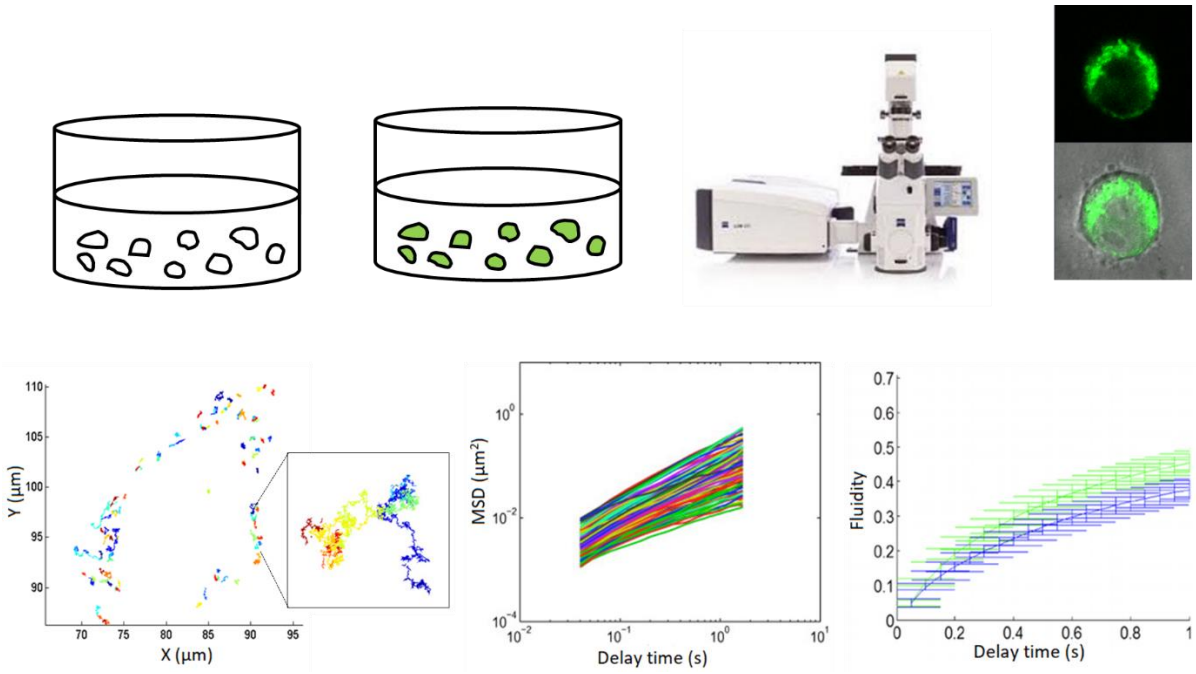

Figure 2.2: Procedure for MPTM. From left to right on the top row are an illustration of treated and untreated WHCO1 cells in 2D and 3D environments. It is followed by a representative of cells fluorescently labelled with MitoTracker green solution (green color represents the mitochondria of the cells fluorescently labelled with Mitotrackers), a confocal microscope used for time-lapse imaging of cells, and lastly, examples of images captured with a confocal microscope. The second row illustrates the procedure for post-image processing and data analysis. On the left is a representation of particle trajectories (see inset) constructed using TrackMate in Image J to trace the displacement of mitochondria within the cell cytoplasm. In the centre is a graph representing time-dependent MSDs that were computed from particle trajectories using custom algorithms in MATLAB, and at the right is the plot of fluidity calculated from the slope of time-dependent logarithmic MSDs.

2.6 Cell morphological analysis

Analysis of the morphology of cells in all conditions was carried out using the Visually Aided Morpho-Phenotyping Image Recognition (VAMPIRE) algorithm, as described by Wu *et al.* (2015). VAMPIRE assay analyses irregular cell shapes to facilitate direct visual comparison of cell morphologies. Briefly, brightfield images of the treated and untreated WHCO1 cells in 2D and 3D environments captured as described in section 2.5 were processed and then segmented using the Trainable Weka Segmentation

plugin in Fiji Image J as described by Arganda-Carreras *et al.* (2017) to identify the boundaries of the cells.

The segmented images were then imported into the VAMPIRE graphical user interface to build a cell shape analysis model. This model works by assigning a corresponding shape mode to individual cells. One thousand evenly spaced points on any contours of the cells were used to represent the potential total number of cell shape modes. Next, we determined the number of shape modes to be identified from the cell population. From our dataset, cells were categorized into ten different shape modes. The shape analysis model was then applied to analyze the shapes of WHCO1 cells across all conditions and determine the fractional abundance for cells within each shape mode. VAMPIRE analysis results based on the shape analysis model include bar graphs showing a fractional lot of cells within each shape mode and parameters such as cell area, perimeter, circularity, and aspect ratio for all cells in the different conditions. See Figure 2.3 for an overview of the VAMPIRE analysis.

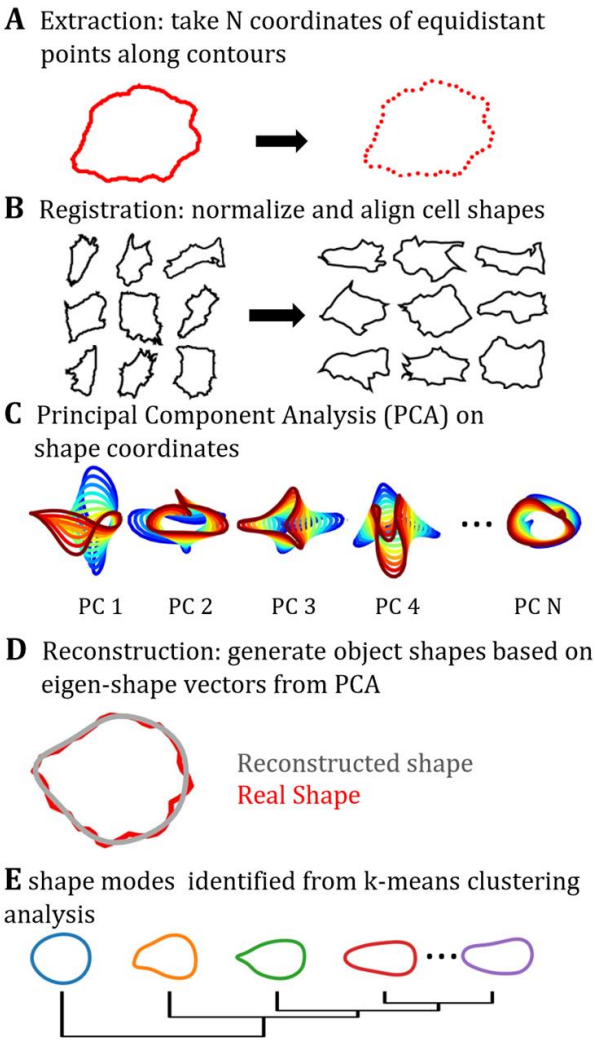

Figure 2.3: Illustration of the VAMPIRE analysis. A: a thousand equidistant points along the contour of cells were used to describe the contour of the cells. B: The unaligned identified cell shapes (left) were

then combined and aligned as shown on the right. C: principal component analysis of the coordinates on the contours of the aligned cells was performed to acquire principal components (PC 1, PC 2…, PC N). D: the cell shapes were then reconstructed from a reduced number of principal components comprising 95 % shape variations among all analyzed cells. E: K-means clustering was then applied to the group of cell data described by the principal components to obtain representative shape modes. Reused with permission from Phillip et al. (2021).

2.7 Statistical analysis

Statistical analysis was performed using a two-way ANOVA unless otherwise declared. The assumptions of a two-way ANOVA were evaluated using residual analysis as follows. Box plots were examined to determine the presence of outliers. Shapiro-Wilk's normality test was performed to assess the normality of data, and Levene's test was carried out to evaluate the homogeneity of variance. Data that failed the normality test were transformed using a logarithmic and square root function and then re-tested for the assumptions of a two-way ANOVA. Following a statistically significant interaction, pairwise comparisons were performed for every simple main effect with a 95 % confidence interval and *p*-values Bonferroni-adjusted for all the simple main effects. Statistical significance was considered at $p < 0.05$. SPSS Statistics for Windows 26.0. (IBM Corp, Armonk, NY) was used for all the statistical analyses. All experiments were performed in duplicate.

Chapter 3 Results

3.1 Intracellular stiffness of WHCO1 cells

3.1.1 Effect of Paclitaxel treatment on the intracellular stiffness of WHCO1 cells in 2D environments

Mitochondrial particle-tracking microrheology experiments were performed as described in section 2.5 to assess drug treatment's effect on the intracellular stiffness of non-resistant human oesophageal squamous cell carcinoma in 2D environments. WHCO1 cells representing OSCC of South African origin were cultured in 2D and then treated with Paclitaxel over 48 hours as described in section 2.4.1. Intracellular stiffness of treated and untreated cells was then evaluated after 24 and 48 hours of treatment. Untreated cells were used as controls, and ethanol was used as vehicle control. Statistical analysis was performed using a two-way ANOVA as described in section 2.7. Figure 3.1 shows Paclitaxel-treated, ethanol-treated, and untreated cells in 2D environments after 24 and 48 hours of treatment. The images with green MitoTracker were used for MPTM experiments.

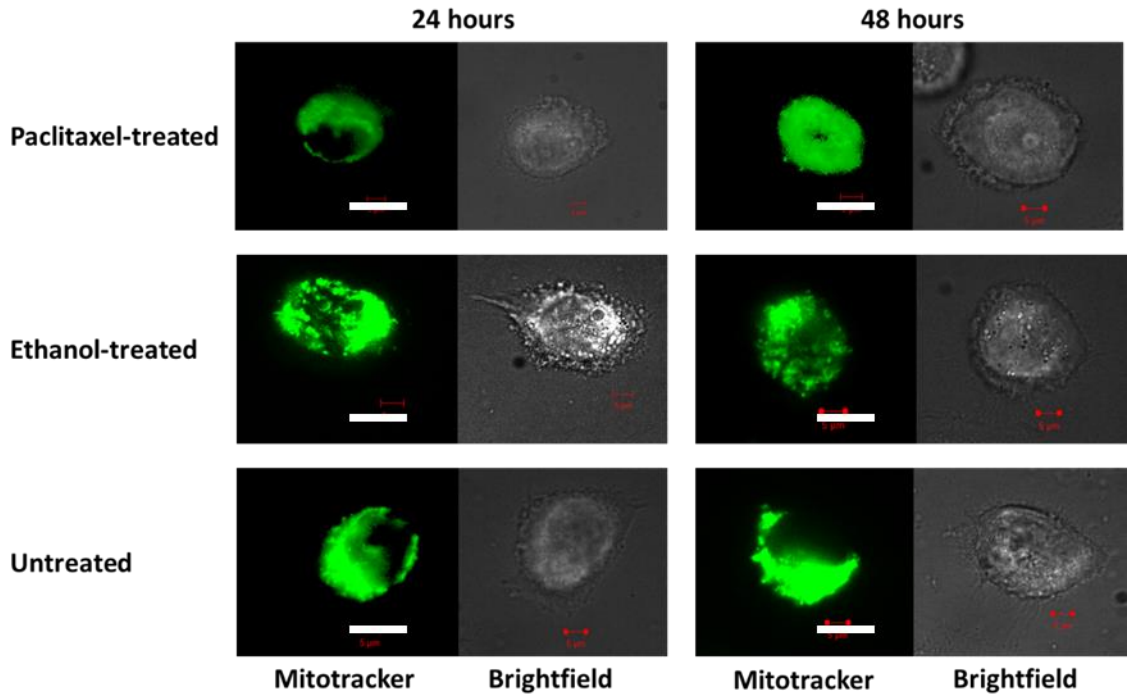

Figure 3.1: Confocal images of Paclitaxel-treated, ethanol-treated, and untreated WHCO1 cells in 2D environments after 24 and 48 hours of treatment. The images are taken from a pool of 1000 frames captured in 140 seconds using a confocal microscope. The images were captured for N = 12 and 14 Paclitaxel treated cells at 24 and 48 hours of treatment, 11 for each of the ethanol-treated cells at 24 and 48 hours, and 17 and 14 for untreated cells at 24 and 48 hours, respectively. Scale bars (white) represent 5 µm.

The fluctuations of mitochondria within the cytoplasm of cells were traced using TrackMate for a total of 79 isolated cells from one repeat experiment (n = 2), with at least 75 mitochondria captured and

tracked per cell. Time-dependent MSDs were calculated from the particle trajectories describing the movement of mitochondria within the cytoplasm. The MSDs were then converted to logarithmic MSD ensemble averages for statistical analysis (two-way ANOVA). Larger MSDs show that the mitochondria within the cells have a greater ability to travel longer distances within a given time interval across the cell cytoplasm compared to mitochondria with lower MSDs. The slope of the log-log plot of MSDs (fluidity or diffusivity coefficient, α) was used to interpret the intracellular mechanical properties of cells. Lower and flat MSDs signify stiffer or solid-like materials, whereas high and sloped MSDs demonstrate a more fluid-like or softer material.

Additionally, a fluidity value close to zero represents a stiffer or solid-like cell cytoplasm, whereas a fluidity value close to one corresponds to a softer or fluid-like cell cytoplasm (Baker E. L. *et al.* 2009, Mason *et al.* 1997, Selvaggi *et al.* 2010, Wirtz 2009). Enhanced molecular motor activities inside the cells can lead to additional stresses on top of thermal fluctuations leading to increased MSDs and fluidity values at longer time scales (Guo *et al.* 2014, Mak *et al.* 2014). Therefore, we present our results at short time scales of τ = 10 and 4 s for the MSDs and fluidity, respectively, to eliminate the effect of molecular motor activity on the cell cytoplasm's mitochondrial fluctuations.

Paclitaxel-treated cells at 24 hours exhibited significantly higher MSDs than the Paclitaxel-treated cells at 48 hours at all delay times ($p < .05$) except at τ = 0.14 s, Figure 3.2 (a). Similarly, the fluidity of Paclitaxel-treated cells at 24 hours was noticeably higher than that of the treated cells at 48 hours at all delay times, as shown in Figure 3.2 (b). Statistically significant differences in the Paclitaxel-treated cells at 24 and 48 hours were found between τ = 0.28 and 2.1 s ($p < .05$), however, no statistically significant differences were observed between τ = 3.5 and 4 s.

The MSD for ethanol-treated cells at 48 hours was found to be slightly higher, although not statistically significant, than those of the cells treated with ethanol for 24 hours at all the delay times, Figure 3.2 (c). Although not statistically significant, discernible differences were observed between the ethanol-treated cells at 24 and 48 hours of treatment at all delay times, Figure 3.2 (d).

No significant differences were found in the MSDs of untreated cells at 24 and 48 hours of incubation at all delay times, as shown by the MSD versus delay time curves in Figure 3.2 (e). Furthermore, no significant differences in fluidity were found between untreated cells at 24 and 48 hours of incubation at any delay times, as illustrated by the fluidity versus delay time curves in Figure 3.2 (f).

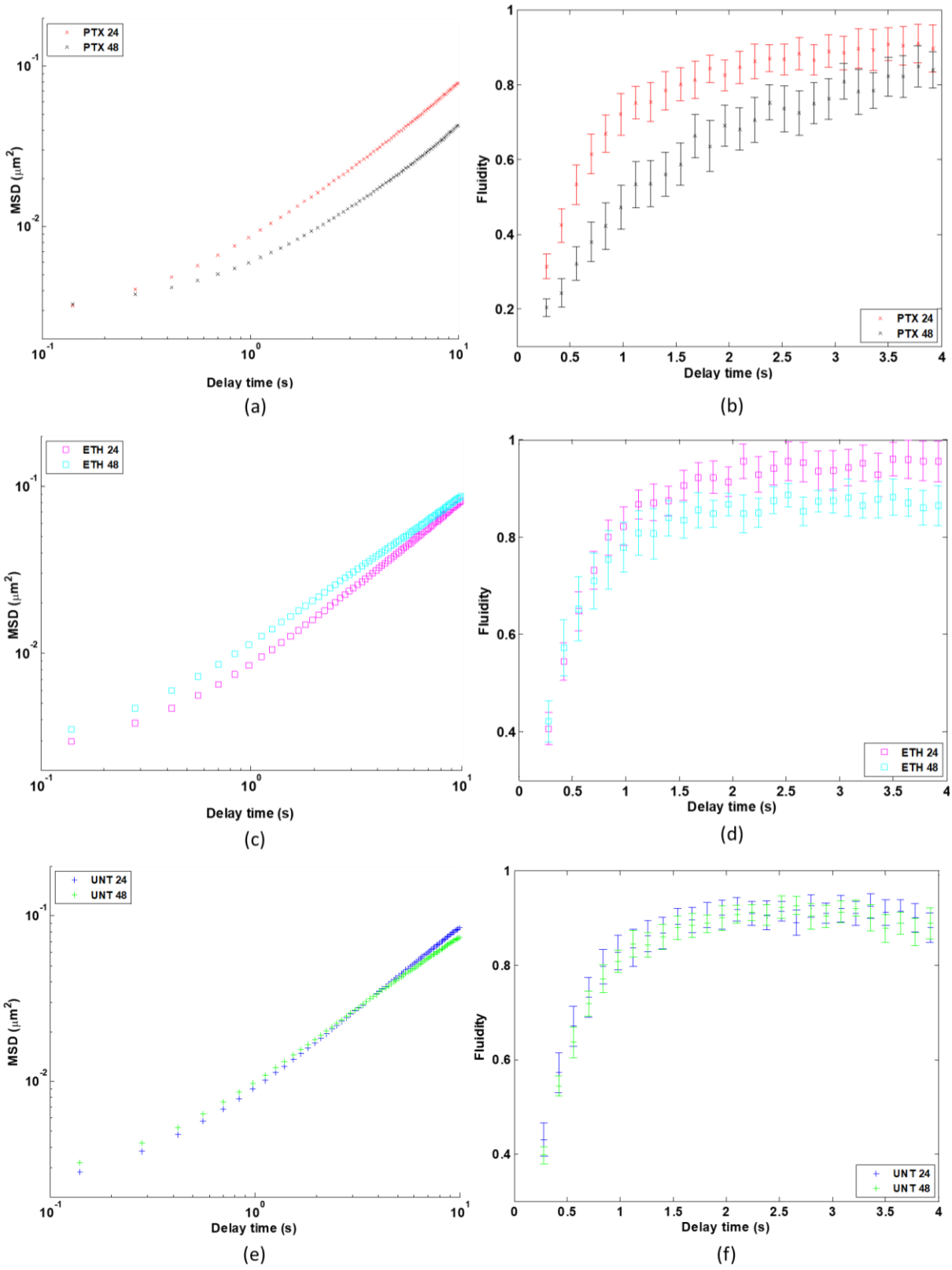

Figure 3.2: Microrheological characterization of WHCO1 cells in 2D environments. (a) MSD versus delay time curves for Paclitaxel-treated cells at 24 (PTX 24) and 48 (PTX 48) hours of incubation. (b) Fluidity versus delay time curves for Paclitaxel-treated cells at 24 and 48 hours of treatment. (c) MSD versus delay time plots for cells treated with ethanol for 24 (ETH 24) and 48 (ETH 48) hours. (d) Fluidity versus delay time curves for ethanol-treated cells at 24 and 48 hours of treatment. (e) MSD curves for the untreated at 24 (UNT 24) and 48 (UNT 48) hours of incubation. (f) Fluidity curves for untreated cells at

24 and 48 hours. Error bars are SEM for one independent repeat experiment (n = 2), N = 12 and 14 for Paclitaxel-treated cells at 24 and 48 hours of treatment, respectively, N = 11 for each of the ethanol-treated cells at 24 and 48 hours of treatment, and N =17 and 14 for untreated cells incubated for 24 hours 48 hours, respectively. Statistical analysis was carried out using a two-way ANOVA.

Additionally, no statistically significant differences in MSDs were observed between Paclitaxel-treated and the untreated cells at 24 hours of treatment at all delay times except at $\tau = 0.7$ s ($p = 0.031$). No statistically significant differences in MSDs were observed between the untreated and ethanol-treated cells and Paclitaxel-treated and ethanol-treated cells at any delay times. See Figure 3.3 (a). The fluidity of Paclitaxel-treated cells at 24 hours was relatively lower than that of both ethanol-treated and untreated cells at all delay times, as shown in Figure 3.3 (b). Statistically significant differences were only observed between Paclitaxel-treated and untreated cells at $\tau = 0.28$ s ($p = 0.026$). No statistically significant differences were observed between ethanol-treated and untreated cells and Paclitaxel-treated and ethanol-treated cells at 24 hours of treatment at all delay times.

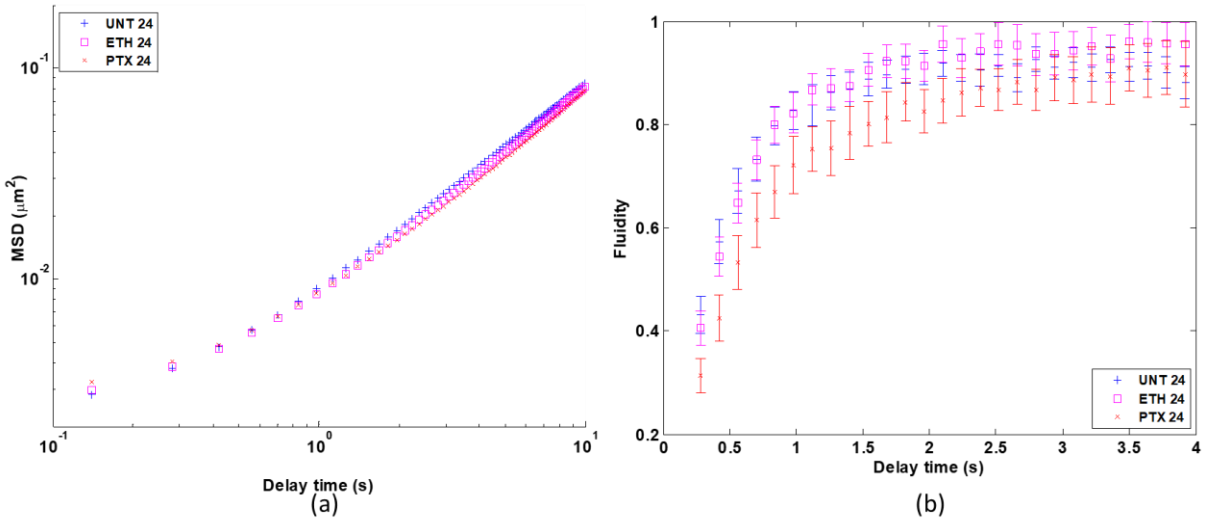

Figure 3.3: Microrheology of WHCO1 cells at 24 hours of treatment in 2D environments. (a) MSD versus delay time curves for untreated (UNT), ethanol-treated (ETH), and Paclitaxel-treated cells (PTX). (b) Fluidity versus delay time curves for untreated, ethanol-treated, and Paclitaxel-treated cells. Error bars are SEM for one independent repeat experiments (n = 2), N=17 (UNT), 11 (ETH), and 12 (PTX). N refers to the number of cells in each condition. A total of 40 cells were analyzed. Statistical analysis was carried out using a two-way ANOVA.

Furthermore, the MSDs of Paclitaxel-treated cells at 48 hours were significantly lower than that of ethanol-treated cells ($p < .05$) and untreated cells ($p < .005$) at all delay times except at $\tau = 0.14$ s, Figure 3.4 (a). No statistically significant differences in MSDs were observed between the ethanol-treated and untreated cells during the delay times. The fluidity of Paclitaxel-treated cells at 48 hours was significantly lower than that of the ethanol-treated cells ($p < .05$) and untreated cells ($p < .0005$) at all delay times except between $\tau = 3.5$ and 4 s. No statistically significant differences in fluidity were observed between ethanol-treated and untreated cells at all delay times.

See Figure 3.4 (b). See Table S. 1 and Table S. 2 for the MSDs and fluidity, respectively, and Table S. 4 and Table S. 5 for the pairwise comparisons for the treated and untreated cells in 2D environments at all delay times.

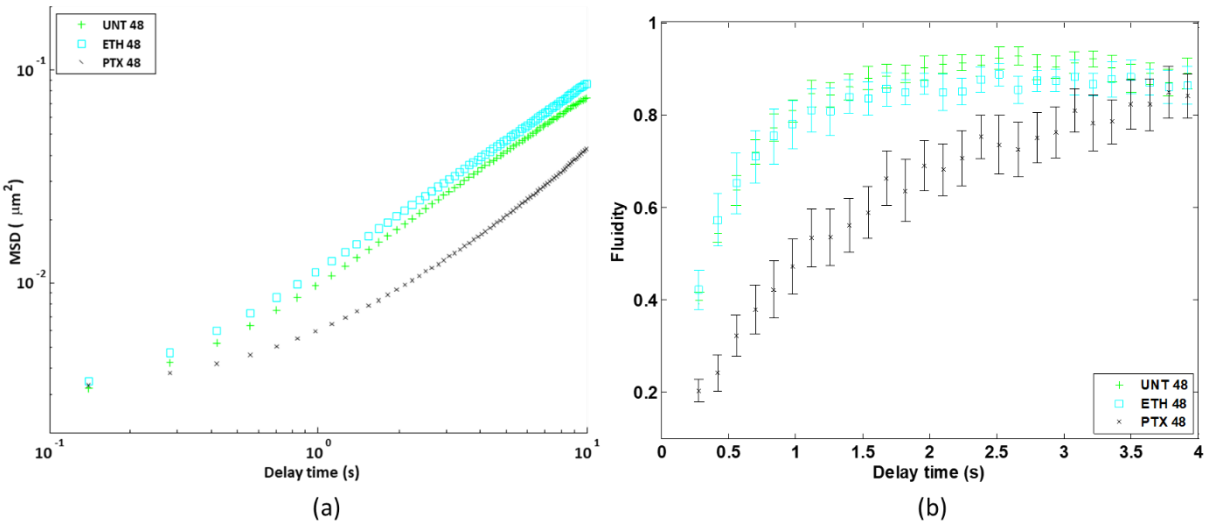

Figure 3.4: Microrheology of WHCO1 cells at 48 hours of treatment in 2D environments. (a) MSD versus delay time curves for Untreated, ethanol-treated, and Paclitaxel-treated cells. (b) Fluidity versus delay time curves for untreated, ethanol-treated, and Paclitaxel-treated cells. Error bars show SEM for one independent repeat experiment (n = 2), N=14, 11, and 14 for untreated, ethanol-treated, and Paclitaxel-treated cells, respectively. Statistical analysis was carried out using a two-way ANOVA.

3.1.2 Effect of Paclitaxel treatment on the intracellular stiffness of WHCO1 cells in 3D environments

Mitochondrial-particle-tracking microrheology experiments were conducted as described in section 2.5 to investigate the effect of drug treatment on the intracellular stiffness of non-resistant human oesophageal squamous cell carcinoma in 3D environments. WHCO1 cells were embedded as single cells in a 2 mg/ml concentration of collagen and then treated with Paclitaxel as described in section 2.4.2 for up to 48 hours. Untreated cells were used as controls. Intracellular stiffness of treated and untreated cells was then evaluated after 24 and 48 hours of treatment. Statistical analysis was performed using a two-way ANOVA as described in section 2.7. Figure 3.5 shows Paclitaxel-treated and untreated cells embedded in 3D environments after 24 and 48 hours of treatment. The images with the green MitoTrackers were used for the MPTM experiments.

The intracellular displacement of the mitochondria was tracked for a total of 63 isolated cells from one repeat experiment (n = 2), with at least 75 mitochondria captured and tracked per cell. The time-dependent MSDs were computed from the particle trajectories constructed from the mitochondria

displacements within the cell cytoplasm and converted to logarithmic MSD ensemble averages for statistical analysis. The slope of the log-log plot of MSDs (fluidity or diffusivity coefficient, α) was then used to infer the mechanical properties of cells as described in section 1.8.5.1. An increase in the molecular motor activities within the cells can lead to additional stresses on top of thermal fluctuations leading to increased MSDs and fluidity values at longer time scales (Guo *et al.* 2014, Mak *et al.* 2014). Therefore, the results are presented at shorter time scales to leave out the effect of molecular motor activity on the mitochondrial fluctuations within the cell cytoplasm.

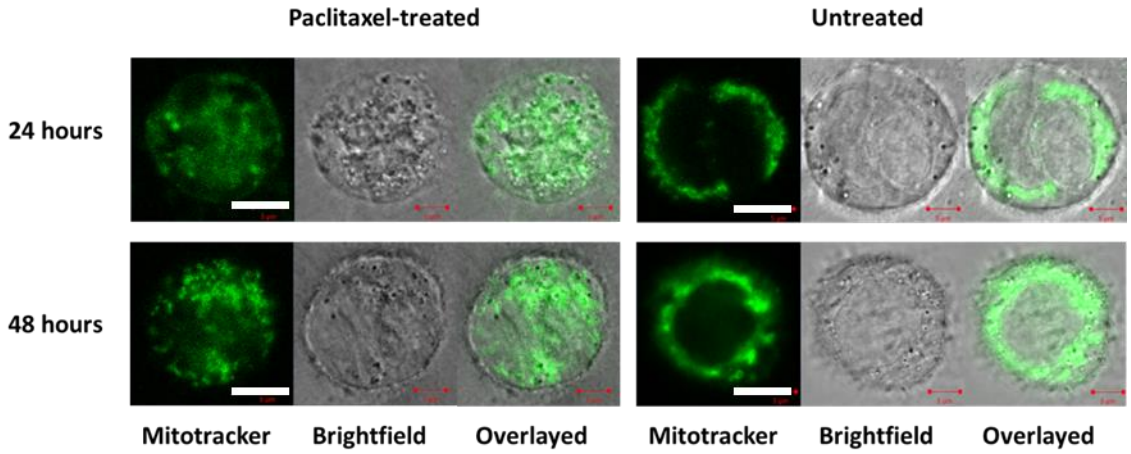

Figure 3.5: Confocal images of Paclitaxel-treated and untreated WHCO1 cells embedded in 3D environments after 24 and 48 hours. The images are taken from a pool of 1000 frames captured in 150 seconds using a confocal microscope. The images were captured for N = 21 and 10 Paclitaxel treated cells at 24 and 48 hours of treatment, respectively, and 19 and 13 for the untreated cells at 24 and 48 hours. Scale bars (white) represent 5 µm.

The MSDs of Paclitaxel-treated cells at 48 hours were significantly higher than those of the Paclitaxel-treated cells at 24 hours for all the delay times ($p < .05$) except at $\tau = 0.15$ s ($p = 0.056$). See Figure 3.6 (a). Additionally, the fluidity of Paclitaxel-treated cells at 48 hours was found to be significantly higher than that of the treated cells at 24 hours at all delay times ($p < .05$) except at $\tau = 1.2$, 1.5, and 2.1 s, Figure 3.6 (b).

The MSDs for untreated cells at 24 hours were higher than those for the untreated cells at 48 hours of incubation at all delay times. Statistically significant differences in MSDs were found between $\tau =$ 0.9 and 3.6 s ($p < .05$), however, no statistically significant differences were found between $\tau = 0.15$ and 0.9 s, Figure 3.6 (c). Statistically significant differences in the fluidity of untreated cells at 24 and 48 hours of incubation were only observed between $\tau = 0.15$ and 0.9 s ($p < .05$). Discernible differences, although not statistically significant, were observed between $\tau = 1.2$ and 4 s. See Figure 3.6 (d).

The MSDs for untreated cells were significantly higher than those for the Paclitaxel-treated cells at 24 hours of treatment at all delay times ($p < .05$) as shown in Figure 3.7 (a) except between $\tau = 0.15$ and

0.3 s. The fluidity of untreated cells was also significantly higher than that of Paclitaxel-treated cells at all delay times ($p < .05$). See Figure 3.7 (b).

The MSDs of Paclitaxel-treated cells at 48 hours were noticeably higher than those of the untreated cells, with statistically significant differences between τ = 0.3 and 4.2 s ($p < .05$). No statistically significant differences occurred at τ = 0.15 s and between 4.2 and 10 s. See Figure 3.8 (a). In contrast, no statistically significant differences were observed between paclitaxel-treated and untreated cells at 48 hours at any of the delay times. See Figure 3.8 (b).

Please see Table S. 6 and Table S. 7 for the MSD and fluidity, respectively, and Table S. 9 and Table S. 10 for the pairwise comparisons for the treated and untreated cells in 3D environments at all delay times.

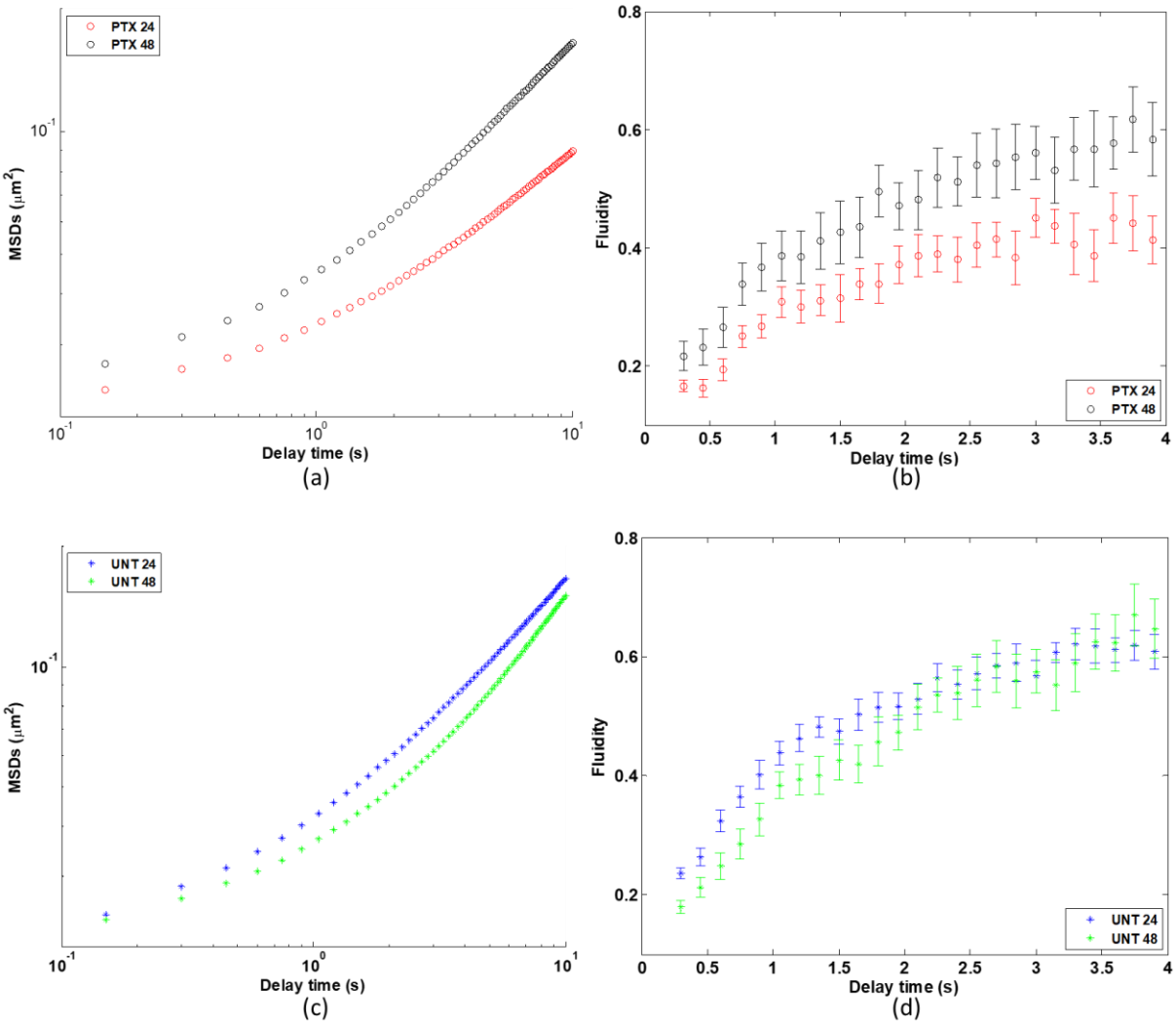

Figure 3.6: Microrheological characterization of WHCO1 cells in 3D environments. (a) MSD versus delay time curves for Paclitaxel-treated cells at 24 and 48 incubation hours. (b) Fluidity versus delay time curves for Paclitaxel-treated cells at 24 and 48 hours. (c) MSD versus delay time plots for untreated cells 24 and 48 hours of incubation. (d) Fluidity versus delay time curves for untreated cells at 24 and 48 hours of incubation. Error bars indicate SEM for one independent repeat experiment (n = 2), N = 21

and 10 for Paclitaxel-treated cells at 24 and 48 hours of treatment, respectively, and N = 19 and 13 for untreated cells incubated for 24 hours 48 hours, respectively. Statistical analysis was carried out using a two-way ANOVA.

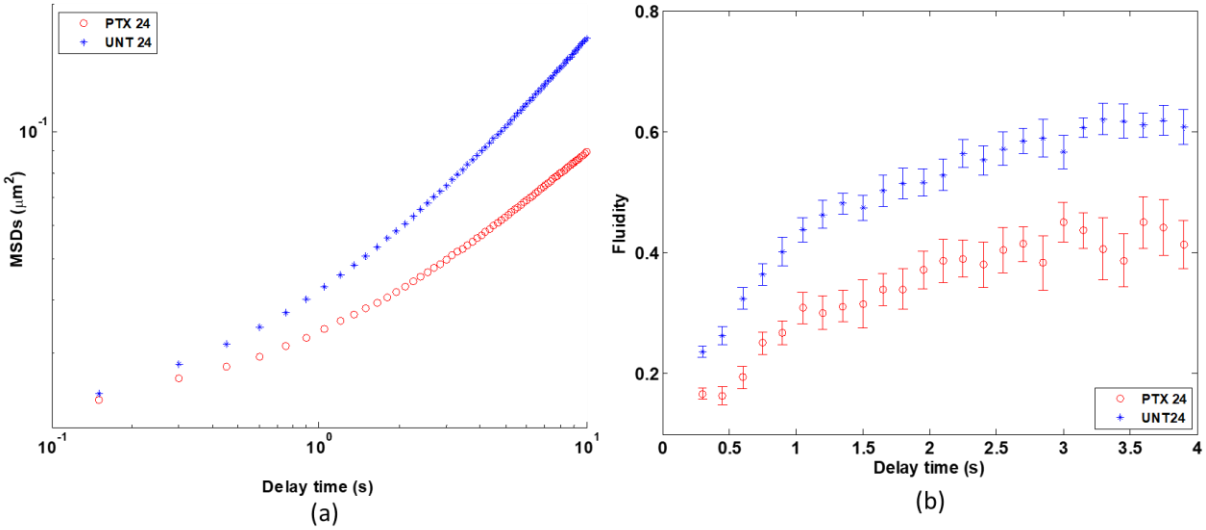

Figure 3.7: Microrheology of WHCO1 cells at 24 hours of treatment in 3D environments. (a) MSD versus delay time curves for Untreated and Paclitaxel-treated cells. (b) Fluidity versus delay time curves for untreated and Paclitaxel-treated cells. Error bars show SEM for one independent repeat experiment (n = 2), N = 19 and 21 for untreated and Paclitaxel-treated cells, respectively. Statistical analysis was carried out using a two-way ANOVA.

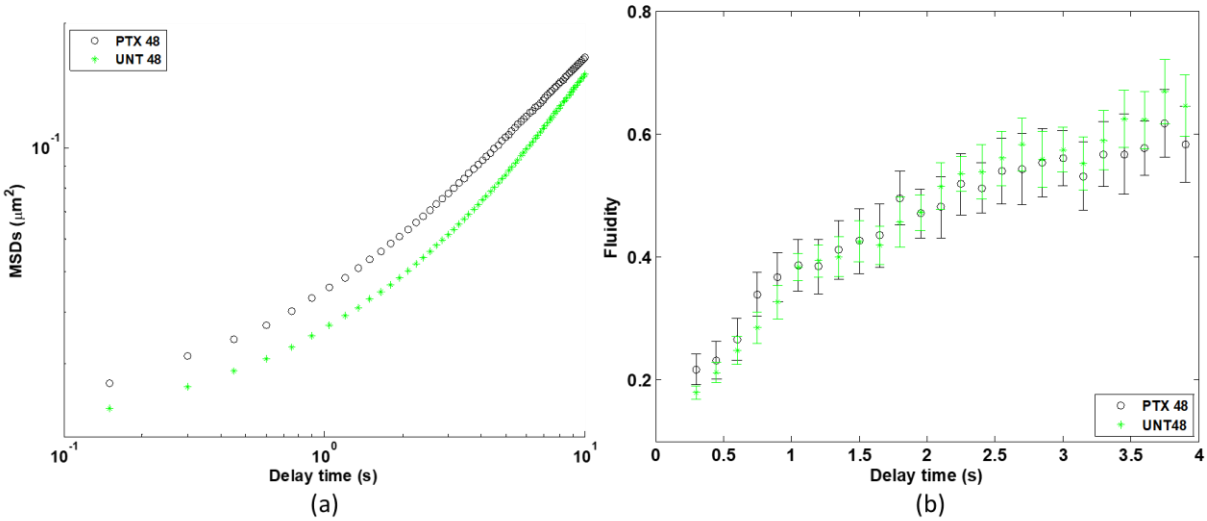

Figure 3.8: Microrheology of WHCO1 cells at 48 hours of treatment in 3D environments. (a) MSD versus delay time curves for Untreated and Paclitaxel-treated cells. (b) Fluidity versus delay time curves for untreated and Paclitaxel-treated cells. Error bars show SEM for one independent repeat experiment (n = 2), N = 13 and 10 for untreated and Paclitaxel-treated cells, respectively. Statistical analysis was carried out using a two-way ANOVA.

In summary, Paclitaxel-treated cells in 3D at 24 hours of treatment had smaller mitochondrial fluctuations and were stiffer (lower fluidity values) than the untreated cells at 24 hours and the Paclitaxel-treated cells at 48 hours. See Figure 3.7 (b) and Figure 3.6 (b), respectively. However, the intracellular stiffness of Paclitaxel-treated cells was comparable to that of the untreated cells at 48

hours (no significant differences in fluidity values), as shown in Figure 3.8 (b). Untreated cells in 3D also exhibited a reduction in intracellular stiffness at shorter time delays (between τ = 0.15 and 1.5 s) when incubated for more than 24 hours (higher fluidity values at 48 hours of incubation than at 24 hours at shorter time delays), as shown in Figure 3.6 (d).

3.1.3 Effect of dimensionality on the intracellular stiffness of WHCO1 cells

The MSDs and fluidity for untreated and Paclitaxel-treated cells in 2D and 3D environments were compared to evaluate the effect of dimensionality on the intracellular stiffness of WHCO1 OSCC cells. It was found that cells embedded in 3D environments exhibited larger MSDs than those in 2D environments. Additionally, cells in 2D were more fluid-like (had higher fluidity values) than those in 3D environments. A three-way ANOVA was conducted to compare the MSDs and fluidity of treated and untreated cells in 2D and 3D environments at τ = 2.1 s to determine whether dimensionality had any effect on the intracellular stiffness of WHCO1 OSCC cells.

The MSDs were transformed using a square root function, and fluidity was normally distributed ($p > .05$) as assessed by Shapiro-Wilk's normality test except for fluidity of untreated cells in 2D at 24 hours of treatment, $p = 0.022$. The variance was homogeneous ($p > 0.05$) in both MSD data and fluidity as assessed by Levene's test for equality of variance. A statistically significant three-way interaction ($p < .05$) was detected between dimensionality (2D versus 3D), drug treatment (Paclitaxel-treated versus untreated cells), and exposure time (24 versus 48 hours). Statistical significance was accepted at $p < 0.025$, based on three groups, for simple two-way interactions and simple-simple main effects. All simple-simple pairwise comparisons were performed with a Bonferroni adjustment applied.

The MSDs for Paclitaxel-treated and untreated cells in 3D were noticeably higher than those in 2D environments, as seen in Figure 3.9 (a). In contrast, fluidity for both Paclitaxel-treated and untreated cells in 3D was notably lower than that of the cells in 2D environments, as illustrated in Figure 3.9 (b). The MSDs for Paclitaxel-treated cells in 3D were significantly larger than those of the treated cells in 2D environments at 24 hours of treatment ($p < .0005$). Additionally, MSDs for untreated cells in 3D were significantly larger than those of the untreated cells in 2D environments ($p < .0005$). Furthermore, Paclitaxel-treated cells in 2D exhibited a considerably larger fluidity than the Paclitaxel-treated cells in 3D environments ($p < .0005$). Similarly, untreated cells in 2D had a significantly larger fluidity than the untreated cells in 3D environments ($p < .0005$).

The MSDs of Paclitaxel-treated cells in 3D were also significantly larger than those of the treated cells in 2D environments at 48 hours of treatment ($p < .0005$), and the same was observed for the untreated cells. In contrast, the fluidity of Paclitaxel-treated cells in 3D was substantially lower than that of the

treated cells in 2D environments ($p < .005$). The fluidity of untreated cells in 3D was also significantly lower than that of the untreated cells in 2D environments ($p < .0005$).

See Table S. 11 for the MSD and fluidity and Table S. 12 for the pairwise comparisons for the MSDs and fluidity of treated and untreated WHCO1 cells in 2D and 3D environments at $\tau = 2.1$ s.

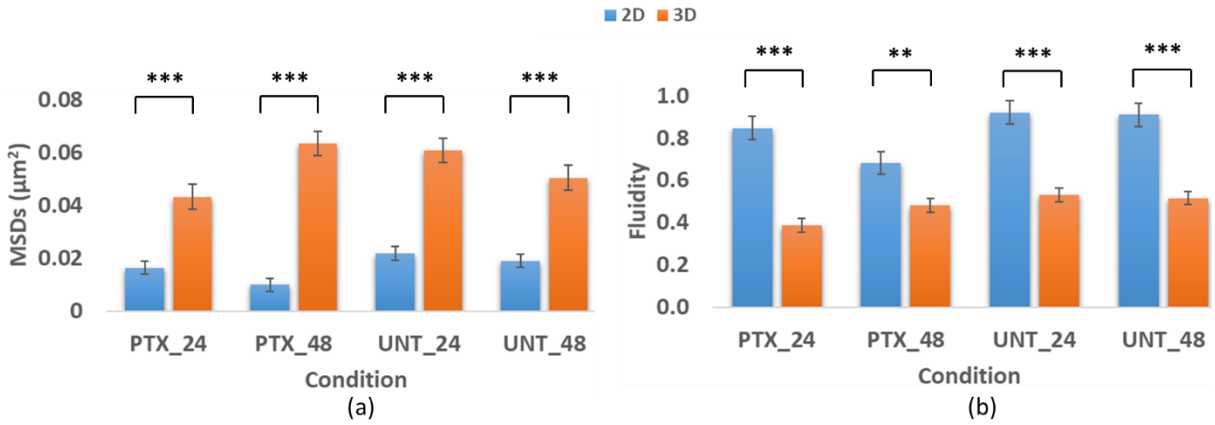

*Figure 3.9: Comparison of MSDs and fluidity for WHCO1 cells in 2D and 3D environments at a delay time of 2.1 seconds. (a) MSDs for Paclitaxel-treated and untreated WHCO1 cells at 24 and 48 hours of treatment. (b) Fluidity for Paclitaxel-treated and untreated WHCO1 cells at 24 and 48 hours of treatment. PTX_24, PTX_48, UNT_24, and UNT_48 stand for Paclitaxel-treated and Untreated cells at 24 and 48 hours of treatment. Error bars indicate SEM. ** and *** indicate $p < 0.005$ and 0.0005, respectively. Statistical analysis was carried out using a three-way ANOVA.*

3.2 Morphology for WHCO1 cells

As discussed in section 2.6, VAMPIRE software was used to examine the visual characteristics of the treated and untreated WHCO1 cells in 2D and 3D environments. VAMPIRE analysis was performed on the brightfield images (as in Figure 3.1 and Figure 3.5) for a total of 251 cells from one repeat experiment ($n = 2$), with 194 and 57 cells analyzed in 2D and 3D experiments, respectively. Shape analysis and heterogeneity of the treated and untreated WHCO1 cells in 2D and 3D environments were performed to identify the shape modes associated with individual cells within the different conditions.

Additionally, parameters such as cell area, perimeter, circularity, and aspect ratio were also determined to facilitate morphological comparison of the treated and untreated WHCO1 cells in 2D and 3D environments. Circularity describes a circular shape of cells, whereas aspect ratio is a ratio of the long axis to the short axis of the cells. Cells with an aspect ratio and circularity equalling one are assumed to be perfectly circular. However, when the aspect ratio value increases and the circularity decrease from one, the cell is described as elongated (Chen B *et al.* 2015, Gautam *et al.* 2021, Liu X *et al.* 2010). A three-way ANOVA was conducted to determine the statistical differences in the cell area, perimeter, circularity, and aspect ratio of the treated and untreated cells in 2D and 3D environments. Simple-simple pairwise comparisons were also performed with a Bonferroni adjustment after

obtaining statistically significant simple two-way interactions and simple-simple main effects ($p < 0.025$). The study was based on the hypothesis that treating OSCC cells with chemotherapeutic drugs is associated with cell morphology changes.

3.2.1 Effect of Paclitaxel treatment on the morphology of WHCO1 cells in 2D environments

3.2.1.1 Paclitaxel-treated cells are larger than the untreated and ethanol-treated cells

Paclitaxel-treated cells at 24 hours of treatment had a significantly larger cell area than the untreated cells ($p < .005$) and ethanol-treated cells ($p < .0005$). Paclitaxel-treated cells at 48 hours of treatment were also significantly larger in cell area than the untreated cells ($p < .0005$) and ethanol-treated cells ($p < .0005$). No statistically significant difference in cell area was observed between the untreated and ethanol-treated cells at both 24 and 48 hours of treatment. Also, no statistically significant differences in cell area were observed between the cells (treated and untreated) at 24 and 48 hours of treatment. See Figure 3.10 (a).

Paclitaxel-treated cells at both 24 and 48 hours of treatment exhibited a significantly larger perimeter than ethanol-treated cells ($p < .005$). Additionally, Paclitaxel-treated cells at 48 hours of treatment had a considerably larger perimeter than the untreated cells ($p < .0005$). However, no statistically significant difference in perimeter was observed between Paclitaxel-treated cells and untreated cells at 24 hours of treatment. Additionally, no statistically significant differences were observed between untreated and ethanol-treated cells at both 24 and 48 hours of treatment. Furthermore, Paclitaxel-treated cells at 48 hours of treatment were significantly larger in perimeter than the Paclitaxel-treated cells at 24 hours of treatment ($p < .005$). No statistically significant differences in perimeter were observed in the control cells (untreated and ethanol-treated cells) between 24 and 48 hours of treatment. See Figure 3.10 (b).

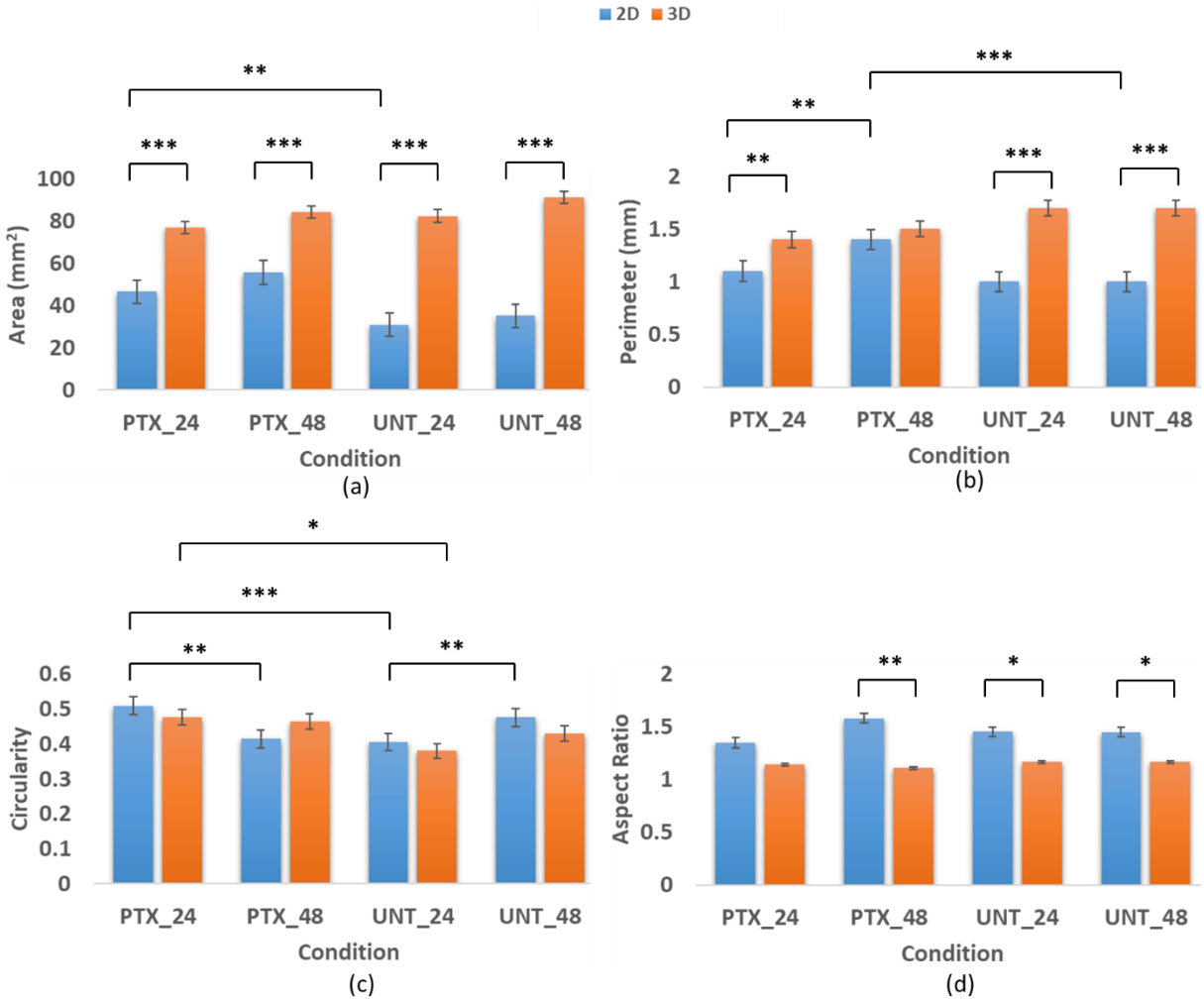

*Figure 3.10: Morphology analysis of treated and untreated cells. (a) Cell area, (b) perimeter, (c) circularity, and (d) aspect ratio of Paclitaxel-treated and Untreated WHCO1 cells at 24 and 48 hours of treatment in 2D and 3D environments. Error bars are SEM for one independent repeat experiment (n = 2). For 2D experiments, N = 27 and 22 for Paclitaxel-treated cells at 24 and 48 hours, respectively. N = 43 and 23 for the ethanol-treated cells at 24 and 48 hours and 42 and 37 for the untreated cells at 24 and 48 hours, respectively. For the 3D experiments, N = 15, 11 for Paclitaxel-treated cells at 24 (PTX_24) and 48 (PTX_48) hours of treatment, respectively, and 16 and 15 for untreated cells at 24 (UNT_24) and 48 (UNT_48) hours of treatment, respectively. *, **, *** indicate p < 0.025, 0.005, and 0.0005, respectively. Statistical analysis was carried out using a three-way ANOVA.*

3.2.1.2 The circularity and aspect ratio of treated and untreated cells at 24 and 48 hours of treatment

Paclitaxel-treated cells at 24 hours of treatment were significantly more circular than the untreated cells ($p < .0005$), and the same was observed for the ethanol-treated cells. Furthermore, Paclitaxel-treated cells at 24 hours of treatment were significantly more circular than the Paclitaxel-treated cells at 48 hours ($p < .005$). At 24 hours of treatment, the ethanol-treated cells were also substantially more circular than the ethanol-treated cells at 48 hours ($p < .0005$). In contrast, the untreated cells at 48 hours of treatment were significantly more circular than those at 24 hours ($p < .005$). No statistically significant differences in circularity were observed between Paclitaxel-treated and ethanol-treated

cells at both 24 and 48 hours of treatment and between Paclitaxel-treated and untreated cells and untreated and ethanol-treated cells at 48 hours of treatment. See Figure 3.10 (c).

No statistically significant differences in the aspect ratio were observed in all conditions (Paclitaxel-treated, ethanol-treated, and untreated) between cells at 24 and 48 hours of treatment and between Paclitaxel-treated and ethanol-treated cells and Paclitaxel-treated and untreated cells at both 24 and 48 hours of treatment. See Figure 3.10 (d).

3.2.2 Effect of Paclitaxel treatment on the morphology of WHCO1 cells in 3D environments

No statistically significant differences in cell area and perimeter were observed between Paclitaxel-treated and untreated cells at both 24 and 48 hours of treatment. Additionally, no statistically significant differences in cell area and perimeter were observed between cells (Paclitaxel-treated and untreated) at 24 and 48 hours of treatment. See Figure 3.10 (a and b).

A statistically significant difference in circularity was only observed between Paclitaxel-treated and untreated cells at 24 hours of treatment ($p < .05$). No statistically significant differences in circularity were found between cells (Paclitaxel-treated and untreated) at 24 and 48 hours of treatment and between Paclitaxel-treated and untreated cells at 48 hours of treatment. See Figure 3.10 (c).

Furthermore, no statistically significant differences in aspect ratio were observed between Paclitaxel-treated and untreated cells at 24 and 48 hours of treatment and between cells (Paclitaxel-treated and untreated) at 24 and 48 hours of treatment. See Figure 3.10 (d).

3.2.3 Effect of dimensionality on the morphology of WHCO1 cells

Paclitaxel-treated cells in 3D were significantly larger in cell area than the Paclitaxel-treated cells in 2D environments at 24 and 48 hours of treatment ($p < .0005$). Additionally, Paclitaxel-treated cells in 3D were significantly larger in perimeter than the Paclitaxel-treated cells in 2D environments at 24 hours of treatment ($p < .005$), but no significant differences were found at 48 hours. Furthermore, the untreated cells in 3D were significantly larger in cell area and perimeter than the untreated cells in 2D environments at 24 and 48 hours of treatment ($p < .0005$). See Figure 3.10 (a and b).

No statistically significant differences in circularity were observed between Paclitaxel-treated and untreated cells in 2D and 3D environments at 24 and 48 hours of treatment. See Figure 3.10 (c).

At 24 hours of treatment, untreated cells in 2D had a significantly bigger aspect ratio than the untreated cells in 3D environments ($p < .05$). However, no statistically significant differences in aspect ratio were observed between Paclitaxel-treated cells in 2D and 3D environments. Additionally, Paclitaxel-treated and untreated cells in 2D had considerably larger aspect ratios than the cells in 3D environments ($p < .05$). Figure 3.10 (d).

See Table S. 13 for the mean area, perimeter, circularity, and aspect ratio, and Table S. 14 for the pairwise comparisons of the treated and untreated WHCO1 cells in 2D and 3D environments.

3.2.4 Shape analysis and heterogeneity of the treated and untreated WHCO1 cells

The results in this section are based on the hypothesis that cancer cells within a tumour can have different responses to the same chemotherapeutic drug. Therefore, variants of the cancer cells that do not respond to the drug can result in mechanisms leading to cellular heterogeneity and reduced response treatment.

Figure *3.11* illustrates the shape modes associated with the treated and untreated WHCO1 cells in 2D and 3D environments. The shape modes were obtained using the VAMPIRE software as described in section 2.6 and used to describe inherent cell shapes. The first shape mode (1) was more elongated than the rest, whereas the second shape mode (2) was more circular than the other shape modes. The rest of the shape modes (3 through 10) were irregular and differed slightly. Cell heterogeneity was then computed using the shape mode distributions, representing each shape mode among the experimental condition. See Table S. 15 for the abundance of cells in each experimental condition for each shape mode.

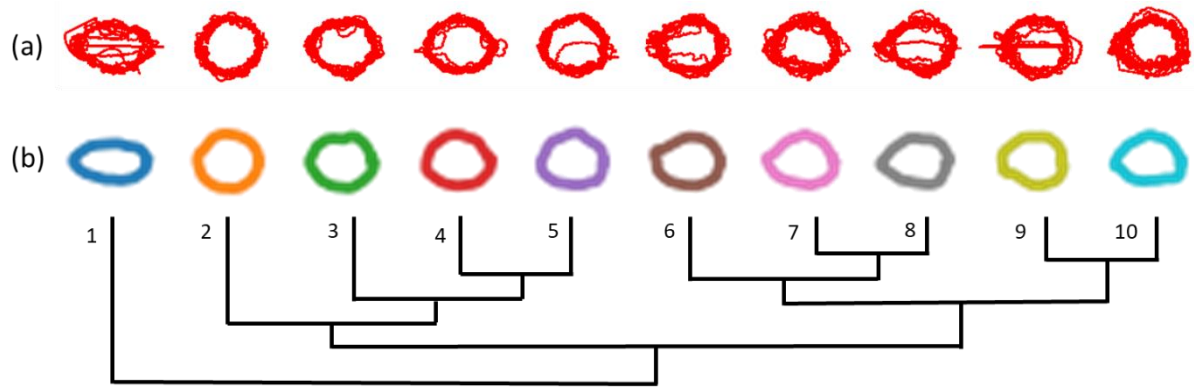

Figure 3.11: Shape modes obtained for WHCO1 cells in 2D and 3D environments. (a) Registered objects are showing actual boundaries of cells selected randomly from individual shape modes. (b) Shape mode dendrogram demonstrating the morphology of the different shape modes (1 through 10) detected and their similarity.

3.2.5 Heterogeneity in the treated and untreated WHCO1 cells in 2D environments

Paclitaxel-treated cells at 48 hours exhibited a slightly lower heterogeneity than the Paclitaxel-treated cells at 24 hours, with no cells classified under shape modes 5 and 9. The highest number of Paclitaxel-treated cells at 24 hours were classified under shape modes 6, 7, and 10 (18.2 %), whereas the majority of the Paclitaxel-treated cells at 24 hours were categorized under shape mode 2 (18.5 %) and the least number of cells in shape mode 10 (3.7 %), Figure *3.12* (a and b).

Ethanol-treated cells at 24 and 48 hours exhibited similar heterogeneity with cells distributed across all shape modes except for shape modes 9 and 6, respectively, which had no cells classified under them. Most ethanol-treated cells at 24 hours were grouped under shape modes 4 and 8 (18.6 %), whereas the highest number of ethanol-treated cells at 48 hours were categorized under shape modes 4, 5, and 10 (17.4 %), see Figure *3.12* (c and d).

Untreated cells at 48 hours also exhibited a slightly lower heterogeneity than the untreated cells at 24 hours, with no cells classified under shape modes 3 and 7. The highest number of untreated cells at 24 hours was grouped under shape mode 7 (19 %), whereas most untreated cells at 48 hours were classified under shape mode 1 (23.3 %), see Figure *3.12* (e and f).

At both 24 and 48 hours of treatment, no significant differences in heterogeneity were observed among all study conditions, that is, Paclitaxel-treated, ethanol-treated, and untreated cells (Figure *3.12*).

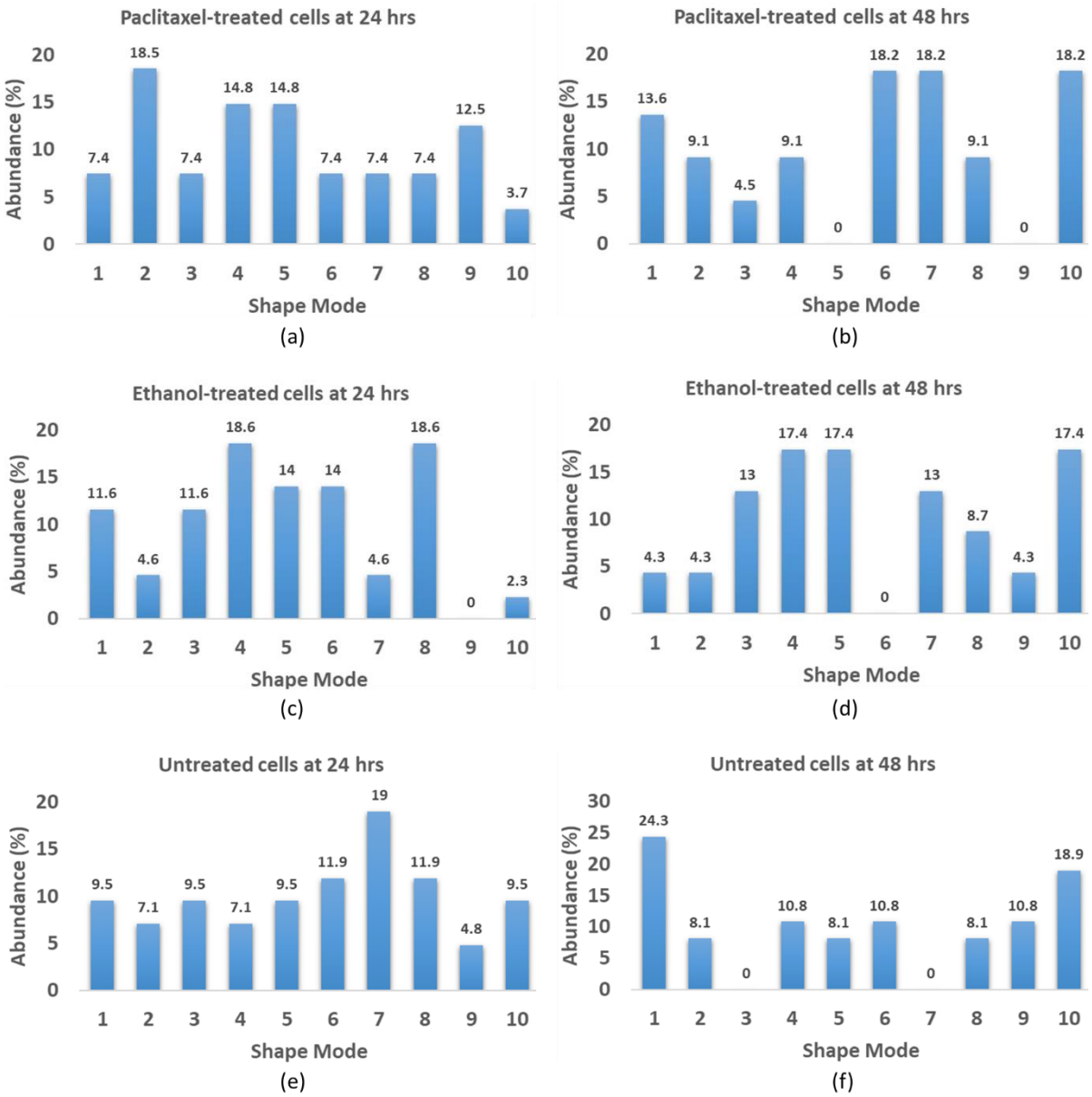

Figure 3.12: Cellular heterogeneity for treated and untreated WHCO1 cells in 2D environments, (a) cells treated with Paclitaxel for 24 hours (N = 27), (b) cells treated with Paclitaxel for 48 hours (N = 22), (c) cells treated with ethanol for 24 hours (N = 43), (d) ethanol-treated cells at 48 hours of treatment (N = 23), (e) and (f) untreated cells at 24 (N = 42) and 48 (N = 37) hours of incubation, respectively obtained using VAMPIRE analysis. The numbers above the bars are representative of the abundance of cells in each shape mode. The shape modes are shown in Figure 3.11 (b).

3.2.6 Heterogeneity in the treated and untreated WHCO1 cells in 3D environments

Paclitaxel-treated cells at 48 hours exhibited a significantly lower heterogeneity than the Paclitaxel-treated cells at 24 hours, with all the cells classified under shape modes 2 (36.4 %), 4 (27.3 %), 7 (9.3 %), and 9 (27.3 %). The Paclitaxel-treated cells at 24 hours were well distributed across all shape modes except for 8 and 10, which had no cells classified under them. Most of the treated cells at 24 and 48 hours were categorized under shape mode 2 (33.3 % and 36.4 %, respectively). See Figure *3.13* (a and b).

The untreated cells at 48 hours exhibited a significantly lower heterogeneity than the untreated cells at 24 hours, with most cells classified under shape 2 (26.7 %) and no cells grouped under shape modes 1, 6 and 7. The most untreated cells at 24 hours were classified under shape mode 9 (25 %), and no cells were grouped under shape mode 1. See Figure *3.13* (c and d).

After 24 hours of treatment, Paclitaxel-treated cells exhibited a lower heterogeneity than the untreated cells: treated cells were distributed amongst eight shape modes (1-7 and 9) compared to nine shape modes (2-10) for untreated cells. Furthermore, at 48 hours, Paclitaxel-treated cells exhibited a significantly lower heterogeneity than the untreated cells, with no cells classified under six shape modes compared to three in the untreated cells (Figure *3.13*).

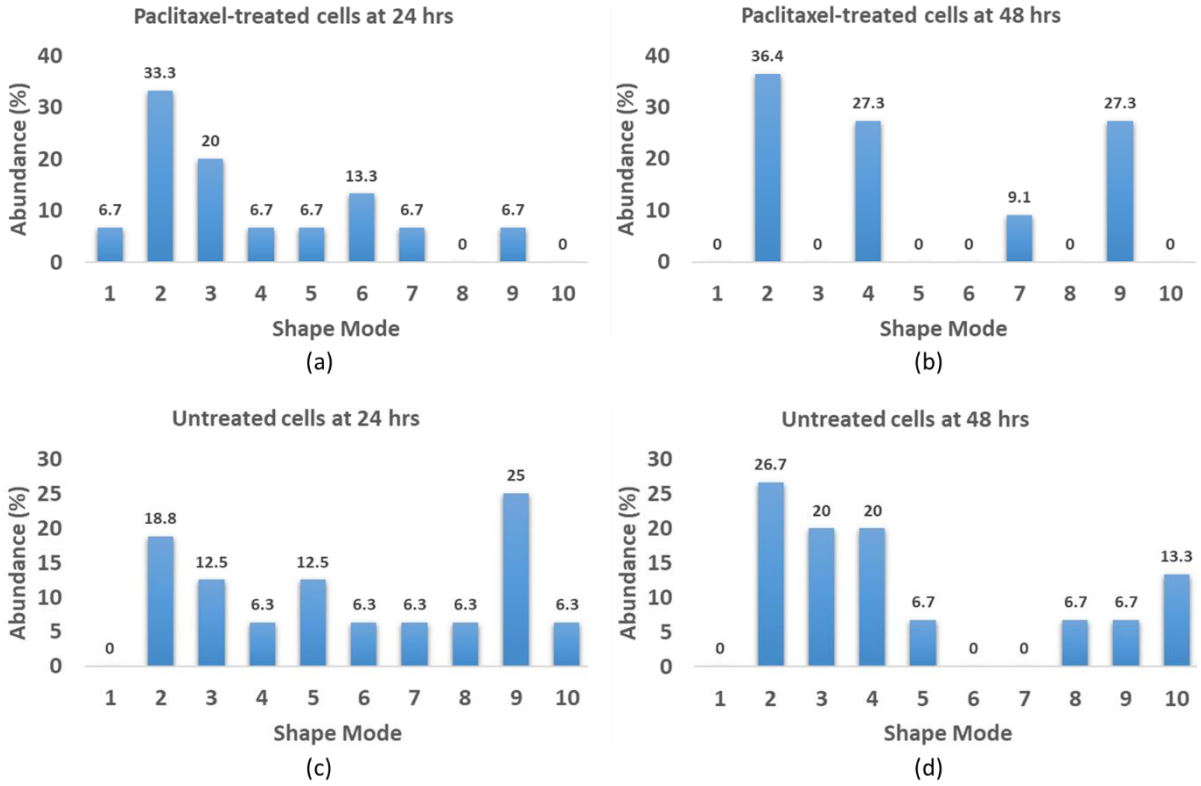

Figure 3.13: Cellular heterogeneity for treated and untreated cells in 3D environments, (a) cells treated with Paclitaxel for 24 hours (N = 15), (b) cells treated with Paclitaxel for 48 hours (N = 11), (c) untreated cells incubated for 24 hours (N = 16), and (d) untreated cells incubated for 48 hours (N = 15) obtained using VAMPIRE analysis. The numbers above the bars are representative of the abundance of cells in each shape mode. The shape modes are shown in Figure 3.11(b).

Chapter 4 Discussion

This study characterised the intracellular stiffness and morphology of treated and untreated WHCO1 OSCC cells in 2D and 3D environments at 24 and 48 hours of treatment using mitochondrial particle-tracking microrheology and VAMPIRE analysis, respectively. The study aimed to determine the effect of chemotherapeutic treatment on the intracellular stiffness and morphology of WHCO1 OSCC cells in 2D and 3D environments. Paclitaxel was used as the chemotherapeutic drug, whereas the untreated cells and ethanol-treated cells were used as the controls.

4.1 Intracellular stiffness

In 2D environments, WHCO1 OSCC cells treated with Paclitaxel exhibited a stiffer intracellular domain (lower fluidity) than the control cells at 24 and 48 hours (Figure 3.3 and Figure 3.4). Additionally, the intracellular stiffness of Paclitaxel-treated cells increased significantly (decrease in fluidity) when drug exposure time increased from 24 to 48 hours (Figure 3.2). However, no significant differences in intracellular stiffness were observed between the control cells indicating that the increase in intracellular stiffness of Paclitaxel-treated was due to chemotherapeutic drug treatment (Figure 3.3 and Figure 3.4).

In 3D environments, Paclitaxel-treated WHCO1 OSCC cells exhibited an increased intracellular stiffness (lower fluidity) than the control cells at 24 hours of treatment. However, the intracellular stiffness of Paclitaxel-treated cells significantly decreased (higher fluidity) when the drug exposure time increased from 24 to 48 hours. At 48 hours of treatment, no significant difference in fluidity was detected between Paclitaxel-treated cells and the controls. The untreated cells at 48 hours also exhibited a stiffer intracellular environment (lower fluidity) than those at 24 hours at the short delay times (between τ = 0.15 and 1.5 s)(Figure 3.6 toFigure 3.8).

Results for 2D (at both 24 and 48 hours) and 3D experiments at 24 hours of treatment agree with several previous studies that indicated that the treatment of cancer cells with chemotherapeutic drugs increases their stiffness. These include an investigation by Islam *et al.* (2018) which using AFM demonstrated that the stiffness of leukaemia cancer cells (K562 and Jurkat) significantly increased on treatment with daunorubicin. Another study by Lam *et al.* (2007), using AFM, found that the stiffness of acute myeloid and acute lymphoblastic leukaemia cancer cells increased on treatment with daunorubicin and dexamethasone chemotherapeutic agents.

Similarly, a study by Ren *et al.* (2015) also demonstrated using AFM that the stiffness of pancreatic cancer cells (PC-3) increases due to treatment with drugs such as disulfiram, and paclitaxel, tomatine and valproic acid. Furthermore, Raudenska *et al.* (2019) also demonstrated using AFM that the

stiffness of cancer cells (PNTIA, 22Rv1 and PC-3) increased on treatment with cisplatin and docetaxel drugs.

The increase in the stiffness of the cancer cells on treatment with chemotherapeutic drugs has previously been attributed to alterations in the cytoskeleton structure and its associated proteins, as most chemotherapeutic drugs work by targeting the cytoskeleton to induce the cytotoxic effect. Paclitaxel, a chemotherapeutic drug used in this study, for example, works by promoting the formation and stabilization of microtubules with the cancer cells, which leads to a reduction in the depolymerization and normal dynamic reorganization of the microtubules required for mitosis and cell proliferation (Fan 1999, Gascoigne and Taylor 2009, Weaver 2014).

The stabilization of the microtubules increases the density of the cytoskeleton and may reduce its dynamic behaviour. Additionally, the stabilized microtubules also push the actin cortex outward to a point where it strain-hardens (Kubitschke *et al.* 2017). Paclitaxel's effect on the microtubules explains the increase in the intracellular stiffness of the Paclitaxel-treated WHCO1 OSCC observed in this study, especially for the cells in 2D at both 24 and 48 hours and those in 3D at 24 hours of treatment.

Changes in intracellular stiffness observed in the treated and untreated cells embedded in 3D at 48 hours of treatment can be attributed to the remodelling of the cytoskeleton and the extracellular matrix. Cells can sense external forces from the physical environment that directly regulate biochemical signalling within the cell and drive cell fate decisions (Humphrey *et al.* 2014, Janmey and Weitz 2004, Staunton *et al.* 2019). They can also apply the internally generated forces to the physical environment in which they attach. In doing so, cells can change their structure, motility, growth, morphology, and response to drugs and alter the physical properties of their surrounding environments (Cavo *et al.* 2016, Doyle and Yamada 2016, Flanagan *et al.* 2002, Janmey and Weitz 2004, Pelham and Wang 1997). The change in the structure, motility and growth of the cells is governed by the cytoskeleton and the proteins and organelles that regulate it (Gkretsi and Stylianopoulos 2018, Janmey 1998, Park 2016, Staunton *et al.* 2019).

The cytoskeleton is linked to the extracellular matrix through transmembrane proteins such as integrins. These transmembrane proteins transfer signals due to internal and external forces between the cytoskeleton and the ECM, which can lead to the remodelling of both the cytoskeleton and the ECM (Helmke and Davies 2002, Hu *et al.* 2003, Janmey and Weitz 2004). Additionally, the cytoskeleton and ECM remodelling can also lead to the activation of mechanisms responsible for drug efflux from the cells. Consequently, the concentration levels of drugs (Paclitaxel) reduce within the cells, yet its effectiveness depends on the accumulation of drugs (Weaver 2014). Hence, the decrease in the intracellular stiffness of WHCO1 OSCC cells as drug exposure time was increased from 24 to 48 hours.

Furthermore, it is assumed that Paclitaxel only kills the parent cells that divide in its existence. The daughter cells from cells that underwent mitosis in the absence of Paclitaxel are not affected by the drug since its effects cannot be carried to subsequent generations (Gascoigne and Taylor 2009). Thus, the lack of significant difference in intracellular stiffness between Paclitaxel-treated and untreated WHCO1 OSCC cells in 3D at 48 hours of treatment.

4.2 Morphology

In 2D environments, Paclitaxel-treated WHCO1 OSCC cells exhibited a significantly larger cell area than control cells at both 24 and 48 hours of treatment. However, no significant differences in cell area were detected between the control cells at both time points. Also, increasing the drug exposure time from 24 to 48 hours of treatment did not significantly affect the cell area of WHCO1 OSCC cells. In contrast to 2D experiments, no significant differences in cell area were detected between the treated and untreated cells embedded in 3D environments at any of the time points (Figure 3.10).

Additionally, Paclitaxel-treated WHCO1 OSCC cells in 2D environments exhibited a significantly larger perimeter than the control cells at 24 and 48 hours of treatment. However, no significant differences were detected among the control cells. Increasing drug exposure time from 24 to 48 hours also significantly increased the perimeter of WHCO1 OSCC cells. On the other hand, no significant differences in perimeter were detected between the treated and untreated cells embedded in 3D environments at any of the time points (Figure 3.10).

Furthermore, Paclitaxel-treated WHCO1 OSCC cells in 2D environments at 24 hours of treatment were significantly more circular than the untreated cells. Similarly, ethanol-treated cells were substantially more circular than untreated cells. However, no significant differences were detected between Paclitaxel-treated and ethanol-treated cells at 24 hours and among all the conditions at 48 hours of treatment. Untreated WHCO1 OSCC cells at 48 hours were significantly more circular than those at 24 hours, whereas Paclitaxel-treated and ethanol-treated cells at 24 hours were significantly more circular than those at 48 hours of treatment. Compared to 2D results, significant differences in circularity were only detected between the treated and untreated cells at 24 hours for the WHCO1 OSCC cells embedded in 3D environments with Paclitaxel-treated cells more circular than the untreated cells (Figure 3.10).

The above findings on the morphology (cell area and perimeter) of WHCO1 OSCC cells agree with previous studies, demonstrating that cancer cells enlarge on treatment with chemotherapeutic drugs (Abubaker *et al.* 2013, Bouzekri *et al.* 2019, Rasbridge *et al.* 1994). This enlargement of cells can be attributed to the formation and stabilization of the microtubules due to Paclitaxel treatment, leading to reduced depolymerization and dynamics and increased cytoskeleton density (Fan 1999, Gascoigne

and Taylor 2009, Weaver 2014). Cell enlargement can also be attributed to the formation of multi-nuclei caused by Paclitaxel inhibiting the mitotic cycle, hence cells failing to divide into daughter cells (Abubaker *et al.* 2013, Jordan *et al.* 1996).

Results on cell morphological heterogeneity in the WHCO1 OSCC cells in 2D environments show that treatment of the cells with Paclitaxel has no significant effect on cell heterogeneity. No substantial differences in morphological heterogeneity were observed between the Paclitaxel-treated and the control cells at 24 and 48 hours of treatment. In contrast to 2D results, treatment of WHCO1 OSCC cells with Paclitaxel significantly affected the morphological heterogeneity of cancer cells in 3D environments. The morphological heterogeneity of Paclitaxel-treated and untreated cells decreased by 40 and 20 %, respectively, as the incubation time was increased from 24 to 48 hours. Additionally, the morphological heterogeneity observed in Paclitaxel-treated cells at 48 hours was significantly lower (30 %) than in the untreated cells, whereas no significant differences were detected at 24 hours of treatment (Figure *3.12* andFigure *3.13*). The results in 3D environments show that treatment of cancer cells with Paclitaxel has the potential of inducing changes in morphological heterogeneity within the tumour. This can be attributed to differences in the way tumour cells respond to drug treatment over time leading to changes in several cellular mechanisms, morphology and reduction in drug response.

4.3 Dimensionality

Comparing the intracellular stiffness and morphology of WHCO1 OSCC cells in 2D and 3D environments shows that cells in 3D in all conditions exhibited significantly lower fluidity (stiffer) than the cells in 2D environments. These results on intracellular stiffness agree with previous studies, demonstrating that cancer cells embedded in 3D environments are significantly more rigid than those in 2D (Baker E. L. *et al.* 2009, Mak *et al.* 2014, Staunton *et al.* 2019). Additionally, cells in 3D environments in all conditions exhibited significantly larger cell area and perimeter than those in 2D except for Paclitaxel-treated cells at 48 hours with no significant differences in perimeter between cells in 2D and 3D. No significant differences in circularity were also detected between cells in 2D and 3D in any experimental conditions. These morphological results agree with a previous study by Cavo *et al.* (2016), which demonstrated that cells embedded in 3D environments exhibit larger cell area and perimeter than those in 2D.

The observed differences in the intracellular stiffness and morphology of Paclitaxel-treated and untreated WHCO1 OSCC cells in 2D and 3D can be attributed to the differences in the physical environments in which the cells were cultured and the geometry of the cytoskeleton (Gkretsi and Stylianopoulos 2018, Park 2016). Cells cultured in the traditional 2D environments adhere and grow

on a flat surface and can spread freely in the horizontal plane; however, they do not have the support to grow in the vertical dimension. Consequently, they appear stretched and flattened with a flatter cytoskeleton (Baker BM and Chen 2012, Xu K *et al.* 2012).

In contrast to 2D, cells cultured in 3D environments and their cytoskeleton appear rounder and resemble the *in vivo* architecture. The roundness of the cells in 3D is due to fewer geometrical constraints in the environment in which they are growing and improved cell-cell and cell-extracellular matrix interactions (Cukierman *et al.* 2001, Tibbitt and Anseth 2009, Xu K *et al.* 2012). Therefore, cells in 3D are connected to the extracellular matrix across the entire surface membrane, making their cytoskeletal network more constrained and rigid than that of the cells in 2D.

Chapter 5 Conclusion and recommendations

This study has demonstrated that treating OSCC cells with Paclitaxel increases their intracellular stiffness as early as one day after treatment and increases over time for cells in 2D environments. For cells in 3D, the intracellular stiffness starts decreasing after the first day of treatment and decreases over time and matches the untreated cells by the second day. No significant differences in intracellular stiffness were observed between the controls at both 24 and 48 hours for the cells in 2D, implying that the detected changes were due to Paclitaxel treatment. Additionally, the observed differences in the intracellular stiffness of untreated cells in 3D between 24 and 48 hours of incubation indicate that the detected changes in the stiffness of OSCC in 3D were not only due to Paclitaxel treatment.

Furthermore, this study has demonstrated that treating OSCC cells with Paclitaxel increases the cell area and perimeter of the cells in 2D but not in 3D. Additionally, the circularity of OSCC cells in 2D and 3D also increases after one day of treatment with Paclitaxel. Besides, increasing the exposure time of OSCC cells in 2D to Paclitaxel leads to a decrease in their circularity.

This study has also demonstrated that the morphological heterogeneity of OSCC cells embedded in 3D environments decreases due to treatment with Paclitaxel. In contrast, Paclitaxel treatment does not significantly affect the morphological heterogeneity of cells in 2D environments. Heterogeneity of OSCC cells describes the abundance of cells with distinct morphological and phenotypic profiles within the tumour, which was previously understood at genetic and molecular levels (Lin L and Lin 2019, Wang *et al.* 2019, Yan *et al.* 2019). This study shows that measurement of morphological heterogeneity could complement genetic and molecular heterogeneities as markers to determine the efficacy of Paclitaxel treatment and drug resistance in OSCC patients.

In summary, this study has shown that there are changes in the mechanical properties of cells (intracellular stiffness and morphology) associated with the treatment of OSCC cells in 2D and 3D with Paclitaxel. This study was carried out using clonal cell lines derived from biopsies of primary OSCC; however, additional studies need to be performed using primary OSCC cells and results compared to ascertain the observed changes. Additionally, the cell lines in this study were treated for a short time (two days), and therefore, long term treatment of OSCC primary cells and cell lines with Paclitaxel needs to be performed to determine whether it can lead to the onset of chemoresistance in OSCC patients. Furthermore, changes in intracellular stiffness and morphology associated with long-term exposure of OSCC cells to Paclitaxel need to be studied to determine whether they could serve as markers for the onset of chemoresistance to improve the efficacy of Paclitaxel treatment in OSCC patients. Only two biological repeats were performed in this study due to time limitations as the university's research laboratories were closed for the majority of the master's degree period due to the COVID-19 pandemic and lockdowns.

References

Abubaker K, Latifi A, Luwor R, Nazaretian S, Zhu H, Quinn MA, Thompson EW, Findlay JK, Ahmed N. *Short-term single treatment of chemotherapy results in the enrichment of ovarian cancer stem cell-like cells leading to an increased tumor burden*. Mol Cancer 2013, **12**(1): 24.

Adamo A, Sharei A, Adamo L, Lee B, Mao S, Jensen KF. *Microfluidics-based assessment of cell deformability*. Anal Chem 2012, **84**(15): 6438-43.

Alexandersson VD, Gabriella. *Multimodality treatment of oesophageal cancer: Effects and side effects*. Department of Oncology-Pathology, Karolinska Institutet, 2018.

Anand P, Kunnumakara AB, Sundaram C, Harikumar KB, Tharakan ST, Lai OS, Sung BY, Aggarwal BB. *Cancer is a preventable disease that requires major lifestyle changes*. Pharm Res 2008, **25**(9): 2097-116.

Arganda-Carreras I, Kaynig V, Rueden C, Eliceiri KW, Schindelin J, Cardona A, Sebastian Seung H. *Trainable weka segmentation: A machine learning tool for microscopy pixel classification*. Bioinformatics 2017, **33**(15): 2424-6.

Arnold M, Laversanne M, Brown LM, Devesa SS, Bray F. *Predicting the future burden of esophageal cancer by histological subtype: International trends in incidence up to 2030*. Am J Gastroenterol 2017, **112**(8): 1247-55.

Arnold M, Soerjomataram I, Ferlay J, Forman D. *Global incidence of oesophageal cancer by histological subtype in 2012*. Gut 2015, **64**(3): 381-7.

Babahosseini H, Ketene AN, Schmelz EM, Roberts PC, Agah M. *Biomechanical profile of cancer stem-like/tumor-initiating cells derived from a progressive ovarian cancer model*. Nanomedicine 2014, **10**(5): 1013-9.

Baker BM, Chen CS. *Deconstructing the third dimension - how 3d culture microenvironments alter cellular cues*. J Cell Sci 2012, **125**(13): 3015-24.

Baker EL. *Integrated roles of mechanics, motility, and disease progression in cancer*. Biomedical Engineering. UT Electronic Theses and Dissertations, The University of Texas at Austin, 2010.

Baker EL, Bonnecaze RT, Zaman MH. *Extracellular matrix stiffness and architecture govern intracellular rheology in cancer*. Biophys J 2009, **97**(4): 1013-21.

Baker EL, Srivastava J, Yu D, Bonnecaze RT, Zaman MH. *Cancer cell migration: Integrated roles of matrix mechanics and transforming potential*. PLoS One 2011, **6**(5): e20355.

Bao G, Suresh S. *Cell and molecular mechanics of biological materials*. Nat Mater 2003, **2**(11): 715-25.

Bausch AR, Kroy K. *A bottom-up approach to cell mechanics*. Nat Phys 2006, **2**(4): 231-8.

Bird-Lieberman EL, Fitzgerald RC. *Early diagnosis of oesophageal cancer*. Br J Cancer 2009, **101**(1): 1-6.

Bloomfeld RS, Bridgers DI, 3rd, Pineau BC. *Sensitivity of upper endoscopy in diagnosing esophageal cancer*. Dysphagia 2005, **20**(4): 278-82.

Bober BG, Shah SB. *Paclitaxel alters sensory nerve biomechanical properties*. J Biomech 2015, **48**(13): 3559-67.

Bouzekri A, Esch A, Ornatsky O. *Multidimensional profiling of drug-treated cells by imaging mass cytometry*. FEBS Open Bio 2019, **9**(9): 1652-69.

Bray F, Ferlay J, Soerjomataram I, Siegel RL, Torre LA, Jemal A. *Global cancer statistics 2018: Globocan estimates of incidence and mortality worldwide for 36 cancers in 185 countries*. CA Cancer J Clin 2018, **68**(6): 394-424.

Butcher DT, Alliston T, Weaver VM. *A tense situation: Forcing tumour progression*. Nat Rev Cancer 2009, **9**(2): 108-22.

Cavo M, Fato M, Penuela L, Beltrame F, Raiteri R, Scaglione S. *Microenvironment complexity and matrix stiffness regulate breast cancer cell activity in a 3d in vitro model*. Sci Rep 2016, **6**(1): 35367.

Chadwick G, Riley S, Hardwick RH, Crosby T, Hoare J, Hanna G, Greenaway K, Varagunam M, Cromwell DA, Groene O. *Population-based cohort study of the management and survival of patients with early-stage oesophageal adenocarcinoma in england*. Br J Surg 2016, **103**(5): 544-52.

Charoen KM, Fallica B, Colson YL, Zaman MH, Grinstaff MW. *Embedded multicellular spheroids as a biomimetic 3d cancer model for evaluating drug and drug-device combinations*. Biomaterials 2014, **35**(7): 2264-71.

Chen B, Co C, Ho CC. *Cell shape dependent regulation of nuclear morphology*. Biomaterials 2015, **67**: 129-36.

Chen CS, Tan J, Tien J. *Mechanotransduction at cell-matrix and cell-cell contacts*. Annu Rev Biomed Eng 2004, **6**: 275-302.

Cooper GM, Hausman RE. The cell: A molecular approach, The Yale Journal of Biology and Medicine, 2004.

Cross SE, Jin YS, Rao J, Gimzewski JK. *Nanomechanical analysis of cells from cancer patients*. Nat Nanotechnol 2007, **2**(12): 780-3.

Cukierman E, Pankov R, Stevens DR, Yamada KM. *Taking cell-matrix adhesions to the third dimension*. Science 2001, **294**(5547): 1708-12.

Dapri G, Himpens J, Cadiere GB. *Minimally invasive esophagectomy for cancer: Laparoscopic transhiatal procedure or thoracoscopy in prone position followed by laparoscopy?* Surg Endosc 2008, **22**(4): 1060-9.

De Forges H, Bouissou A, Perez F. *Interplay between microtubule dynamics and intracellular organization*. Int J Biochem Cell Biol 2012, **44**(2): 266-74.

Decitre M, Gleyzal C, Raccurt M, Peyrol S, Aubert-Foucher E, Csiszar K, Sommer P. *Lysyl oxidase-like protein localizes to sites of de novo fibrinogenesis in fibrosis and in the early stromal reaction of ductal breast carcinomas*. Lab Invest 1998, **78**(2): 143-51.

Deng Z, Lulevich V, Liu FT, Liu GY. *Applications of atomic force microscopy in biophysical chemistry of cells*. J Phys Chem B 2010, **114**(18): 5971-82.

Ding YX, Cheng Y, Sun QM, Zhang YY, You K, Guo YL, Han D, Geng L. *Mechanical characterization of cervical squamous carcinoma cells by atomic force microscopy at nanoscale*. Med Oncol 2015, **32**(3): 71.

Doyle AD, Yamada KM. *Mechanosensing via cell-matrix adhesions in 3d microenvironments*. Exp Cell Res 2016, **343**(1): 60-6.

Dzobo K, Hassen N, Senthebane DA, Thomford NE, Rowe A, Shipanga H, Wonkam A, Parker MI, Mowla S, Dandara C. *Chemoresistance to cancer treatment: Benzo-alpha-pyrene as friend or foe?* Molecules 2018, **23**(4).

Fan W. *Possible mechanisms of paclitaxel-induced apoptosis*. Biochem Pharmacol 1999, **57**(11): 1215-21.

Faria EC, Ma N, Gazi E, Gardner P, Brown M, Clarke NW, Snooka RD. *Measurement of elastic properties of prostate cancer cells using afm*. Analyst 2008, **133**(11): 1498-500.

Findlay JM, Bradley KM, Maile EJ, Braden B, Maw J, Phillips-Hughes J, Gillies RS, Maynard ND, Middleton MR. *Pragmatic staging of oesophageal cancer using decision theory involving selective endoscopic ultrasonography, pet and laparoscopy*. Br J Surg 2015, **102**(12): 1488-99.

Flanagan LA, Ju YE, Marg B, Osterfield M, Janmey PA. *Neurite branching on deformable substrates*. Neuroreport 2002, **13**(18): 2411-5.

Fletcher DA, Mullins RD. *Cell mechanics and the cytoskeleton*. Nature 2010, **463**(7280): 485-92.

Folkman J, Moscona A. *Role of cell shape in growth control*. Nature 1978, **273**(5661): 345-9.

Fuhrmann A, Staunton JR, Nandakumar V, Banyai N, Davies PC, Ros R. *Afm stiffness nanotomography of normal, metaplastic and dysplastic human esophageal cells*. Phys Biol 2011, **8**(1): 015007.

Gascoigne KE, Taylor SS. *How do anti-mitotic drugs kill cancer cells?* J cell Sci 2009, **122**(15): 2579-85.

Gautam S, Sharma C, Purohit SD, Singh H, Dinda AK, Potdar PD, Chou CF, Mishra NC. *Gelatin-polycaprolactone-nanohydroxyapatite electrospun nanocomposite scaffold for bone tissue engineering*. Mater Sci Eng C Mater Biol Appl 2021, **119**: 111588.

Geiger B, Bershadsky A. *Exploring the neighborhood: Adhesion-coupled cell mechanosensors*. Cell 2002, **110**(2): 139-42.

Gkretsi V, Stylianopoulos T. *Cell adhesion and matrix stiffness: Coordinating cancer cell invasion and metastasis*. Front Oncol 2018, **8**: 145.

Goley ED, Welch MD. *The arp2/3 complex: An actin nucleator comes of age*. Nat Rev Mol Cell Biol 2006, **7**(10): 713-26.

Gosse C, Croquette V. *Magnetic tweezers: Micromanipulation and force measurement at the molecular level*. Biophys J 2002, **82**(6): 3314-29.

Grady ME, Composto RJ, Eckmann DM. *Cell elasticity with altered cytoskeletal architectures across multiple cell types*. J Mech Behav Biomed Mater 2016, **61**: 197-207.

Guo M, Ehrlicher AJ, Jensen MH, Renz M, Moore JR, Goldman RD, Lippincott-Schwartz J, Mackintosh FC, Weitz DA. *Probing the stochastic, motor-driven properties of the cytoplasm using force spectrum microscopy*. Cell 2014, **158**(4): 822-32.

Gurusamy KS, Pallari E, Midya S, Mughal M. *Laparoscopic versus open transhiatal oesophagectomy for oesophageal cancer*. Cochrane Database Syst Rev 2016, **3**(3): CD011390.

Helmke BP, Davies PF. *The cytoskeleton under external fluid mechanical forces: Hemodynamic forces acting on the endothelium*. Ann Biomed Eng 2002, **30**(3): 284-96.

Herrmann H, Bar H, Kreplak L, Strelkov SV, Aebi U. *Intermediate filaments: From cell architecture to nanomechanics*. Nat Rev Mol Cell Biol 2007, **8**(7): 562-73.

Hochmuth RM. *Micropipette aspiration of living cells*. J Biomech 2000, **33**(1): 15-22.

Hu S, Chen J, Fabry B, Numaguchi Y, Gouldstone A, Ingber DE, Fredberg JJ, Butler JP, Wang N. *Intracellular stress tomography reveals stress focusing and structural anisotropy in cytoskeleton of living cells*. Am J Physiol Cell Physiol 2003, **285**(5): C1082-90.

Huang S, Ingber DE. *Cell tension, matrix mechanics, and cancer development*. Cancer Cell 2005, **8**(3): 175-6.

Humphrey JD, Dufresne ER, Schwartz MA. *Mechanotransduction and extracellular matrix homeostasis*. Nat Rev Mol Cell Biol 2014, **15**(12): 802-12.

Hynes RO. *The extracellular matrix: Not just pretty fibrils*. Science 2009, **326**(5957): 1216-9.

Islam M, Mezencev R, Mcfarland B, Brink H, Campbell B, Tasadduq B, Waller EK, Lam W, Alexeev A, Sulchek T. *Microfluidic cell sorting by stiffness to examine heterogenic responses of cancer cells to chemotherapy*. Cell Death Dis 2018, **9**(2): 239.

Isomoto H, Yamaguchi N, Minami H, Nakao K. *Management of complications associated with endoscopic submucosal dissection/endoscopic mucosal resection for esophageal cancer*. Dig Endosc 2013, **25**: 29-38.

Janmey PA. *The cytoskeleton and cell signaling: Component localization and mechanical coupling*. Physiol Rev 1998, **78**(3): 763-81.

Janmey PA, Weitz DA. *Dealing with mechanics: Mechanisms of force transduction in cells*. Trends Biochem Sci 2004, **29**(7): 364-70.

Jemal A, Bray F, Center MM, Ferlay J, Ward E, Forman D. *Global cancer statistics*. CA Cancer J Clin 2011, **61**(2): 69-90.

Jordan MA, Wendell K, Gardiner S, Derry WB, Copp H, Wilson L. *Mitotic block induced in hela cells by low concentrations of paclitaxel (taxol) results in abnormal mitotic exit and apoptotic cell death*. Cancer Res 1996, **56**(4): 816-25.

Jordan MA, Wilson L. *Microtubules as a target for anticancer drugs*. Nat Rev Cancer 2004, **4**(4): 253-65.

Kasza KE, Rowat AC, Liu JY, Angelini TE, Brangwynne CP, Koenderink GH, Weitz DA. *The cell as a material*. Curr Opin Cell Biol 2007, **19**(1): 101-7.

Kim HH, Park SJ, Lee SH, Park HU, Song CS, Park MI, Moon W. *Efficacy of endoscopic submucosal resection with a ligation device for removing small rectal carcinoid tumor compared with endoscopic mucosal resection: Analysis of 100 cases*. Dig Endosc 2012, **24**(3): 159-63.

Kim JE, Reynolds DS, Zaman MH, Mak M. *Characterization of the mechanical properties of cancer cells in 3d matrices in response to collagen concentration and cytoskeletal inhibitors*. Integr Biol (Camb) 2018, **10**(4): 232-41.

Kim JJ, Tannock IF. *Repopulation of cancer cells during therapy: An important cause of treatment failure*. Nat Rev Cancer 2005, **5**(7): 516-25.

Kim SH, Turnbull J, Guimond S. *Extracellular matrix and cell signalling: The dynamic cooperation of integrin, proteoglycan and growth factor receptor*. J Endocrinol 2011, **209**(2): 139-51.

Klevebro F, Alexandersson Von Dobeln G, Wang N, Johnsen G, Jacobsen AB, Friesland S, Hatlevoll I, Glenjen NI, Lind P, Tsai JA, Lundell L, Nilsson M. *A randomized clinical trial of neoadjuvant chemotherapy versus neoadjuvant chemoradiotherapy for cancer of the oesophagus or gastro-oesophageal junction*. Ann Oncol 2016, **27**(4): 660-7.

Kubitschke H, Schnauss J, Nnetu KD, Warmt E, Stange R, Kaes J. *Actin and microtubule networks contribute differently to cell response for small and large strains*. New J Phys 2017, **19**(9): 093003.

Kumar S, Weaver VM. *Mechanics, malignancy, and metastasis: The force journey of a tumor cell*. Cancer Metastasis Rev 2009, **28**(1-2): 113-27.

Lagergren J, Lagergren P. *Oesophageal cancer*. BMJ 2010, **341**: c6280.

Lagergren J, Smyth E, Cunningham D, Lagergren P. *Oesophageal cancer*. Lancet 2017, **390**(10110): 2383-96.

Lam WA, Rosenbluth MJ, Fletcher DA. *Chemotherapy exposure increases leukemia cell stiffness*. Blood 2007, **109**(8): 3505-8.

Lekka M, Gil D, Pogoda K, Dulinska-Litewka J, Jach R, Gostek J, Klymenko O, Prauzner-Bechcicki S, Stachura Z, Wiltowska-Zuber J, Okon K, Laidler P. *Cancer cell detection in tissue sections using afm*. Arch Biochem Biophys 2012, **518**(2): 151-6.

Li QS, Lee GY, Ong CN, Lim CT. *Afm indentation study of breast cancer cells*. Biochem Biophys Res Commun 2008, **374**(4): 609-13.

Lin HH, Lin HK, Lin IH, Chiou YW, Chen HW, Liu CY, Harn HI, Chiu WT, Wang YK, Shen MR, Tang MJ. *Mechanical phenotype of cancer cells: Cell softening and loss of stiffness sensing*. Oncotarget 2015, **6**(25): 20946-58.

Lin L, Lin DC. *Biological significance of tumor heterogeneity in esophageal squamous cell carcinoma*. Cancers (Basel) 2019, **11**(8): 1156.

Liu W, Wu C. *Rheological study of soft matters: A review of microrheology and microrheometers*. Macromol Chem Phys 2018, **219**(3): 1700307.

Liu X, Zhang X, Lee I. *A quantitative study on morphological responses of osteoblastic cells to fluid shear stress*. Acta Biochim Biophys Sin (Shanghai) 2010, **42**(3): 195-201.

Louise C, Etienne D, Marie-Pierre R. *Afm sensing cortical actin cytoskeleton destabilization during plasma membrane electropermeabilization*. Cytoskeleton (Hoboken) 2014, **71**(10): 587-94.

Lu P, Weaver VM, Werb Z. *The extracellular matrix: A dynamic niche in cancer progression*. J Cell Biol 2012, **196**(4): 395-406.

Luketich JD, Schauer PR, Christie NA, Weigel TL, Raja S, Fernando HC, Keenan RJ, Nguyen NT. *Minimally invasive esophagectomy*. Ann Thorac Surg 2000, **70**(3): 906-11; discussion 11-2.

Mahoney L, Csima A. *Efficiency of palpation in clinical detection of breast cancer*. Can Med Assoc J 1982, **127**(8): 729-30.

Mak M, Anderson S, Mcdonough MC, Spill F, Kim JE, Boussommier-Calleja A, Zaman MH, Kamm RD. *Integrated analysis of intracellular dynamics of menainv cancer cells in a 3d matrix*. Biophys J 2017, **112**(9): 1874-84.

Mak M, Kamm RD, Zaman MH. *Impact of dimensionality and network disruption on microrheology of cancer cells in 3d environments*. PLoS Comput Biol 2014, **10**(11): e1003959.

Malandrino A, Kamm RD, Moeendarbary E. *In vitro modeling of mechanics in cancer metastasis*. ACS Biomater Sci Eng 2018, **4**(2): 294-301.

Malta DFB, Reticker-Flynn NE, Da Silva CL, Cabral JMS, Fleming HE, Zaret KS, Bhatia SN, Underhill GH. *Extracellular matrix microarrays to study inductive signaling for endoderm specification*. Acta Biomater 2016, **34**: 30-40.

Mandal K, Asnacios A, Goud B, Manneville JB. *Mapping intracellular mechanics on micropatterned substrates*. Proc Natl Acad Sci U S A 2016, **113**(46): E7159-E68.

Mason TG, Ganesan K, Vanzanten JH, Wirtz D, Kuo SC. *Particle tracking microrheology of complex fluids*. Phys Rev Lett 1997, **79**(17): 3282-5.

Mcbeath R, Pirone DM, Nelson CM, Bhadriraju K, Chen CS. *Cell shape, cytoskeletal tension, and rhoa regulate stem cell lineage commitment*. Dev Cell 2004, **6**(4): 483-95.

Mckeown KC. *Total three-stage oesophagectomy for cancer of the oesophagus*. Br J Surg 1976, **63**(4): 259-62.

Mihai C, Bao SY, Lai JP, Ghadiali SN, Knoell DL. *Pten inhibition improves wound healing in lung epithelia through changes in cellular mechanics that enhance migration*. Am J Physiol-Lung C 2012, **302**(3): L287-L99.

Mitchison T, Kirschner M. *Dynamic instability of microtubule growth*. Nature 1984, **312**(5991): 237-42.

Moeendarbary E, Harris AR. *Cell mechanics: Principles, practices, and prospects*. Wiley Interdiscip Rev Syst Biol Med 2014, **6**(5): 371-88.

Moffitt JR, Chemla YR, Smith SB, Bustamante C. *Recent advances in optical tweezers*. Annu Rev Biochem 2008, **77**: 205-28.

Mofrad MRK. *Rheology of the cytoskeleton*. Annu Rev Fluid Mech 2009, **41**: 433-53.

Mucke N, Kreplak L, Kirmse R, Wedig T, Herrmann H, Aebi U, Langowski J. *Assessing the flexibility of intermediate filaments by atomic force microscopy*. J Mol Biol 2004, **335**(5): 1241-50.

Nematbakhsh Y, Pang KT, Lim CT. *Correlating the viscoelasticity of breast cancer cells with their malignancy*. Converg Sci Phys Oncol 2017, **3**(3): 034003.

Network TPS-OC, Agus DB, Alexander JF, Arap W, Ashili S, Aslan JE, Austin RH, Backman V, Bethel KJ, Bonneau R. *A physical sciences network characterization of non-tumorigenic and metastatic cells*. Sci Rep 2013, **3**: 1449.

Ning B, Abdelfatah MM, Othman MO. *Endoscopic submucosal dissection and endoscopic mucosal resection for early stage esophageal cancer*. Ann Cardiothorac Surg 2017, **6**(2): 88-98.

Nyhan MJ, O'donovan TR, Boersma AW, Wiemer EA, Mckenna SL. *Mir-193b promotes autophagy and non-apoptotic cell death in oesophageal cancer cells*. BMC Cancer 2016, **16**(1): 101.

O'sullivan G C, Sheehan D, Clarke A, Stuart R, Kelly J, Kiely MD, Walsh T, Collins JK, Shanahan F. *Micrometastases in esophagogastric cancer: High detection rate in resected rib segments*. Gastroenterology 1999, **116**(3): 543-8.

Orr AW, Helmke BP, Blackman BR, Schwartz MA. *Mechanisms of mechanotransduction*. Dev Cell 2006, **10**(1): 11-20.

Orringer MB, Sloan H. *Esophagectomy without thoracotomy*. J Thorac Cardiov Sur 1978, **76**(5): 643-54.

Paccez JD, Duncan K, Vava A, Correa RG, Libermann TA, Parker MI, Zerbini LF. *Inactivation of gsk3beta and activation of nf-kappab pathway via axl represents an important mediator of tumorigenesis in esophageal squamous cell carcinoma*. Mol Biol Cell 2015, **26**(5): 821-31.

Pachenari M, Seyedpour SM, Janmaleki M, Babazadeh Shayan S, Taranejoo S, Hosseinkhani H. *Mechanical properties of cancer cytoskeleton depend on actin filaments to microtubules content: Investigating different grades of colon cancer cell lines*. J Biomech 2014, **47**(2): 373-9.

Park S. *Nano-mechanical phenotype as a promising biomarker to evaluate cancer development, progression, and anti-cancer drug efficacy*. J Cancer Prev 2016, **21**(2): 73-80.

Pelham RJ, Jr., Wang Y. *Cell locomotion and focal adhesions are regulated by substrate flexibility*. Proc Natl Acad Sci U S A 1997, **94**(25): 13661-5.

Pennathur A, Gibson MK, Jobe BA, Luketich JD. *Oesophageal carcinoma*. Lancet 2013, **381**(9864): 400-12.

Phillip JM, Han KS, Chen WC, Wirtz D, Wu PH. *A robust unsupervised machine-learning method to quantify the morphological heterogeneity of cells and nuclei*. Nat Protoc 2021, **16**(2): 754-74.

Pine DJ, Weitz DA, Zhu JX, Herbolzheimer E. *Diffusing-wave spectroscopy - dynamic light-scattering in the multiple-scattering limit*. J Phys-Paris 1990, **51**(18): 2101-27.

Pogoda K, Jaczewska J, Wiltowska-Zuber J, Klymenko O, Zuber K, Fornal M, Lekka M. *Depth-sensing analysis of cytoskeleton organization based on afm data*. Eur Biophys J 2012, **41**(1): 79-87.

Pogoda K, Pieta E, Roman M, Piergies N, Liberda D, Wrobel TP, Janmey PA, Paluszkiewicz C, Kwiatek WM. *In search of the correlation between nanomechanical and biomolecular properties of prostate cancer cells with different metastatic potential*. Arch Biochem Biophys 2021, **697**: 108718.

Prabhune M, Belge G, Dotzauer A, Bullerdiek J, Radmacher M. *Comparison of mechanical properties of normal and malignant thyroid cells*. Micron 2012, **43**(12): 1267-72.

Pritchard RH, Huang YY, Terentjev EM. *Mechanics of biological networks: From the cell cytoskeleton to connective tissue*. Soft Matter 2014, **10**(12): 1864-84.

Puig-De-Morales M, Grabulosa M, Alcaraz J, Mullol J, Maksym GN, Fredberg JJ, Navajas D. *Measurement of cell microrheology by magnetic twisting cytometry with frequency domain demodulation*. J Appl Physiol (1985) 2001, **91**(3): 1152-9.

Quinlan AMT, Sierad LN, Capulli AK, Firstenberg LE, Billiar KL. *Combining dynamic stretch and tunable stiffness to probe cell mechanobiology in vitro*. Plos One 2011, **6**(8): e23272.

Radmacher M, Tillamnn RW, Fritz M, Gaub HE. *From molecules to cells: Imaging soft samples with the atomic force microscope*. Science 1992, **257**(5078): 1900-5.

Rajagopalan P, Marganski WA, Brown XQ, Wong JY. *Direct comparison of the spread area, contractility, and migration of balb/c 3t3 fibroblasts adhered to fibronectin- and rgd-modified substrata*. Biophys J 2004, **87**(4): 2818-27.

Ramos JR, Pabijan J, Garcia R, Lekka M. *The softening of human bladder cancer cells happens at an early stage of the malignancy process*. Beilstein J Nanotech 2014, **5**(1): 447-57.

Rasbridge SA, Gillett CE, Seymour AM, Patel K, Richards MA, Rubens RD, Millis RR. *The effects of chemotherapy on morphology, cellular proliferation, apoptosis and oncoprotein expression in primary breast carcinoma*. Br J Cancer 1994, **70**(2): 335-41.

Raudenska M, Kratochvilova M, Vicar T, Gumulec J, Balvan J, Polanska H, Pribyl J, Masarik M. *Cisplatin enhances cell stiffness and decreases invasiveness rate in prostate cancer cells by actin accumulation*. Sci Rep 2019, **9**(1): 1660.

Remmerbach TW, Wottawah F, Dietrich J, Lincoln B, Wittekind C, Guck J. *Oral cancer diagnosis by mechanical phenotyping*. Cancer Res 2009, **69**(5): 1728-32.

Ren J, Huang H, Liu Y, Zheng X, Zou Q. *An atomic force microscope study revealed two mechanisms in the effect of anticancer drugs on rate-dependent young's modulus of human prostate cancer cells*. PLoS One 2015, **10**(5): e0126107.

Reynolds DS, Tevis KM, Blessing WA, Colson YL, Zaman MH, Grinstaff MW. *Breast cancer spheroids reveal a differential cancer stem cell response to chemotherapeutic treatment*. Sci Rep 2017, **7**(1): 10382.

Rianna C, Radmacher M. *Comparison of viscoelastic properties of cancer and normal thyroid cells on different stiffness substrates*. Eur Biophys J 2017, **46**(4): 309-24.

Rice TW, Ishwaran H, Ferguson MK, Blackstone EH, Goldstraw P. *Cancer of the esophagus and esophagogastric junction: An eighth edition staging primer*. J Thorac Oncol 2017, **12**(1): 36-42.

Rodriguez ML, Mcgarry PJ, Sniadecki NJ. *Review on cell mechanics: Experimental and modeling approaches*. Appl Mech Rev 2013, **65**(6).

Rosenbluth MJ, Lam WA, Fletcher DA. *Force microscopy of nonadherent cells: A comparison of leukemia cell deformability*. Biophys J 2006, **90**(8): 2994-3003.

Samuel MS, Lopez JI, Mcghee EJ, Croft DR, Strachan D, Timpson P, Munro J, Schroder E, Zhou J, Brunton VG, Barker N, Clevers H, Sansom OJ, Anderson KI, Weaver VM, Olson MF. *Actomyosin-mediated cellular tension drives increased tissue stiffness and beta-catenin activation to induce epidermal hyperplasia and tumor growth*. Cancer Cell 2011, **19**(6): 776-91.

Schlansky B, Dimarino AJ, Jr., Loren D, Infantolino A, Kowalski T, Cohen S. *A survey of oesophageal cancer: Pathology, stage and clinical presentation*. Aliment Pharmacol Ther 2006, **23**(5): 587-93.

Schultz KM, Furst EM. *Microrheology of biomaterial hydrogelators*. Soft Matter 2012, **8**(23): 6198-205.

Selvaggi L, Salemme M, Vaccaro C, Pesce G, Rusciano G, Sasso A, Campanella C, Carotenuto R. *Multiple-particle-tracking to investigate viscoelastic properties in living cells*. Methods 2010, **51**(1): 20-6.

Senkowski CK, Adams MT, Beck AN, Brower ST. *Minimally invasive esophagectomy: Early experience and outcomes*. Am Surg 2006, **72**(8): 677-83; discussion 83.

Shapiro J, Van Lanschot JJB, Hulshof M, Van Hagen P, Van Berge Henegouwen MI, Wijnhoven BPL, Van Laarhoven HWM, Nieuwenhuijzen GaP, Hospers GaP, Bonenkamp JJ, Cuesta MA, Blaisse RJB, Busch ORC, Ten Kate FJW, Creemers GM, Punt CJA, Plukker JTM, Verheul HMW, Bilgen EJS, Van Dekken H, Van Der Sangen MJC, Rozema T, Biermann K, Beukema JC, Piet AHM, Van Rij CM, Reinders JG, Tilanus HW, Steyerberg EW, Van Der Gaast A, Group CS. *Neoadjuvant chemoradiotherapy plus surgery versus surgery alone for oesophageal or junctional cancer (cross): Long-term results of a randomised controlled trial*. Lancet Oncol 2015, **16**(9): 1090-8.

Sharma S, Santiskulvong C, Rao J, Gimzewski JK, Dorigo O. *The role of rho gtpase in cell stiffness and cisplatin resistance in ovarian cancer cells*. Integr Biol (Camb) 2014, **6**(6): 611-7.

Sharp DJ, Rogers GC, Scholey JM. *Microtubule motors in mitosis.* Nature 2000, **407**(6800): 41-7.

Siyo V, Schafer G, Hunter R, Grafov A, Grafova I, Nieger M, Katz AA, Parker MI, Kaschula CH. *The cytotoxicity of the ajoene analogue bispmb in whco1 oesophageal cancer cells is mediated by chop/gadd153*. Molecules 2017, **22**(6).

Smith M, Hunter R, Stellenboom N, Kusza DA, Parker MI, Hammouda AN, Jackson G, Kaschula CH. *The cytotoxicity of garlic-related disulphides and thiosulfonates in whco1 oesophageal cancer cells is dependent on s-thiolation and not production of ros*. Biochim Biophys Acta 2016, **1860**(7): 1439-49.

Staunton JR, So WY, Paul CD, Tanner K. *High-frequency microrheology in 3d reveals mismatch between cytoskeletal and extracellular matrix mechanics*. P Natl Acad Sci USA 2019, **116**(29): 14448-55.

Stern MM, Myers RL, Hammam N, Stern KA, Eberli D, Kritchevsky SB, Soker S, Van Dyke M. *The influence of extracellular matrix derived from skeletal muscle tissue on the proliferation and differentiation of myogenic progenitor cells ex vivo*. Biomaterials 2009, **30**(12): 2393-9.

Su XD, Zhang DK, Zhang X, Lin P, Long H, Rong TH. *Prognostic factors in patients with recurrence after complete resection of esophageal squamous cell carcinoma*. J Thorac Dis 2014, **6**(7): 949-57.

Sun M, Chi G, Li P, Lv S, Xu J, Xu Z, Xia Y, Tan Y, Xu J, Li L, Li Y. *Effects of matrix stiffness on the morphology, adhesion, proliferation and osteogenic differentiation of mesenchymal stem cells*. Int J Med Sci 2018, **15**(3): 257-68.

Suresh S. *Biomechanics and biophysics of cancer cells*. Acta Biomater 2007, **3**(4): 413-38.

Tan C, Qian X, Guan Z, Yang B, Ge Y, Wang F, Cai J. *Potential biomarkers for esophageal cancer*. Springerplus 2016, **5**: 467.

Tarantino N, Tinevez JY, Crowell EF, Boisson B, Henriques R, Mhlanga M, Agou F, Israel A, Laplantine E. *Tnf and il-1 exhibit distinct ubiquitin requirements for inducing nemo-ikk supramolecular structures*. J Cell Biol 2014, **204**(2): 231-45.

Thoumine O, Ott A. *Comparison of the mechanical properties of normal and transformed fibroblasts*. Biorheology 1997, **34**(4-5): 309-26.

Thun M, Linet MS, Cerhan JR, Haiman CA, Schottenfeld D. Cancer epidemiology and prevention, Oxford University Press, 2017.

Tibbitt MW, Anseth KS. *Hydrogels as extracellular matrix mimics for 3d cell culture*. Biotechnol Bioeng 2009, **103**(4): 655-63.

Tilghman RW, Cowan CR, Mih JD, Koryakina Y, Gioeli D, Slack-Davis JK, Blackman BR, Tschumperlin DJ, Parsons JT. *Matrix rigidity regulates cancer cell growth and cellular phenotype*. PLoS One 2010, **5**(9): e12905.

Tinevez J-Y, Herbert S. *The nemo dots assembly: Single-particle tracking and analysis* Bioimage data analysis workflows, Springer, Cham, 2020: 67-96.

Tinevez JY, Perry N, Schindelin J, Hoopes GM, Reynolds GD, Laplantine E, Bednarek SY, Shorte SL, Eliceiri KW. *Trackmate: An open and extensible platform for single-particle tracking*. Methods 2017, **115**: 80-90.

Trickey WR, Lee GM, Guilak F. *Viscoelastic properties of chondrocytes from normal and osteoarthritic human cartilage*. J Orthop Res 2000, **18**(6): 891-8.

Tseng Y, Kole TP, Wirtz D. *Micromechanical mapping of live cells by multiple-particle-tracking microrheology*. Biophys J 2002, **83**(6): 3162-76.

Ulrich TA, De Juan Pardo EM, Kumar S. *The mechanical rigidity of the extracellular matrix regulates the structure, motility, and proliferation of glioma cells*. Cancer Res 2009, **69**(10): 4167-74.

Unal M, Alapan Y, Jia H, Varga AG, Angelino K, Aslan M, Sayin I, Han C, Jiang Y, Zhang Z, Gurkan UA. *Micro and nano-scale technologies for cell mechanics*. Nanobiomedicine (Rij) 2014, **1**: 5.

Von Dobeln GA, Klevebro F, Jacobsen AB, Johannessen HO, Nielsen NH, Johnsen G, Hatlevoll I, Glenjen NI, Friesland S, Lundell L, Yu J, Nilsson M. *Neoadjuvant chemotherapy versus neoadjuvant chemoradiotherapy for cancer of the esophagus or gastroesophageal junction: Long-term results of a randomized clinical trial*. Dis Esophagus 2019, **32**(2): doy078.

Wakatsuki T, Schwab B, Thompson NC, Elson EL. *Effects of cytochalasin d and latrunculin b on mechanical properties of cells*. J Cell Sci 2001, **114**(Pt 5): 1025-36.

Wang X, Jia Y, Deng H, Liu Y, Liu Y. *Intratumoral heterogeneity of esophageal squamous cell carcinoma and its clinical significance*. Pathol Res Pract 2019, **215**(2): 308-14.

Weaver BA. *How taxol/paclitaxel kills cancer cells*. Mol Biol Cell 2014, **25**(18): 2677-81.

Weber A, Iturri J, Benitez R, Zemljic-Jokhadar S, Toca-Herrera JL. *Microtubule disruption changes endothelial cell mechanics and adhesion*. Sci Rep 2019, **9**(1): 14903.

Weihs D, Mason TG, Teitell MA. *Bio-microrheology: A frontier in microrheology*. Biophys J 2006, **91**(11): 4296-305.

Weinberg RA. *The biology of cancer. New york, USA: Garland science*, Taylor & Francis Group, LLC, 2007.

Wirtz D. *Particle-tracking microrheology of living cells: Principles and applications*. Annu Rev Biophys 2009, **38**: 301-26.

Working MRCOC. *Surgical resection with or without preoperative chemotherapy in oesophageal cancer: A randomised controlled trial*. The Lancet 2002, **359**(9319): 1727-33.

World Health Organization. *Who report on cancer: Setting priorities, investing wisely and providing care for all*, 2020.

Wu PH, Phillip JM, Khatau SB, Chen WC, Stirman J, Rosseel S, Tschudi K, Van Patten J, Wong M, Gupta S, Baras AS, Leek JT, Maitra A, Wirtz D. *Evolution of cellular morpho-phenotypes in cancer metastasis*. Sci Rep 2015, **5**: 18437.

Xu K, Babcock HP, Zhuang X. *Dual-objective storm reveals three-dimensional filament organization in the actin cytoskeleton*. Nat Methods 2012, **9**(2): 185-8.

Xu WW, Mezencev R, Kim B, Wang LJ, Mcdonald J, Sulchek T. *Cell stiffness is a biomarker of the metastatic potential of ovarian cancer cells*. Plos One 2012, **7**(10): e46609.

Yamamoto M, Weber JM, Karl RC, Meredith KL. *Minimally invasive surgery for esophageal cancer: Review of the literature and institutional experience*. Cancer Control 2013, **20**(2): 130-7.

Yan T, Cui H, Zhou Y, Yang B, Kong P, Zhang Y, Liu Y, Wang B, Cheng Y, Li J, Guo S, Xu E, Liu H, Cheng C, Zhang L, Chen L, Zhuang X, Qian Y, Yang J, Ma Y, Li H, Wang F, Liu J, Liu X, Su D, Wang Y, Sun R, Guo S, Li Y, Cheng X, Liu Z, Zhan Q, Cui Y. *Multi-region sequencing unveils novel actionable targets and spatial heterogeneity in esophageal squamous cell carcinoma*. Nat Commun 2019, **10**(1): 1670.

Ychou M, Boige V, Pignon JP, Conroy T, Bouche O, Lebreton G, Ducourtieux M, Bedenne L, Fabre JM, Saint-Aubert B, Geneve J, Lasser P, Rougier P. *Perioperative chemotherapy compared with surgery alone for resectable gastroesophageal adenocarcinoma: An fnclcc and ffcd multicenter phase iii trial*. J Clin Oncol 2011, **29**(13): 1715-21.

Zaman MH, Trapani LM, Sieminski AL, Mackellar D, Gong H, Kamm RD, Wells A, Lauffenburger DA, Matsudaira P. *Migration of tumor cells in 3d matrices is governed by matrix stiffness along with cell-matrix adhesion and proteolysis*. Proc Natl Acad Sci 2006, **103**(29): 10889-94.

Zhang H, Liu KK. *Optical tweezers for single cells*. J R Soc Interface 2008, **5**(24): 671-90.

Zhen Q, Gao LN, Wang RF, Chu WW, Zhang YX, Zhao XJ, Lv BL, Liu JB. *Lncrna pcat-1 promotes tumour growth and chemoresistance of oesophageal cancer to cisplatin*. Cell Biochem Funct 2018, **36**(1): 27-33.

Zimmerman SB, Minton AP. *Macromolecular crowding: Biochemical, biophysical, and physiological consequences*. Annu Rev Biophys Biomol Struct 1993, **22**(1): 27-65.

Appendix

Supplementary Information for Chapter 2

Preparation of DMEM

A vial of powdered DMEM and 3.7 g of sodium bicarbonate ($NaHCO_3$) were added to 900 ml of distilled water and stirred with a magnetic stirrer until it dissolved. The solution's pH was adjusted to 7.4 using either hydrochloric acid (1N HCl) or sodium hydroxide (1N NaOH). The DMEM solution was then brought up to 1 litre with distilled water. Lastly, it was filtered and sterilized using a 0.2 µm membrane filter.

Preparation of cell culture growth media

10 % FBS and 1 % Streptomycin-Penicillin stock were added to DMEM prepared in the section above 0to make growth media for the WHCO1 cells. For example, to make 500 ml of growth media, 50 ml of FBS and 5 ml of Streptomycin-Penicillin stock were added to a sterile container and then brought to 500 ml by adding 445 ml of DMEM.

Preparation of PBS

2.9 g of 8 mM $Na_2HPO_412H_2O$ (Sodium phosphate dibasic dodecahydrate), 0.2 g of 1.4 mM KH_2PO_4 (Potassium dihydrogen phosphate), 0.2 g of 2.7 mM KCl (Potassium chloride), and 8 g of 137 mM NaCl (Sodium chloride) were dissolved in 900 ml of distilled water and stirred with a magnetic stirrer until they completely dissolved. The solution's pH was adjusted to 7.4 using either 1N HCl or 1N NaOH and then topped with distilled water to make one litre of PBS solution. It was then labelled and autoclaved before use in cell culture.

Preparation of Paclitaxel

A stock solution of 1 mM of Paclitaxel was prepared from 16.7 ml of Paclitaxel drug containing 49.7 % ethanol. The stock solution was then diluted with fresh growth media to make the required concentrations of Paclitaxel. I mM of Paclitaxel drug contains 5.988 mg of Paclitaxel. The molecular weight of Paclitaxel is 853.906.

$$mg = mM \times molecular\ weight \times volume\ in\ litres \quad (a.\ 1)$$

$$mM = \frac{(5.988 \times 1000)}{853.906} = 7.0125\ mM = 7012.5\ \mu M \quad (a.\ 2)$$

$$C1V1 = C2V2 \quad (a.\ 3)$$

$$V1 = \frac{(1000 \times 1.5)}{7012.5} = 214\ \mu l \quad (a.\ 4)$$

Where:

- C_1 represents the initial concentration (e.g., 7012.5 µM of Paclitaxel),
- C_2 the required concentration (e.g., 1 mM of Paclitaxel),
- V_1 the unknown volume to be pipetted from the original/stock solution, and
- V_2 represents the required volume (e.g., 1.5 ml of Paclitaxel).

From Eq. (a. 1) and (a. 2), 5.988 mg/ml contains 7012.5 µM of Paclitaxel. 1286 µl of growth was added to 213.9 µl of the initial concentration of Paclitaxel, obtained using Eq. (a. 3) and (a. 4), to make 1.5 ml of 1mM of Paclitaxel stock solution. The stock solution was diluted further to make up the required concentration of Paclitaxel using Eq. (a. 3). For example, to make 1.5 ml of 10 µM of Paclitaxel, 15 µl of stock solution was added to 1485 µl of fresh growth media.

Preparation of collagen

Firstly, the collagen concentrations, neutralizing solution (HEPES buffer), PBS, and cell suspension required to prepare the collagen solution were calculated. For example, preparing 2 gels, collagen concentration of 2 mg/ml and a gel volume of 50 µl, the calculations as shown in Eq. (a. 5) and (a. 6) were done:

$$Collagen\ solution\ needed = \frac{\#gels \times collagen\ concentration \times gel\ vol}{stock\ solution\ concentration} \quad (a.\ 5)$$

$$collagen\ solution\ needed = \left(\frac{2\ gels \times 2\ mg/ml \times 50\ \mu l}{8.21\ mg/ml}\right) = 24.4\ \mu l \quad (a.\ 6)$$

Collagen and the neutralizing solution were used in a ratio of 1:1; therefore, to 24.4 µl of collagen solution, 24.4 µl of the neutralisation solution (100 mM HEPES buffer) was added.

Cell suspension volume is 10 % of the gels' required total volume and was calculated using Eq. (a. 7) below. For example, the volume of cell suspension seeded in 50 µl of gel solution was 10 µl.

$$Cell\ suspension\ volume\ = \left(\frac{10}{100} \times\ (2\ gels\ \times 50\ \mu l\ volume\ of\ gels)\right) = 10\ \mu l \qquad (a.\ 7)$$

The rest of the gel was diluted in PBS to the desired collagen concentration, as shown in Eq. (a. 8) and (a. 9).

$$PBS\ volume\ = (total\ gel\ volume) -\ (volume\ of\ collagen\ solution) - (volume\ of\ neutrazing\ solution) -\ (volume\ of\ cell\ suspension) \qquad (a.\ 8)$$

$$PBS\ volume\ =\ [(2\ gels\ \times 50\ \mu l) - 24.4\ \mu l - 24.4\ \mu l - 10\ \mu l]\ =\ 41.2\ \mu l \qquad (a.\ 9)$$

MitoTracker dilution

A package of MitoTracker green contains 20 vials, each of 50 µg. The molecular weight of Mitotracker green is 671.88 g/mol (obtained from the label on the package). To make 1 mM of stock solution, we diluted the 50 µg of Mitotracker green with 74.42 µl of DMSO calculated as shown in Eq. (a. 10) and (a. 11).

$$\left(\frac{1\ mol}{671.88\ g}\right) \times \left(\frac{50\ \mu g}{x\ l}\right)\ = 1\ mM\ =\ 10^{-3}\ mol/l \qquad (a.\ 10)$$

$$x\ = 74.42\ \mu l \qquad (a.\ 11)$$

The desired concentrations for experimental conditions were obtained by diluting the stock solution of 1 mM Mitotracker green with fresh growth media using Eq. (a. 3) as follows.

For example, to make 100 nM of Mitotracker green solution, dilute 0.5 µl of stock solution in 5 ml of media; for 400 nM, dilute 2 µl of stock solution in 5 ml of media.

Supplementary Information for Chapter 3

Mitochondrial Particle Tracking Microrheology experiments in 2D environments

Descriptive statistics

Table S. 1: Summaries of mean MSDs (μm²) and standard deviations of mitochondrial fluctuations from 79 individual WHCO1 cells in 2D environments at 24 and 48 hours of treatment. PTX and UNT stand for Paclitaxel-treated and untreated cells, respectively. MSDs at τ = 0.7 s were transformed using a logarithmic function, whereas τ = 6.3, 7.7 and 9.1 s were transformed using a square root function, respectively, after failing the normality test.

Delay (s)	Mean (M)						Standard Deviation (SD)					
	PTX		UNT		ETH		PTX		UNT		ETH	
	24	***48***	***24***	***48***	***24***	***48***	***24***	***48***	***24***	***48***	***24***	***48***
0.14	.003	.003	.003	.003	.003	.003	.0002	.0004	.0003	.0002	.0003	.0004
0.7	-2.1	-2.1	-2.1	-2.1	-2.2	-2.3	.1009	.0494	.0673	.1249	.1261	.0886
3.5	0.04	0.03	0.03	0.03	0.03	0.01	.0142	.0054	.0095	.0129	.0138	.0067
6.3	.241	.224	.243	.235	.209	.156	.0540	.0260	.0404	.0492	.0668	.0434
7.7	.263	.241	.268	.257	.231	.172	.061	.031	.049	.054	.078	.051
9.1	.284	.261	.290	.277	.252	.188	.067	.034	.059	.059	.091	.060

Table S. 2: Summaries of mean fluidity and standard deviations of mitochondrial fluctuations from 79 individual WHCO1 cells in 2D environments at 24 and 48 hours of treatment. PTX and UNT stand for Paclitaxel-treated and untreated cells, respectively. Fluidity values at τ = 6.3 and 9.1 s were transformed using a logarithmic and square root function, respectively, after failing the normality test.

Delay (s)	Mean (M)						Standard Deviation (SD)					
	UNT		ETH		PTX		UNT		ETH		PTX	
	24	***48***	***24***	***48***	***24***	***48***	***24***	***48***	***24***	***48***	***24***	***48***
0.28	0.43	0.40	0.41	0.42	0.31	0.20	0.15	0.07	0.11	0.14	0.12	0.09
0.7	0.73	0.72	0.73	0.71	0.61	0.38	0.18	0.10	0.13	0.20	0.19	0.20
2.1	0.92	0.91	0.96	0.85	0.85	0.68	0.10	0.07	0.12	0.13	0.15	0.21
3.5	0.91	0.88	0.96	0.88	0.91	0.82	0.11	0.11	0.11	0.12	0.15	0.18
4.9	0.91	0.83	0.93	0.84	0.95	0.90	0.11	0.14	0.19	0.15	0.23	0.20
6.3	-0.05	-0.08	-0.04	-0.06	-0.04	-0.03	0.07	0.08	0.12	0.07	0.10	0.09
9.1	0.91	0.88	0.92	0.95	0.93	0.95	0.10	0.10	0.22	0.10	0.18	0.21

Two-way ANOVA results

Table S. 3: Two-way ANOVA results summarising the significance of the interaction between drug treatment intervention (untreated and Paclitaxel-treated cells) and duration of treatment (24 and 48 hours) in MSDs and fluidity at the different delay times for the cells in 2D.

Delay (s)	MSDs (μm²)			Delay (s)	Fluidity (α)		
	F (2, 73)	***p***	η_p^2		***F (2, 73)***	***p***	η_p^2
0.14	0.554	0.577	0.015	**0.28**	1.831	0.168	0.048
0.7	2.901	0.061	0.074	**0.7**	3.758	0.028	0.093
2.1	1.943	0.151	0.051	**2.1**	2.325	0.105	0.060
3.5	1.511	0.228	0.040	**3.5**	0.292	0.748	0.008
4.9	2.596	0.081	0.066	**4.9**	0.150	0.861	0.004
6.3	1.511	0.228	0.040	**6.3**	0.382	0.684	0.010
7.7	1.343	0.267	0.035	**7.7**	0.255	0.775	0.007
9.1	1.173	0.315	0.031	**9.1**	0.309	0.735	0.008

Pairwise comparisons

Table S. 4: Pairwise comparisons of MSDs of Paclitaxel-treated (PTX or P) and untreated (UNT or U) in 2D environments at 24 and 48 hours of treatment. For example, PTX (24 Vs 48) compares MSDs for Paclitaxel-treated cells at 24 and 48 hours.

Delay (s)	P-values								
	UNT ***(24 Vs 48)***	**ETH** ***(24 Vs 48)***	**PTX** ***(24 Vs 48)***	**24**			**48**		
				(U Vs E)	***(E Vs P)***	***(P Vs U)***	***(U Vs E)***	***(E Vs P)***	***(P Vs U)***
0.14	0.625	0.362	0.631	1.000	1.000	1.000	0.109	0.411	1.000
0.7	0.382	0.548	0.006	1.000	0.078	0.031	0.580	<.0005	<.0005
3.5	0.245	0.984	0.014	1.000	0.277	0.125	1.000	<.0005	0.002
6.3	0.335	0.683	0.007	1.000	0.271	0.249	1.000	<.0005	0.001
7.7	0.324	0.650	0.008	1.000	0.348	0.370	1.000	0.001	0.003
9.1	0.330	0.646	0.012	1.000	0.477	0.571	1.000	0.002	0.009

Table S. 5: Pairwise comparisons of fluidity for Paclitaxel-treated (PTX or P), ethanol-treated (ETH or E) and untreated (UNT, or U) in 2D environments at 24 and 48 hours of treatment.

Delay (s)	**P-values**								
	UNT	**ETH**	**PTX**	**24**			**48**		
	(24 Vs 48)	***(24 Vs 48)***	***(24 Vs 48)***	***(U Vs E)***	***(E Vs P)***	***(P Vs U)***	***(U Vs E)***	***(E Vs P)***	***(P Vs U)***
0.28	0.424	0.755	0.017	1.000	0.177	0.026	1.000	<.0005	<.0005
0.7	0.831	0.754	0.001	1.000	0.290	0.197	1.000	<.0005	<.0005
2.1	0.832	0.068	0.003	1.000	0.178	0.500	0.838	0.010	<.0005
3.5	0.497	0.191	0.117	1.000	1.000	1.000	1.000	0.858	0.868
4.9	0.204	0.186	0.510	1.000	1.000	1.000	1.000	1.000	0.729
6.3	0.319	0.610	0.802	1.000	1.000	1.000	1.000	1.000	0.407
9.1	0.536	0.663	0.839	1.000	1.000	1.000	0.700	1.000	0.693

Mitochondrial Particle Tracking Microrheology experiments in 3D environments

Descriptive statistics

Table S. 6: Summarises of mean MSDs (μm²) and standard deviations of mitochondrial fluctuations from 63 individual WHCO1 cells embedded in 3D environments at 24 and 48 hours of treatment. PTX and UNT stand for Paclitaxel-treated and untreated cells, respectively.

Delay (s)	Mean (M)				Standard Deviation (SD)			
	PTX		UNT		PTX		UNT	
	24	***48***	***24***	***48***	***24***	***48***	***24***	***48***
0.15	0.0233	0.0268	0.0241	0.0233	0.0063	0.0033	0.0042	0.0034
0.3	0.0261	0.0313	0.0283	0.0264	0.0069	0.0043	0.0047	0.0037
0.6	0.0294	0.0372	0.0345	0.0309	0.0075	0.0063	0.0051	0.0041
0.9	0.0326	0.0432	0.0402	0.0350	0.0081	0.0086	0.0059	0.0048
1.2	0.0357	0.0485	0.0458	0.0392	0.0092	0.0112	0.0068	0.0058
1.5	0.0382	0.0536	0.0510	0.0430	0.0097	0.0120	0.0078	0.0069
1.8	0.0406	0.0586	0.0560	0.0466	0.0103	0.0165	0.0090	0.0077
2.1	0.0431	0.0633	0.0608	0.0504	0.0113	0.0192	0.0102	0.0087
2.4	0.0454	0.0681	0.0655	0.0542	0.0120	0.2193	0.0114	0.0098
2.7	0.0477	0.0729	0.0702	0.0580	0.0128	0.0247	0.0127	0.0110
3	0.0499	0.0777	0.0747	0.0617	0.0136	0.0275	0.0140	0.0121
3.6	0.0540	0.0867	0.0837	0.0689	0.0153	0.0330	0.0164	0.0145
4.2	0.0580	0.0952	0.0921	0.0765	0.0171	0.0382	0.0189	0.0174
4.8	0.0619	0.1038	0.1005	0.0841	0.0187	0.0435	0.0216	0.0207
6	0.0690	0.1195	0.1167	0.0994	0.0217	0.0537	0.0277	0.0275
9.9	0.0848	0.1543	0.1540	0.1381	0.0300	0.0768	0.0416	0.0464

Table S. 7: Summaries of mean fluidity and standard deviations of mitochondrial fluctuations from 63 individual WHCO1 cells embedded in 3D environments at 24 and 48 hours of treatment. PTX and UNT stand for Paclitaxel-treated and untreated cells, respectively. Fluidity at τ = 1.5 s was transformed using a square root function after failing the normality test.

Delay (s)	Mean (M)				Standard Deviation (SD)			
	PTX		UNT		PTX		UNT	
	24	***48***	***24***	***48***	***24***	***48***	***24***	***48***
0.3	0.1666	0.2175	0.2365	0.1803	0.0431	0.0773	0.0395	0.0378
0.6	0.1941	0.2661	0.3245	0.2483	0.0850	0.1091	0.0797	0.0798
0.9	0.2675	0.3671	0.4012	0.3264	0.0894	0.1289	0.1044	0.0997
1.2	0.3009	0.3848	0.4633	0.3934	0.1243	0.1378	0.1012	0.0943
1.5	0.5728	0.6406	0.6856	0.6454	0.1240	0.1343	0.0653	0.1014
1.8	0.3397	0.4959	0.5150	0.4572	0.1534	0.1397	0.1096	0.1481
2.1	0.3871	0.4815	0.5289	0.5153	0.1629	0.1584	0.1132	0.1357
2.4	0.3804	0.5125	0.5530	0.5388	0.1727	0.1288	0.1055	0.1620
2.7	0.4144	0.5434	0.5852	0.5831	0.1325	0.1828	0.0918	0.1567
3	0.4509	0.5608	0.5664	0.5748	0.1497	0.1408	0.1215	0.1321
3.6	0.4501	0.5772	0.6113	0.6231	0.1973	0.1400	0.0863	0.1691
4.2	0.5033	0.5387	0.6143	0.6160	0.1547	0.1557	0.1229	0.2098
4.8	0.4386	0.6386	0.6388	0.7123	0.1611	0.1832	0.1258	0.2041
6	0.5235	0.5965	0.6882	0.7222	0.2534	0.2443	0.1458	0.2334
9.9	0.4758	0.6995	0.7084	0.7540	0.4010	0.4908	0.1991	0.2462

Two-way ANOVA results

Table S. 8: Two-way ANOVA results summarising the significance of the interaction between drug treatment intervention (untreated and Paclitaxel-treated cells) and duration of treatment (24 and 48 hours) in MSDs and fluidity at the different delay times for the cells in 3D.

Delay (s)	MSDs (μm²)			Fluidity (α)		
	F (1, 59)	***p***	η_p^2	***F (1, 59)***	***p***	η_p^2
0.15	2.931	0.092	0.047			
0.3	6.270	0.015	0.096	17.908	<.0005	0.233
0.6	12.694	0.001	0.177	10.551	0.002	0.152
0.9	18.390	< .0005	0.238	10.364	0.002	0.149
1.2	19.893	< .0005	0.252	6.522	0.013	0.100
1.5	21.878	< .0005	0.271	3.697	0.059	0.060
1.8	23.484	< .0005	0.285	8.666	0.005	0.128
2.1	23.011	< .0005	0.281	2.052	0.157	0.034
2.4	23.011	< .0005	0.281	3.616	0.062	0.058
2.7	22.734	< .0005	0.278	3.332	0.073	0.053
3	22.393	< .0005	0.275	1.992	0.163	0.033
3.6	21.896	< .0005	0.271	1.977	0.165	0.032
4.2	20.390	< .0005	0.257	0.162	0.688	0.003
4.8	19.268	< .0005	0.246	2.117	0.151	0.035
6	16.773	< .0005	0.221	0.114	0.737	0.002
9.9	12.123	0.001	0.170	0.991	0.324	0.017

Pairwise comparisons

Table S. 9: Pairwise comparisons of MSDs of Paclitaxel-treated (PTX) and untreated (UNT) in 3D environments at 24 and 48 hours of treatment. For example, PTX (24 Vs 48) compares MSDs for Paclitaxel-treated cells at 24 and 48 hours.

Delay (s)	**P-values**			
	PTX ***(24 Vs 48)***	**UNT** ***(24 Vs 48)***	**24** ***(UNT Vs PTX)***	**48** ***(UNT Vs PTX)***
0.15	0.056	0.676	0.596	0.087
0.3	0.015	0.333	0.195	0.036
0.6	0.001	0.107	0.011	0.016
0.9	< .0005	0.042	0.001	0.007
1.2	< .0005	0.030	< .0005	0.010
1.5	< .0005	0.023	< .0005	0.010
1.8	< .0005	0.018	< .0005	0.010
2.1	< .0005	0.020	< .0005	0.014
2.4	< .0005	0.023	< .0005	0.017
2.7	< .0005	0.027	< .0005	0.021
3	< .0005	0.031	< .0005	0.024
3.6	< .0005	0.038	< .0005	0.033
4.2	< .0005	0.056	< .0005	0.051
4.8	< .0005	0.076	< .0005	0.068
6	< .0005	0.132	< .0005	0.133
9.9	< .0005	0.346	< .0005	0.411

Table S. 10: Pairwise comparisons of fluidity for Paclitaxel-treated (PTX) and untreated (UNT) in 3D environments at 24 and 48 hours of treatment.

Delay (s)	**P-values**			
	PTX ***(24 Vs 48)***	**UNT** ***(24 Vs 48)***	**24** ***(UNT Vs PTX)***	**48** ***(UNT Vs PTX)***
0.3	0.008	0.002	< .0005	0.071
0.6	0.035	0.018	< .0005	0.626
0.9	0.014	0.048	< .0005	0.351
1.2	0.061	0.095	< .0005	0.858
1.5	0.105	0.297	0.002	0.914
1.8	0.005	0.250	< .0005	0.508
2.1	0.091	0.794	0.003	0.575
2.4	0.022	0.788	< .0005	0.671
2.7	0.017	0.966	< .0005	0.492
3	0.041	0.866	0.010	0.809
3.6	0.038	0.834	0.002	0.487
4.2	0.565	0.977	0.032	0.254
4.8	0.003	0.220	< .0005	0.292
6	0.391	0.670	0.021	0.180
9.9	0.092	0.711	0.035	0.705

Comparing MSDs and fluidity for WHCO1 cells in 2D and 3D environments

Descriptive statistics

Table S. 11: Summaries of mean MSDs and fluidity and standard deviations of mitochondrial fluctuations from single WHCO1 cells in 2D and 3D environments at 24 and 48 hours of treatment. PTX and UNT stand for Paclitaxel-treated and untreated cells, respectively. The MSDs and fluidity are compared at τ = 2.1 s. MSDs were transformed using the square root function after failing the normality test.

Dependent variable	Time (hours)	Intervention	Dimension	Mean (M)	Standard deviation (SD)
MSDs	24	PTX	2D	0.1245	0.0302
			3D	0.2060	0.0268
		UNT	2D	0.1451	0.0268
			3D	0.2457	0.0206
	48	PTX	2D	0.0973	0.0196
			3D	0.2492	0.0369
		UNT	2D	0.1374	0.0110
			3D	0.2236	0.0195
Fluidity	24	PTX	2D	0.8469	0.1503
			3D	0.3871	0.1629
		UNT	2D	0.9189	0.1032
			3D	0.5289	0.1132
	48	PTX	2D	0.6813	0.2109
			3D	0.4815	0.1584
		UNT	2D	0.9084	0.0730
			3D	0.5153	0.1357

Pairwise comparisons

Table S. 12: Pairwise comparisons of MSDs and fluidity for Paclitaxel-treated (PTX) and untreated (UNT) in 2D and 3D environments at 24 and 48 hours of treatment.

Dependent variable	Time (hours)	Differences	P-Value
MSDs	24	PTX (2D V 3D)	< .0005
		UNT (2D v 3D)	< .0005
	48	PTX (2D v 3D)	< .0005
		UNT (2D v 3D)	< .0005
Fluidity	24	PTX (2D v 3D)	< .0005
		UNT (2D v 3D)	< .0005
	48	PTX (2D v 3D)	0.001
		UNT (2D v 3D)	< .0005

Morphology analysis of WHCO1 cells

Descriptive statistics

Table S. 13: Summaries of mean and standard deviations for the area, perimeter, circularity, and aspect ratio from WHCO1 cells in 2D and 3D environments at 24 and 48 hours of treatment. PTX and UNT stand for Paclitaxel-treated and untreated cells, respectively.

Dependent variable	Time (hours)	Intervention	Dimension	Mean (M)	Standard deviation (SD)
Area	24	PTX	2D	46.553	8.921
			3D	77.061	14.768
		UNT	2D	30.973	5.936
			3D	82.477	15.261
	48	PTX	2D	55.709	10.676
			3D	84.270	16.843
		UNT	2D	35.078	6.722
			3D	91.186	15.615
Perimeter	24	PTX	2D	1.100	0.143
			3D	1.434	0.175
		UNT	2D	1.010	0.123
			3D	1.670	0.258
	48	PTX	2D	1.157	0.141
			3D	1.512	0.171
		UNT	2D	0.964	0.118
			3D	1.658	0.252
Circularity	24	PTX	2D	0.510	0.104
			3D	0.477	0.097
		UNT	2D	0.406	0.083
			3D	0.380	0.073
	48	PTX	2D	0.415	0.084
			3D	0.464	0.071
		UNT	2D	0.476	0.097
			3D	0.430	0.090
Aspect Ratio	24	PTX	2D	1.349	0.113
			3D	1.142	0.096
		UNT	2D	1.451	0.122
			3D	1.165	0.116
	48	PTX	2D	1.580	0.133
			3D	1.109	0.060
		UNT	2D	1.448	0.122
			3D	1.165	0.107

Pairwise comparisons

Table S. 14: Pairwise comparisons for mean area, perimeter, circularity, and aspect ratio for Paclitaxel-treated (PTX) and untreated (UNT) in 2D and 3D environments at 24 and 48 hours of treatment.

Dependent variable	Interventions		Mean Differences	P-Value
Area	2D	24	**PTX** *(2D V 3D)*	< .0005
			UNT *(2D v 3D)*	< .0005
			PTX v UNT	0.001
			PTX v ETH	< .0005
			ETH v UNT	1.000
		48	**PTX** *(3D v 2D)*	< .0005
			UNT *(2D v 3D)*	< .0005
			PTX v UNT	< .0005
			PTX v ETH	< .0005
			ETH v UNT	1.000
	3D	24	*PTX v UNT*	0.399
		48	*PTX v UNT*	0.330
	PTX	2D	*48 v 24*	0.075
		3D	*48 v 24*	0.310
	ETH	2D	*48 v 24*	0.721
	UNT	2D	*48 v 24*	0.308
		3D	*48 v 24*	0.176
Perimeter	2D	24	**PTX** *(2D V 3D)*	0.001
			UNT *(2D v 3D)*	< .0005
			PTX v UNT	0.737
			PTX v ETH	0.001
			ETH v UNT	0.012
		48	**PTX** *(3D v 2D)*	0.190
			UNT *(2D v 3D)*	< .0005
			PTX v UNT	< .0005
			PTX v ETH	< .0005
			ETH v UNT	1.000
	3D	24	*PTX v UNT*	0.037
		48	*PTX v UNT*	0.241
		2D	*48 v 24*	0.004

	PTX	**3D**	*48 v 24*	0.530
	ETH	**2D**	*48 v 24*	0.142
	UNT	**2D**	*48 v 24*	0.512
		3D	*48 v 24*	0.916
Circularity	**2D**	**24**	**PTX** *(2D V 3D)*	0.359
			UNT *(2D v 3D)*	0.436
			PTX v UNT	< .0005
			PTX v ETH	0.142
			ETH v UNT	< .0005
		48	**PTX** *(3D v 2D)*	0.227
			UNT *(2D v 3D)*	0.175
			PTX v UNT	0.124
			PTX v ETH	0.952
			ETH v UNT	1.000
	3D	**24**	*PTX v UNT*	0.015
		48	*PTX v UNT*	0.433
	PTX	**2D**	*48 v 24*	0.003
		3D	*48 v 24*	0.765
	ETH	**2D**	*48 v 24*	< .0005
	UNT	**2D**	*48 v 24*	0.005
		3D	*48 v 24*	0.214
Aspect Ratio	**2D**	**24**	**PTX** *(2D V 3D)*	0.095
			UNT *(2D v 3D)*	0.012
			PTX v UNT	0.855
			PTX v ETH	1.000
			ETH v UNT	0.208
		48	**PTX** *(3D v 2D)*	0.001
			UNT *(2D v 3D)*	0.017
			PTX v UNT	0.609
			PTX v ETH	0.087
			ETH v UNT	0.728
	3D	**24**	*PTX v UNT*	0.870
		48	*PTX v UNT*	0.714
		2D	*48 v 24*	0.038

	PTX	**3D**	*48 v 24*	0.830
	ETH	**2D**	*48 v 24*	0.765
	UNT	**2D**	*48 v 24*	0.974
		3D	*48 v 24*	0.997

Shape Analysis of WHCO1 cells

Table S. 15: VAMPIRE analysis results showing the abundance of cells in each of the conditions in each shape mode. P_24, P_48, E_24, E_48, U_24, and U_48 represent the number of Paclitaxel-treated cells at 24 and 48 hours, ethanol-treated cells at 24 and 48 hours, and untreated cells at 24 and 48 hours, respectively.

Shape Modes	**2D**						**3D**			
	P_24	**P_48**	**E_24**	**E_48**	**U_24**	**U_48**	**P_24**	**P_48**	**U_24**	**U_48**
1	2	3	5	1	4	9	1	0	0	0
2	5	2	2	1	3	3	5	4	3	4
3	2	1	5	3	4	0	3	0	2	3
4	4	2	8	4	3	4	1	3	1	3
5	4	0	6	4	4	3	1	0	2	1
6	2	4	6	0	5	4	2	0	1	0
7	2	4	2	3	8	0	1	1	1	0
8	2	2	8	2	5	3	0	0	1	1
9	3	0	0	1	2	4	1	3	4	1
10	1	4	1	4	4	7	0	0	1	2